Some investigations of the ion acoustic wave problem in collisionless plasmas. (Thesis)

Jensen, V.O.

Publication date:
1976

Document Version
Publisher's PDF, also known as Version of record

Risø Report No. 322

Risø Report No. 322

Research Establishment Risø

Some Investigations of the Ion Acoustic Wave Problem in Collisionless Plasmas

by V.O. Jensen

August 1976

Sales distributors: Jul. Gjellerup, 87, Sølvgade, DK-1307 Copenhagen K, Denmark
Available on exchange from: Library, Research Establishment Risø,
DK-4000 Roskilde, Denmark

UDC 533.9.07/.08: 533.951.3

SOME INVESTIGATIONS OF THE ION ACOUSTIC WAVE PROBLEM IN COLLISIONLESS PLASMAS

by

V.O. Jensen

August 1976 Risø Report No. 322

SOME INVESTIGATIONS OF THE ION ACOUSTIC WAVE PROBLEM IN COLLISIONLESS PLASMAS

by

V.O. Jensen

Physics Department
Research Establishment Risø
Roskilde

Denne afhandling er af det naturvidenskabelige fakultet ved Aarhus Universitet antaget til offentligt at forsvares for den filosofiske doktorgrad.

Aarhus Universitet, den 8. november 1976.

Lauritz B. Holm-Nielsen
dekan

Forsvaret finder sted fredag d. 7. januar 1977 kl. 14^{15} i Fysisk Auditorium, Det fysiske Institut, Aarhus Universitet, Ny Munkegade.

ISBN 87-550-0408-3

Abstract

A survey is presented of the Risø studies of linear ion acoustic waves in a single-ended Q-machine during the period 1969-74. Some of the main results are:

1) The construction of an electrostatic ion energy analyzer for determination of both unperturbed and perturbed ion velocity distribution functions.

2) Propagation properties of grid-excited pulses and waves were calculated analytically by means of Green's functions. It was concluded that a single Landau-mode does not constitute a satisfactory description of the wave propagation close to the grid. This was confirmed experimentally.

3) It was shown that any density wave pattern obtainable as a solution to the Vlasov equation with the collective term included can also be obtained with purely freely streaming ions alone.

4) Clear-cut evidence of collective interaction in connection with density pulses was found by measuring the perturbed ion velocity distribution function.

5) It was concluded that the damping of ion acoustic waves can best be described by a phase mixing of almost freely streaming ions. The wave potential energy in the electron fluid is absorbed by the bulk of the ions in the background plasma; the absorption spectrum is centered around the phase velocity but has a rather wide shape.

CONTENTS

Preface

Since 1969 the Q-machine group at Risø has been engaged in a detailed study of the propagation properties of ion acoustic disturbances in collisionless plasmas. The present treatise describes the part of this work in which the author has been actively involved. Most of the results have already been published. Reprints of the most important of these publications are included as separate chapters as follows·

Chapter 3 S.A. Andersen, V.O. Jensen, P. Michelsen, and P. Nielsen, Determination and Shaping of the Ion-Velocity Distribution Function in a Single-Ended Q Machine, Phys. Fluids 14, 728 (1971).

Chapter 4 S.A. Andersen, G.B. Christoffersen, V.O. Jensen, P. Michelsen, and P. Nielsen, Measurements of Wave-Particle Interaction in a Single-Ended Q Machine, Phys. Fluids 14, 990 (1971).

Chapter 5 G.B. Christoffersen, V.O. Jensen, and P. Michelsen, Investigation of Ion Acoustic Waves in Collisionless Plasmas, Phys. Fluids 17, 390 (1974).

Chapter 6 V.O. Jensen, P. Michelsen and H.C.S. Hsuan, Absolute and Convective Ion Beam Instability Studied through Green's Functions, Phys. Fluids 17, 2208 (1974).
V.O. Jensen, P. Michelsen and H.C.S. Hsuan, Errata: Absolute and Convective Ion Beam Instability Studied through Green's Functions, Phys. Fluids 18, 754 (1975).

The reprint in chapter 6 is not an exact copy of the article as it appeared in Phys. Fluids 17, 2208 (1974), but a version of the paper in which the printer's errors have been corrected.

Besides reprints of the publications, this treatise contains four chapters: an introduction in chapter 1, a description of the Risø Q-machine in chapter 2, some additional remarks on chapters 3 through 6 in chapter 7, and a general discussion and conclusions in chapter 8. In these four chapters references to the above-mentioned publications are labelled chapter 3 through chapter 6. Although chapters 1, 2, 7 and 8 are written exclusive-

ly for the present publication they do contain details which have been previously published. The publications in which these details appeared are not considered important enough to be included here; they took the form of letters, contributions to conferences, or laboratory reports, and are included in the list of references at the end of this report.

During the work described here the author was responsible for activities involving the Risø Q-machine. Only a small part of the work was performed by the author alone. The main part was performed in collaboration with a number of people who have joined the Q-machine group and taken part at various stages of the work. The author wishes to acknowledge the inspiring collaboration of all these colleagues. Poul Michelsen joined the group on a permanent basis during most of the study. The close collaboration and many discussions with him were of much encouragement to the author. Hans Kurt Andersen, Gert Christoffersen, Per Nielsen, Hans Pecseli, Peter I. Petersen, and Lars Prahm have all worked for their licentiate degrees in the Q-machine group during the period in question. Their enthusiasm, ideas and criticism considerably improved the work. Hulbert C.S. Hsuan joined the group as a summer guest twice during the same period. The author enjoyed working closely with him and gained much theoretical insight from this collaboration. N. D'Angelo has been attached to the group during the whole period. His constructive criticism and sophisticated arguments against the need and usefulness of Green's functions in the study of ion acoustic waves provided us with a constant challenge to improve our work. Finally, numerous scientific discussions with C.F. Wandel during more than 15 years are greatly acknowledged.

Without the technical skill and patience of Mogens Nielsen and Børge Reher in maintaining the Q-machine and in building equipment it would have been impossible to perform the experimental work described here.

The author also wishes to thank K.-V. Weisberg for his skilled help with the electronic equipment.

Finally, Otto Kofoed-Hansen and Hans Bjerrum Møller, as successive heads of the Physics Department, are gratefully thanked for their encouragement throughout the course of this research.

The American Institute of Physics has kindly given permission to reproduce the four reprints as part of this treatise.

The work was partly performed under the Association Euratom-Research Establishment Risø.

1. INTRODUCTION

1.1. Collisionless Plasma Description

The work described in this report was concentrated on plasmas in which binary collisions between the charged particles are of very little importance and can thus be neglected. The set of basic equations used in theoretical treatments of such collisionless plasmas consists of the two Vlasov equations

$$\frac{\partial F_{i,e}(\bar{r},\bar{v},t)}{\partial t} + \bar{v}\cdot\nabla_r F_{i,e}(\bar{r},\bar{v},t) + \frac{e_{i,e}}{m_{i,e}} (\bar{E}+\bar{v}\times\bar{B})\cdot\nabla_v F_{i,e}(\bar{r},\bar{v},t) = 0 , \tag{1.1}$$

which are coupled to the Maxwell equations

$$\nabla\cdot\bar{B} = 0 , \quad \nabla\times\bar{B} = \mu_o\bar{j} + \varepsilon_o\mu_o\frac{\partial\bar{E}}{\partial t} ,$$
$$\nabla\cdot\bar{E} = \frac{\rho}{\varepsilon_o} , \quad \nabla\times\bar{E} = -\frac{\partial\bar{B}}{\partial t} \tag{1.2}$$

by the source functions

$$\rho(\bar{r},t) = \sum_{i,e} e_{i,e} \int F_{i,e}(\bar{r},\bar{v},t)\, d^3\bar{v} \tag{1.3}$$

and

$$\bar{j}(\bar{r},t) = \sum_{i,e} e_{i,e} \int \bar{v}\, F_{i,e}(\bar{r},\bar{v},t)\, d^3\bar{v} . \tag{1.4}$$

In this set of equations $\bar{r}$, $\bar{v}$, and t represent the space variable, the velocity space variable, and the time variable. $F_{i,e}$ is the distribution function for ions and electrons, respectively. $e_{i,e}$ is the charge of ions and electrons respectively and $m_{i,e}$ represents the mass of the two kinds of particles. $\bar{B}$ and $\bar{E}$ are the magnetic and the electric fields respectively. $\bar{j}$ represents the current density and ρ the charge density. Finally ε_o is the vacuum dielectric constant and μ_o is the vacuum magnetic permeability. The integrals in Eqs. (1.3) and (1.4) should be performed from $-\infty$ to $+\infty$ over the three components of the velocity $\bar{v}$.

All formulas throughout this paper are expressed in MKSA units.

Although binary collisions are neglected, the charged particles in the plasma do interact. The interaction is caused by collective effects and is described by the third term in the Vlasov equations (1.1). It occurs because of the possibility of a building up of current and charge densities as given by Eqs. (1.3) and (1.4). These densities act as sources of electric and magnetic fields as described by the Maxwell equations (1.2). The fields in turn react on the plasma particle distribution functions through the collective term in the Vlasov equation.

The collective interaction term is peculiar to plasmas; it replaces to some extent the collision terms found in the Boltzmann equations used to describe other many-body systems. This term is responsible for many of the properties characteristic of plasmas, among them all the instabilities encountered in fusion research. Because of the presence of the collective interaction term it is very difficult to solve the Vlasov equation analytically for actual situations. In order to obtain theoretical results, it is normally necessary to introduce various assumptions and approximations; in many cases it is very difficult to assess the validity of these. It is therefore of utmost interest to perform experiments of such quality that the results can confidently be compared with calculations based on the Vlasov equations. One of the purposes of the work described in this treatise was to perform such experiments, and in the light of the results to discuss some of the assumptions and approximations often introduced into theoretical treatments. Another purpose was to obtain a clear experimental proof of plasma properties caused by collective interaction.

In general it is very difficult to design and perform highly reliable experiments in collisionless plasmas. The lifetime of most collisionless laboratory plasmas, such as fusion research plasmas, is very short and the various parameters are poorly known. Only dilute dc-plasmas of the kind produced in Q-machines and in other similar devices seem to be appropriate for this kind of experiment. In these devices the plasmas are produced in a region with a magnetic field by some ionization mechanisms. The charged particles moving freely along the lines of force form a plasma column confined radially by the magnetic field. This kind of plasma is especially suited for studies of longitudinal waves

or other perturbations propagating along the magnetic lines of force. For such phenomena the set of basic equations (1.1) through (1.4) can directly be integrated over the two velocity components perpendicular to the direction of propagation whereby it reduces to

$$\frac{\partial F_{i,e}(x,v,t)}{\partial t} + v \frac{\partial F_{i,e}(x,v,t)}{\partial x} + \frac{e_{i,e}}{m_{i,e}} E(x,t) \frac{\partial F_{i,e}(x,v,t)}{\partial v} = 0 \tag{1.5}$$

and

$$\frac{\partial E(x,t)}{\partial x} = \frac{1}{\varepsilon_o} \sum_{i,e} e_{i,e} \int_{-\infty}^{\infty} F_{i,e}(x,v,t)\, dv \,. \tag{1.6}$$

During the 1960's much experimental work was performed in order to examine and describe propagation properties of longitudinal waves through uniform steady state, collisionless plasmas. Since the wave amplitudes were small in most of this work, it was justifiable to linearize the equations by setting

$$F_{i,e}(x,v,t) = f_{o_{i,e}}(v) + f_{i,e}(x,v,t) \,, \tag{1.7}$$

where $f_{o_{i,e}}(v)$ is assumed to be much larger than $|f_{i,e}(x,v,t)|$. By inserting (1.7) into (1.5) and (1.6), and by neglecting second order terms, we obtain the linearized set of equations

$$\frac{\partial f_{i,e}(x,v,t)}{\partial t} + v \frac{\partial f_{i,e}(x,v,t)}{\partial x} = - \frac{e_{i,e}}{m_{i,e}} E(x,t)\, f'_{o_{i,e}}(v) \,, \tag{1.8}$$

and

$$\frac{\partial E(x,t)}{\partial x} = \frac{1}{\varepsilon_o} \sum_{i,e} e_{i,e} \int_{-\infty}^{\infty} f_{i,e}(x,v,t)\, dv \,. \tag{1.9}$$

To obtain (1.9) we have also used the fact that charge neutrality prevails in the background plasma, i.e. that $\int f_{o_i}(v)\, dv = \int f_{o_e}(v)\, dv$.

A plasma described by Eqs. (1.8) and (1.9) can propagate two kinds of longitudinal waves: high frequency electrostatic electron oscillations and low frequency ion acoustic waves. The first seri-

ous attempt to investigate the high frequency waves was made by Malmberg and his group[1], while Wong, D'Angelo and Motley[2,3] performed the pioneering work within the field of ion acoustic waves.

All the work to be discussed in this treatise is concerned with the ion acoustic wave branch in plasmas with singly charged ions. In most cases, the wavelengths of these waves are long compared to the Debye-length. Therefore it is a good approximation to assume that quasi-neutrality prevails whereby Eqs. (1.9) are omitted, and further to substitute the electron Vlasov equation (1.8) by the isothermal electron fluid equation[4]:

$$E(x,t) = - \frac{\kappa T_e}{e} \frac{1}{n_o} \frac{\partial n(x,t)}{\partial x} \quad . \tag{1.10}$$

In (1.10) e is the ion charge, T_e the electron temperature, κ the Boltzmann constant, n and n_o are the perturbed and unperturbed density, respectively.

By introducing (1.10), (1.8) reduces to

$$\frac{\partial f(x,v,t)}{\partial t} + v \frac{\partial f(x,v,t)}{\partial x} = \frac{c_e^2}{n_o} \frac{\partial n(x,t)}{\partial x} f_o'(v) \quad , \tag{1.11}$$

where

$$n(x,t) = \int_{-\infty}^{\infty} f(x,v,t)\, dv \quad , \tag{1.12}$$

$$n_o = \int_{-\infty}^{\infty} f_o(v)\, dv \tag{1.13}$$

and

$$c_e^2 = \kappa T_e / m_i \quad . \tag{1.14}$$

From now on, when not otherwise indicated, f and f_o without index as in (1.11) stand for the ion velocity distribution functions.

Eqs. (1.11) and (1.12) form the basis of most of the investigations to be discussed here. In a few cases it was necessary to abandon the assumption of quasi-neutrality and to maintain the Poisson equation (1.9) in the treatment (Chapter 6).

1.2. Remarks on Earlier Studies of the Ion Acoustic Wave Problem

The method most commonly used in calculating the propagation properties of longitudinal waves from the Vlasov equation is that of Landau[5]. Since criticism of a somewhat uncritical use of this method for handling experimental situations forms a substantial part of the present work we shall briefly review the Landau method as used in treatments of the ion acoustic wave branch.

Landau considers an induced wave of the form $f(x,v,t=0) = g(v)\exp(ikx)$ as the initial condition and solves the Vlasov equation by applying Laplace transformation in time. By following him and using a Laplace transformation defined as

$$F(\omega) = \int_0^\infty \exp(i\omega t)\, F(t)\, dt \tag{1.15}$$

we get from Eqs. (1.11) and (1.12)

$$n(k,\omega) = \frac{\frac{1}{ik}\int_{-\infty}^{\infty} \frac{g(v)}{v-\omega/k}\, dv}{1 - \frac{c_e^2}{n_o}\int_{-\infty}^{\infty} \frac{f_o'(v)}{v-\omega/k}\, dv} \quad . \tag{1.16}$$

Rather than calculating the inverse transformation

$$n(k,t) = \frac{1}{2\pi}\int_{-\infty+i\delta}^{+\infty+i\delta} n(k,\omega)\exp(-i\omega t)\, d\omega \tag{1.17}$$

exactly, Landau uses the following procedure to determine an asymptotical form of $n(k,t)$ for large values of the time t. The v-integrals in Eq. (1.16) are analytic functions for $\mathrm{Im}\ \omega > 0$. ($g(v)$ and $f_o(v)$ are assumed to be analytic and entire functions of the velocity v). First the v-integrals are defined for $\mathrm{Im}\ \omega \leq 0$ by their analytic continuations, which are obtained by prescribing that the integration paths run below the pole at $v = \omega/k$. As the next step in the procedure the zeros of the denominator in Eq. (1.16) are determined, i.e. ω-values being solutions to the equation

$$1 - \frac{c_e^2}{n_o}\int_b \frac{f_o'(v)}{v-\omega/k}\, dv = 0 \tag{1.18}$$

are found. Index b at the integral indicates that the integration

path runs from $-\infty$ to $+\infty$, but below the pole at $v = \omega/k$. The solution having the largest imaginary part is denoted by ω_p. Now the integration path in Eq. (1.17) is pressed downwards from running above all singularities in $n(k,\omega)$ to running just below ω_p. Eq. (1.17) can then be written

$$n(k,t) = i \text{ Res. } n(k,\omega_p) \exp(-i\omega_p t) + \frac{1}{2\pi} \int_{b.\omega_p} n(k,\omega) \exp(-i\omega t)\, d\omega \qquad (1.19)$$

where Res. stands for "the residue of" and $b.\omega_p$ indicates that the integration path runs below ω_p.

For large t the integral term in Eq. (1.19) is exponentially small in comparison with the residue term and can thus be neglected and we are left with the Landau result

$$n(k,t) = i \text{ Res. } n(k,\omega_p) \exp(-i\omega_p t) \,. \qquad (1.20)$$

Mathematical problems connected to this Landau procedure have been discussed in detail by Backus[6] and by Weitzner[7].

Depending on $f_o(v)$ and c_e^2, ω_p may lie above, on, or below the real ω axis. For the so-called stable plasmas ω_p lies below and Eq. (1.20) shows that the wave amplitude is damped. This damping is the famous Landau damping which has been the subject of intensive studies and discussions during the last fifteen years.

There is some confusion in the literature concerning the exact meaning of the concept "Landau damping". Many authors restrict it to mean only the exponential damping of the first term on the right-hand side of Eq. (1.19). Other authors prefer to call Landau damping the mechanism by which a longitudinal wave in a collisionless plasma is damped, i.e. to them Landau damping is the damping of $n(k,t)$ given by the full expression in Eq. (1.19). In this paper we shall adopt the latter definition. When we specifically discuss the damping that corresponds only to the first term on the right side of Eq. (1.19), we denote it exponential Landau damping.

It should be noted here that ω_p in Eq. (1.19) is determined by means of Eq. (1.18), which only contains the terms found in

the collective interaction term of Eq. (1.11). Therefore a clear-cut experimental verification of exponential Landau damping with the correct complex frequency ω_p would also constitute a convincing demonstration of collective effects in collisionless plasmas.

Much experimental work has been devoted to the study of the propagation properties of ion acoustic waves, especially to their damping characteristics. References 2, 3 and 8-11 are a few representative publications within this field. One of the main objectives of these works has been to verify the existence of exponential Landau damping and to study its features under various conditions. It is not within the scope of the present report to criticize in detail the earlier works in this field. We shall rather restrict ourselves to listing a number of unsolved problems or deficiencies met in varying degrees in all these works:

1) Landau solves the Vlasov equation for an initial value problem: $f(x,v,t=0) = g(v)\exp(ikx)$ and finds that the waves are damped in time. Experimentally the waves are always generated at a fixed position with a <u>real</u> frequency and damped in space. To find the spatial damping several authors have simply inserted their real frequency ω into Eq. (1.18) and found complex k-values fulfilling the equation. Although, as shown by Gould[12], this procedure can lead to approximate solutions within a limited region in space, it is in general neither satisfactory nor mathematically correct.

2) According to Landau's theory one only expects to see the exponentially Landau damped mode for times sufficiently large so that the first right-hand side term in Eq. (1.19) dominates the integral term. Assuming the conversion from damping in time to spatial damping mentioned under 1) to be applicable, one would only expect to see exponential Landau damping in space at distances from the exciter that are sufficiently large to enable the exponentially damped wave to dominate a term corresponding to the last term in Eq. (1.19). Most experiments have been performed within a few wavelengths from the exciter and no real attempt has been made to show that this last term is indeed small.

Therefore the results of these experiments cannot be conceived as convincing experimental proof of exponential Landau damping.

Interesting arguments in this respect were raised by Hirschfield and Jacob[13]. They assumed that a wave was generated at some position in a plasma in which collective interaction was switched off, i.e. in a gas consisting of freely streaming particles. Such a gas, of course, obeys Eq. (1.11) in a form where the right-hand side has been replaced by a zero. For this gas the transformed of the perturbed density $n(k,\omega)$ is simply given by the nominator in Eq. (1.16). As the denominator, being equal to unity, has no zero we find no Landau damped modes. $n(k,t)$ will be given solely by an integral of the same type as the last term in Eq. (1.19). Hirschfield and Jacob showed that their perturbed density propagates and decays in very much the same way as does an exponentially damped Landau mode in a normal plasma. From this they conclude that most experimental results could as well be explained by simple free-streaming effects.

3) From Eq. (1.18) it is clear that ω_p, and thereby the damping of the Landau mode, depends strongly on $f_o(v)$. In order to draw definite conclusions to the effect that exponential Landau damping has been demonstrated experimentally, the $f_o(v)$ function must be known. In most experiments this function has not been measured.

4) Also the function $g(v)$, which enters into both the right-hand side terms in Eq. (1.19), must be known in order to make definite conclusions. No attempt to measure this function has been reported in earlier works on ion acoustic waves.

5) Most investigations have only been concerned with measurements of the perturbed density and have neglected the perturbed velocity distribution function. Since $n(x,t) = \int_{-\infty}^{\infty} f(x,v,t)\, dv$, it is very likely that there are interesting features in the v-dependence of

$f(x,v,t)$ that cannot be recovered in measurements of $n(x,t)$ because they disappear in the integration.

Having realized that there was a gap between the work that was performed up to about 1969 and the work that was needed in order to understand the propagation properties of ion acoustic perturbations in collisionless plasmas in detail, the Q-machine group at Risø decided to undertake a study in this field. Our main purpose was to perform an experimental and theoretical study without the deficiencies mentioned above. This has been done partly by improving the experimental technique, and partly by solving the ion acoustic wave problem analytically for conditions as found in our experimental device, a single-ended Q-machine. To obtain the theoretical results we applied mathematical techniques that emphasize the accuracy of the part of the solution which is comparable with experiments, i.e. the solution relatively close to the exciter. Finally, based on the results of this study, we obtained some results concerning the general solution to the Vlasov equation.

The work performed is presented in this treatise. A short description of the Risø Q-device is given in chapter 2. Chapter 3 describes a part of the work that was devoted to measurements of the undisturbed ion velocity distribution function $f_o(v)$ and to the possibilities of obtaining various shapes of this function. In chapter 4 the Green's functions for Eqs. (1.11) and (1.12) with a given initial value are derived and tested experimentally. The Green's functions for a boundary value problem are derived in chapter 5 and used to calculate propagation properties of waves; the results are compared with experiments. The last reprint in chapter 6 describes a theoretical work on Green's functions for an unstable plasma. A few additional remarks on the four reprints are given in chapter 7. Before reading the reprint chapters, the reader of this treatise is advised to consult the list of notations, corrections and misprints given in 7.1. Finally, a general discussion and conclusions are presented in chapter 8.

2. THE RISØ Q-MACHINE

The Q-machine at Risø was built in 1966-67 under the supervision of Dr. N. D'Angelo. During this period the author was on leave of absence from Risø and he was therefore not involved in the construction but only in various improvements introduced later. Since the Q-machine resembles many other similar devices, only the main features are described below.

2.1. Description of Hardware

A schematic of the machine is shown in Fig. 1. The device consists of a stainless steel tube connected at the one end to a vacuum pump. The tube is surrounded by a number of coils producing an axial magnetic field. A circular tantalum plate, 3 cm in diameter, is placed on the axis of the system and normal to the magnetic field lines at the one end of the tube. This plate can be heated by bombardment of electrons emitted from a filament and accelerated through an electric field. During operation the front side of the tantalum plate is irradiated by a beam of neutral cesium emitted from a Cs-oven. The plasma ions are formed by surface ionization of the neutrals in the beam on the hot Ta-

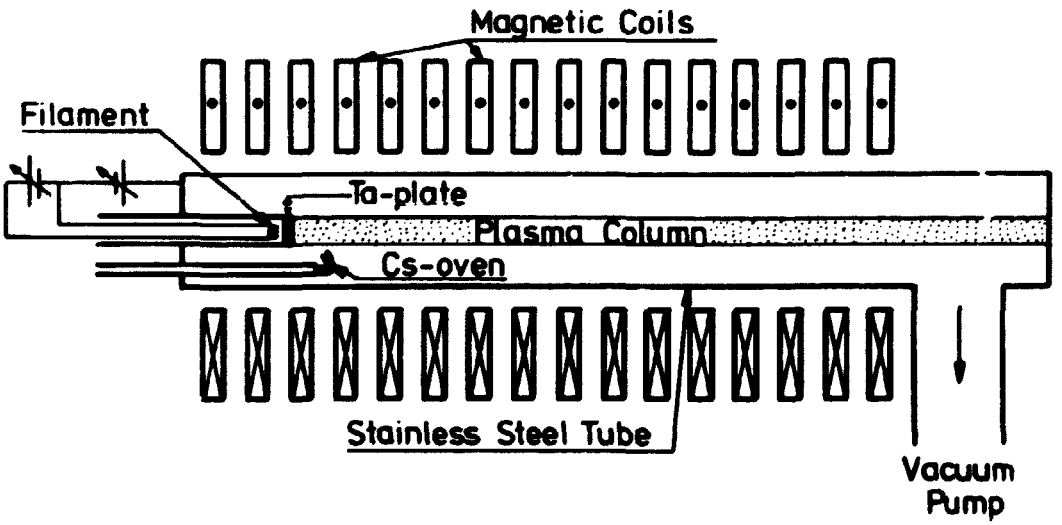

Fig. 1. Schematic drawing of the Risø Q-machine.

plate; the plasma electrons are emitted from this plate through Richardson emission. The plasma particles flow freely in the axial direction while they are confined radially by the magnetic field and thus form a plasma column. Various ports placed around the tube give access to the plasma for diagnostics. Although plasmas of most of the alkali metals can be produced in Q-machines, all the work described in this paper was performed with Cs-plasmas.

The main dimensions and parameters are as follows:

Length of plasma column:	up to 120 cm
Diameter of plasma column:	$\simeq$ 3 cm
Magnetic field on axis, B:	up to 1.0 T
Ripple on magnetic field on axis:	< 2%
Background pressure during operation:	$\lesssim 10^{-5}$ mm Hg
Temperature of Ta-plate, T_{hp}:	$\simeq$ 2500 K
Plasma densities obtainable, n_o:	10^8-10^{12} ions cm^{-3}
Plasma temperature varies with operation conditions but is normally close to the temperature of the Ta-plate:	$\simeq$ 2500 K ($\simeq$ 0.2 eV)

2.2. Characteristic Plasma Parameters

A number of basic parameters characterising a plasma are listed in this subsection. Numerical values of the parameters are calculated for a tandard Q-machine plasma where B = 1T, $n_o = 10^9$ ions/cm^3, $T = T_i = T_e = 0.2$ eV and $m_i = 2.2 \cdot 10^{-25}$ kg (Cs-plasma). The list is meant to facilitate an assessment of the properties of a Q-machine plasma. At the end of the subsection we base a discussion of the importance of binary collisions on the values given in the list, and show that it is indeed justified to apply the collisionless Vlasov equation to calculations of Q-machine plasmas, at least at densities below 10^9 cm^{-3}.

Debye length

$$\lambda_D = (\varepsilon_o \kappa T/n_o e^2)^{\frac{1}{2}} = 1.05 \cdot 10^{-4} \text{ m} \qquad (2.1)$$

Velocity of thermal Cs ion

$$\langle v\rangle_i = (\kappa T_i/m_i)^{\frac{1}{2}} = 3.81\cdot10^{2}\ \mathrm{ms}^{-1} \qquad (2.2)$$

Velocity of thermal electron

$$\langle v\rangle_e = (\kappa T_e/m_e)^{\frac{1}{2}} = 1.88\cdot10^{5}\ \mathrm{ms}^{-1} \qquad (2.3)$$

Larmor radius of thermal ion

$$\rho_i = m_i\langle v\rangle_i/eB = 5.24\cdot10^{-4}\ \mathrm{m} \qquad (2.4)$$

Larmor radius of thermal electron

$$\rho_e = m_e\langle v\rangle_e/eB = 1.07\cdot10^{-6}\ \mathrm{m} \qquad (2.5)$$

Ion Larmor frequency

$$\omega_{ci} = eB/m_i = 7.27\cdot10^{5}\ \mathrm{rad\ s}^{-1} \qquad (2.6)$$

Electron Larmor frequency

$$\omega_{ce} = eB/m_e = 1.76\cdot10^{11}\ \mathrm{rad\ s}^{-1} \qquad (2.7)$$

Ion plasma frequency

$$\omega_{pi} = (n_o e^2/m_i\varepsilon_o)^{\frac{1}{2}} = 3.63\cdot10^{6}\ \mathrm{rad\ s}^{-1} \qquad (2.8)$$

Electron plasma frequency

$$\omega_{pe} = (n_o e^2/m_e\varepsilon_o)^{\frac{1}{2}} = 1.78\cdot10^{9}\ \mathrm{rad\ s}^{-1} \qquad (2.9)$$

Ion self-collision time[14]

$$t_{ci} = 5.44\cdot10^{54}\ \frac{m_i^{1/2}(\kappa T_i)^{3/2}}{\ln\Lambda\ n_o} = 1.46\cdot10^{-3}\ \mathrm{s} \qquad (2.10)$$

Electron self-collision time

$$t_{ce} = 5.44\cdot10^{54}\ \frac{m_e^{1/2}(\kappa T_e)^{3/2}}{\ln\Lambda\ n_o} = 2.97\cdot10^{-6}\ \mathrm{s} \qquad (2.11)$$

Mean free path between ion-ion collisions

$$\lambda_{ii} = \langle v\rangle_i\cdot t_{ci} = 0.56\ \mathrm{m} \qquad (2.12)$$

Mean free path between electron-electron collisions

$$\lambda_{ee} = \lambda_{ii} = \langle v \rangle_e \, t_{ce} \qquad = \quad 0.56 \text{ m} \qquad (2.13)$$

To calculate numerical values for Eqs. (2.10) and (2.11) we have used $\ln \Lambda = 10$, a value taken from table 5.1 in [14].

For densities below 10^9 cm^{-3} we see from Eq. (2.12) that the mean free path for ion-ion collisions is larger than or comparable to the length of the plasma column. For these densities it is therefore safe to use a collisionless theory.

In chapter 3 it is shown that the plasma ions drift along the plasma column with a relatively high drift velocity. As explained below, it is even safer to use a collisionless theory for calculations of a drifting plasma than of a stationary one. The mean free path given in Eq. (2.12) is measured in a frame of reference in which the bulk of the plasma is at rest, and it corresponds roughly to a 90 degree deflection. One of the results of the work described in chapter 3 is that the plasma drifts through the Q-device with a drift velocity, v_{do}, that is characteristically three times the ion thermal velocity $\langle v \rangle_i$ as defined in Eq. (2.2). Because of the high drift velocity the mean free path as measured in the laboratory system will be about three times that given by Eq. (2.12). Furthermore, a 90 degree deflection in the frame of reference moving with velocity v_{do} corresponds to much weaker deflections in the laboratory frame. On the basis of the findings in chapter 3 we can therefore conclude that Eq. (2.12) constitutes a pessimistic estimate of the mean free path between ion-ion collisions for a plasma in a single-ended Q-machine.

Reprinted from *Printed in U.S.A.*

THE PHYSICS OF FLUIDS VOLUME 14, NUMBER 3 MARCH 1971

3. Determination and Shaping of the Ion-Velocity Distribution Function in a Single-Ended *Q* Machine

S. A. ANDERSEN, V. O. JENSEN, P. MICHELSEN, AND P. NIELSEN*
Danish Atomic Energy Commission, Research Establishment Risø, Roskilde, Denmark
(Received 13 March 1970; final manuscript received 2 July 1970)

An electrostatic energy analyzer with a resolution better than 0.03 eV was constructed. This analyzer was used to determine the ion-velocity distribution function at different densities and plate temperatures in a single-ended *Q* machine. In all regions good agreement with theoretical predictions based on simple, physical pictures is obtained. It is shown that within certain limits the velocity distribution function can be shaped; double-humped distribution functions have been obtained. The technique used here is suggested as an accurate method for determination of plasma densities within 10% in single-ended *Q* machines.

I. INTRODUCTION

In recent years many experiments have been performed in order to study the propagation properties of density perturbations in single-ended *Q* machines. The phase velocity and damping characteristics of grid-excited, ion-acoustic waves have been examined by Doucet and Gresillon[1] and by Sato *et al.*[2] Reports of work on ion-wave echoes in single-ended *Q* machines have been published by Ikezi *et al.*[3] and by Baker *et al.*[4] Finally, the propagation of short density pulses has been studied by Andersen *et al.*[5,6] All the experiments mentioned above were performed in order to test theoretical predictions based on the linearized, collisionless Boltzmann equation. The density perturbations studied in these experiments were generated by a grid placed in the plasma column. In order to make quantitative comparisons between the experimental results and the theoretical predictions it is essential to know the undisturbed ion-velocity distribution function, $f(v)$, and the initial velocity distribution of the ions in the perturbation. The latter point has been stressed very clearly by Hirschfield and Jacob,[7] and experiments performed in order to determine the velocity distribution function in the perturbation have been reported by Andersen *et al.*,[8] and more recently by Ikezi and Taylor.[9] A few measurements of the undisturbed distribution function in plasmas in single-ended *Q* machines have also been reported.[8,10]

In this paper we describe a rather accurate measurement of $f(v)$ as a function of plasma density, temperature of the hot Ta plate, and distance from the Ta plate. The method used to determine $f(v)$ further allows us to measure the plasma potential as a function of the parameters mentioned above. In this paper we also demonstrate that we can shape $f(v)$ within certain limits; e.g., we can construct a double-humped distribution function which appears to be interesting for the study of Landau growth. As a by-product of our work we obtained a fairly accurate method of determination of the plasma density.

II. EXPERIMENTAL SET-UP

A schematic drawing of the single-ended *Q* device used in this experiment is shown in Fig. 1. The plasma is produced by surface ionization of a beam of cesium atoms from oven A on the hot tantalum plate ($\sim$ 2500°K) and is confined radially by a uniform, axial magnetic field of intensity up to 10 000 G. The plasma column is 3 cm in diameter and up to 1.2 m long; in the experiments to be described in this paper it ends at an ion-energy analyzer movable along the axis. A copper tube 5 cm in diameter and 15 cm long is placed round the plasma near the hot tantalum plate. This tube is connected with Cs oven B and indirectly heated from the hot plate and provides a spatially limited region with high neutral Cs pressure in the plasma column. In the work of Andersen[11] this tube was used for differential cooling of the plasma ions. A third Cs oven, C, is placed at the far end of the column. By means of this oven we can obtain a cloud of neutral Cs far away from the hot plate. The vacuum system, consisting of a stainless-steel tube (not shown in Fig. 1), is cooled to −20°C in order to reduce the Cs background pressure. In operation the vacuum system is pumped down to below 10^{-6} Torr.

A detailed drawing of the analyzer is shown in Fig. 2. This analyzer closely resembles the one described by Buzzi *et al.*[10] It consists of a brass housing 38 mm long and 22 mm in diameter. A hole 8 mm in diameter in one end of the housing is covered by a copper mesh, 35 μm thick and with

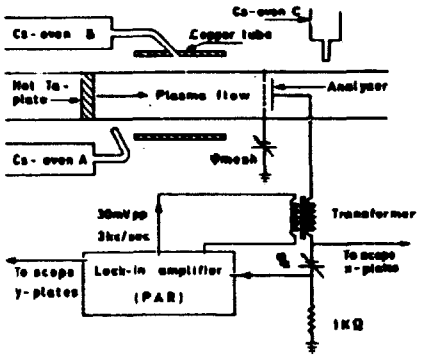

FIG. 1. Schematics of the experimental set-up.

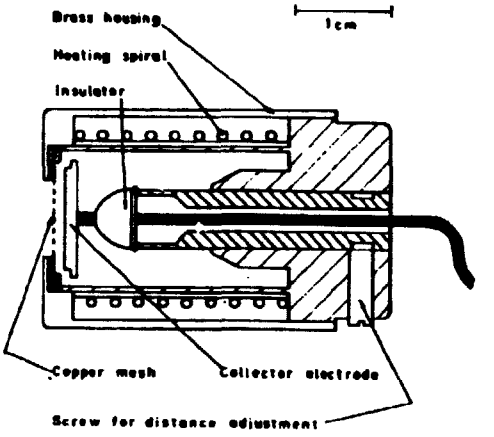

FIG. 2. Detailed drawing of the electrostatic analyzer.

40 000 25 μm × 25 μm holes per cm^2. A collector electrode is placed at a variable distance d (up to 1.2 mm) behind the mesh. In order to avoid cesium condensation on the mesh–collector system the analyzer can be heated electrically to about 500°C by a heating spiral.

In operation the analyzer is placed in the plasma as indicated in Fig. 1. The mesh and the whole housing is biased negatively (−6 to −10 V) with respect to the earth in order to reflect the electrons. The distribution of ion energies parallel to the magnetic field lines is determined by measurement of the current–voltage characteristic of the collector plate. If we assume that the analyzer resolution function is very narrow, then the ion current to the collector plate as a function of collector voltage, φ_c, is given by

$$I(\varphi_c) = enA \int_{v_{min}}^{\infty} vf(v)\, dv, \qquad (1)$$

where A is the effective mesh area, n is the ion density, and $f(v)$ is the ion-velocity distribution function. The minimum velocity, v_{min}, accepted by the collector is given by $\frac{1}{2}mv_{min}^2 = e(\varphi_c - \varphi_{pl})$, φ_{pl} being the plasma potential and m the ion mass. By differentiation of (1) with respect to φ_c we get

$$\frac{dI(\varphi_c)}{d\varphi_c} \begin{cases} \propto f\left[v = \left(\frac{2e(\varphi_c - \varphi_{pl})}{m}\right)^{1/2}\right] & \text{for } \varphi_c \geq \varphi_{pl}, \\ = 0 & \text{for } \varphi_c < \varphi_{pl}. \end{cases} \qquad (2)$$

Thus, we get

$$f\left[v = \left(\frac{2e(\varphi_c - \varphi_{pl})}{m}\right)^{1/2}\right]$$

directly by differentiation of the collector current–voltage characteristic with respect to φ_c.

The electrical circuit shown schematically in Fig. 1 is arranged to show this differentiated characteristic on a scope. Through the transformer a 3 kc/sec 0.03 V peak-to-peak voltage from the generator in the Princeton Applied Research lock-in amplifier is added to the collector dc voltage, φ_c. The ac current to the collector is measured by its corresponding voltage drop across the 1 kΩ resistor. The part of this voltage which is in-phase with the transformer voltage is proportional to $dI(\varphi_c)/d\varphi_c$. (The out-of-phase part is determined by the capacity and self-induction in the circuit.) The lock-in amplifier is adjusted to measure the in-phase part, which is displayed on the scope as a function of φ_c. Thus, the scope simply displays $dI(\varphi_c)/d\varphi_c$ as a function of φ_c.

A calculation of the width of the analyzer resolution function is very complicated. Longitudinal energy loss or gain by deflection of the ion orbits in the holes in the mesh will widen the resolution function, so will changes in the collector work function over the surface. Such changes might be caused by inhomogeneities in the collector material or by variation in the thickness of the Cs layer covering the collector. Also instabilities in the space charge layer round the mesh might broaden the resolution function. We obtained an upper limit for the width of the resolution function experimentally. Figure 3 shows an example of a differentiated characteristic obtained by means of the technique described above at a rather low density ($n \approx 10^9$ cm^{-3}) and with Cs oven B heated. As will be discussed below, the distribution function of the plasma generated on the Ta plate at this low density is close to a truncated Maxwellian with a minimum velocity given by $\frac{1}{2}mv_{min}^2 = e(\varphi_{bp} - \varphi_{pl}) = e\varphi_0$. This truncated Maxwellian corresponds to the wide right-hand peak in Fig. 3. When the ions pass the neutral Cs cloud in

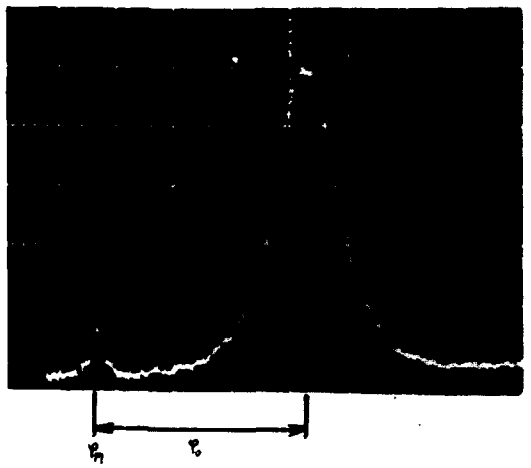

FIG. 3. Typical example of differentiated analyzer characteristic

$$f\left[v = \left[\frac{2e(\varphi_a - \varphi_{pl})}{m}\right]^{1/2}\right].$$

Sweep 0.5 V/large div. Analyzer positioned at $x = 26$ cm, Ta plate at $x = 0$. $n \approx 10^9$ cm^{-3}.

the copper tube, some of them will undergo charge exchange and leave cold (tube temperature $\sim$500°K) ions behind. These ions are formed in a region with plasma potential and are therefore accepted by the analyzer when φ_a is close to and a little above φ_{pl}. The narrow left-hand peak in Fig. 3 corresponds to the contribution from these cold ions. From the positive slope of this peak, which theoretically should be vertical, we can get an upper limit for the width of the analyzer resolution function. The width has been measured at different densities and temperatures and always found to be less than 0.03 eV. The width of the curves of the form (2) measured in this experiment is typically around 2–3 V; therefore, it is justifiable to neglect the influence of a finite width of the resolution function in writing (1).

To find $f(v)$ from (2) and curves like the one shown in Fig. 3, one has to know φ_{pl}. As already mentioned, the cold charge exchange ions are formed in a region with plasma potential. Therefore, the position of the left-hand side of the narrow peak on curves like the one in Fig. 3 determines φ_{pl}.

At high densities the width of the resolution function will increase owing to space-charge-limited current. An upper pessimistic limit for the allowed collector current density is given by Child's law

$$I_{max} = \frac{2}{9}\epsilon_0\left(\frac{2e}{m}\right)^{1/2} d^{-2}(\varphi_a - \varphi_{mesh})^{3/2}. \qquad (3)$$

In the experiments, $\varphi_a - \varphi_{mesh}$ was around 5 V, and the distance d between mesh and collector was around 0.1 mm; so the maximum allowed current density is calculated to be $I_{max} \approx 0.1$ mA/cm^2. In all our experiments the collector current density was kept below this value, and no sign of space charge limitation was seen.

In all experiments the plasma column ended at the analyzer housing, which was kept on a negative voltage in order to reflect all electrons. Thus, the electron cloud in thermal contact only with the hot tantalum plate will take on a temperature, T_e, equal to the temperature, T_{hp}, of the hot plate.

All the measurements to be reported in this paper were performed with B fields around 8000 G. Variation of the magnetic field had little influence on the results.

III. RESULTS OF MEASUREMENTS

By means of the technique just described the ion-velocity distribution function was measured at various plate temperatures and ion densities. The presentation of the results is divided into three parts: low-density region, medium-density region, and high-density region.

A. Low-Density Region ($n \lesssim 10^9$ cm^{-3})

This region is characterized by ion-ion mean free paths long compared with the length of the machine. The distribution function, therefore, does not change appreciably along the plasma column. As already pointed out[10,12] in this case one would expect the ion distribution function to be a truncated Maxwellian with a minimum velocity corresponding to the potential drop, $\varphi_0 (= \varphi_{hp} - \varphi_{pl})$, at the tantalum plate.

In normalized form a truncated Maxwellian is written

$$f(v) = \begin{cases} \left(\frac{2m}{\pi T_e}\right)^{1/2} \frac{1}{1 - \mathrm{erf}\,(e\varphi_0/T_e)^{1/2}} \exp\left(-\frac{mv^2}{2T_e}\right) \\ \qquad\qquad \text{for } v \geq \left(\frac{2e\varphi_0}{m}\right)^{1/2}, \qquad (4) \\ 0 \qquad\qquad \text{for } v < \left(\frac{2e\varphi_0}{m}\right)^{1/2}. \end{cases}$$

Throughout this paper temperatures are measured in energy units.

In Fig. 3 a typical picture of the differentiated analyzer characteristic (2) is shown. As already mentioned, the main peak corresponds to the contribution of the main plasma, while the small left-hand peak is made up of ions formed by charge exchange in the neutral Cs cloud in the copper tube. In this series of experiments the Cs oven B was

only slightly heated so that only a few charge exchange ions were formed. The contribution from these ions was only used to determine the plasma potential. As is clearly seen from the picture, and as was also noticed by Buzzi *et al.*,[10] the left-hand wing of the main peak is not upright as would be expected if the distribution function were a truncated Maxwellian. Buzzi *et al.*[10] explain this smoothing out as being caused by zero relative velocity Coulomb collisions. Experimentally, we have found that the shape of the left wing in this low-density region is nearly independent of distance between the Ta plate and the analyzer and of the density. We would therefore suggest that the smooth shape is at least in part caused by variation, either in the Ta plate work function or in temperature over the surface. Variation in the work function is to be expected because the Ta plate does not form a single crystal, and it is known that the work function depends on the orientation of the surface with respect to the crystal axis. The variation in plate temperature has been measured by means of a pyrometer to be about 100°C.

We define the effective ion temperature by

$$T' = m \int_{-\infty}^{\infty} (v - v_d)^2 f(v)\, dv, \tag{5}$$

where the drift velocity

$$v_d = \int_{-\infty}^{\infty} v f(v)\, dv.$$

Because of the smooth shape of the experimental curves the effective temperature calculated from these curves will be higher than that calculated from (4).

Photographs like the one shown in Fig. 3 were taken with the analyzer placed at different distances from the hot plate. Inspection of these photographs show that the distribution function becomes slightly wider at long distances, and the noise level increases. The broadening of the distribution function is probably caused by the noise.

With the analyzer 5 cm from the end of the copper tube traces like the one shown in Fig. 3 have been taken. From these we checked the following two expected plasma features.

Although the effective parallel ion temperature decreases as the ion flow is accelerated through the potential drop, φ_0, the plate temperature can be deduced from the negative slope of the main peak on the differentiated characteristics.[10] In semilogarithmic plots the right-hand wings of the curves are linear over one decade. From the slope of these

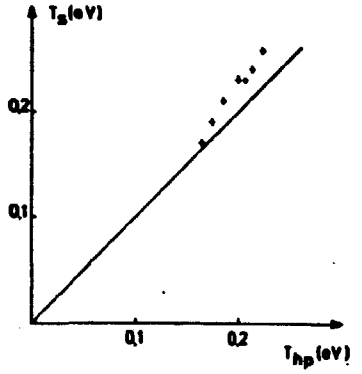

FIG. 4. Plate temperature T_p deduced from the slope of the differentiated characteristics as a function of the plate temperature, T_{hp}.

plots the temperature T_p was deduced. The crosses in Fig. 4 show the results of such measurements as a function of the plate temperature T_{hp}. The straight line shows the expected dependence (slope 45°). The plate temperature was measured by means of a pyrometer. The good agreement in Fig. 4 allows us to conclude that the ions are formed with a parallel temperature equal to that of the hot plate.

From a simple physical picture the variation of φ_0 with plate temperature can be calculated. The Richardson electron emission current density from the hot plate is given by

$$I_R = A\left(\frac{T_{hp}}{\kappa}\right)^2 \exp\left(-\frac{ew}{T_{hp}}\right), \tag{6}$$

where κ is the Boltzmann constant, $A = 120\text{A/cm}^2\,^\circ\text{K}^2$, and w is the plate work function (= 4.1 V). If we assume the electron distribution function to be a Maxwellian, we have the balance equation

$$I_R \exp\left(-\frac{e\varphi_0}{T_{hp}}\right) = \frac{1}{4} en\langle v_e\rangle = en\left(\frac{T_e}{2\pi m_e}\right)^{1/2}, \tag{7}$$

where m_e is the electron mass.

From (6) and (7) and by using $T_{hp} = T_e$ we get

$$\varphi_0 = \frac{T_{hp}}{e} \ln\left(\frac{(2\pi)^{1/2} m_e^{1/2} A T_{hp}^{3/2}}{en\kappa^2}\right) - w. \tag{8}$$

In the experiment the argument of the logarithm is around 10^{12} and only varies by a factor of less than 10. Therefore, the logarithm itself is around 28 and can be considered constant. In Fig. 5, (8) has been verified. The crosses are experimental points obtained by measuring φ_0 on traces like the one in Fig. 3. The straight line has been drawn through $(0, -w)$ and the majority of the experimental points. The slope of the straight line differs from that pre-

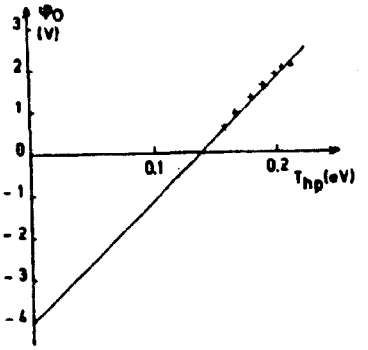

FIG. 5. Potential drop φ_0 at the hot plate as a function of plate temperature. The crosses are the experimental points deduced from traces like the one shown in Fig. 3. The full line shows the expected slope given by formula (8). $n \approx 10^8$ cm^{-3}.

dicted by (8) by less than 5%. Similar results were obtained by Buzzi *et al.*[10]

B. Medium-Density Region (10^8 cm^{-3} $\lesssim n \lesssim$ 5×10^9 cm^{-3})

This region is characterized by ion-ion mean free paths comparable to the length of the plasma column. The distribution function is close to a truncated Maxwellian at the hot plate and changes to approach a drifting Maxwellian along the column. This change was studied experimentally by means of the energy analyzer.

The plasma flow is governed by the following three conservation laws:

Mass flow

$$n(x)v_d(x) = c_1; \tag{9}$$

Momentum flow

$$nm\int_{-\infty}^{\infty} v^2 f(v)\,dv + nT_e = c_2; \tag{10}$$

Energy flow

$$\frac{1}{2}nm\int_{-\infty}^{\infty} v^3 f(v)\,dv + nv_dT_\perp + nv_dT_e = c_3. \tag{11}$$

x is the coordinate along the flow and $x = 0$ at the hot plate. $f(v)$ is the normalized velocity distribution function, which is a function of x. $T_\perp(x)$ is the perpendicular ion temperature, which equals T_{ip} at $x = 0$. c_1, c_2, and c_3 are constants along the flow and can be calculated from the conditions near $x = 0$.

In deriving the conservation equations, interactions between electrons and ions caused by Coulomb collisions were neglected, while allowance was made for ion-ion collisions. Also interaction between ions and electrons as a result of all kinds of instabilities was neglected. The electrons are assumed to act on the ion flow only through a static electric field, which, because of quasineutrality, is given by

$$E(x) = -\frac{T_e}{e}\frac{1}{n}\frac{dn}{dx}. \tag{12}$$

Upon introduction of the effective temperature T' given by (5), (9) and (10) combine to give

$$\frac{v_d^2}{T_e/m_i} - \frac{c_2}{c_1}\frac{v_d}{T_e} + 1 + \frac{T'}{T_e} = 0. \tag{13}$$

In a T'-v_d diagram (13) corresponds to a family of parabolas, one for each value of c_2/c_1. c_1 and c_2 were calculated from (9) and (10) on the assumption that $f(v)$ for $x = 0$ is a truncated Maxwellian of the form (4). It is found that c_2/c_1 is only a function of $(e\varphi_0/T_e)^{1/2}$. In Fig. 6 experimentally interesting parts of the parabolas of the form (13) are drawn for five values of $(e\varphi_0/T_e)^{1/2}$.

The curve tm is drawn through points in the diagram calculated from (5) for $f(v)$ as truncated Maxwellians of the form (4). As the plasma flows away from the hot plate, the distribution function approaches a drifting Maxwellian of the form

$$f(v) = \left(\frac{m}{2\pi T}\right)^{1/2}\exp\left(-\frac{m(v-v_d)^2}{2T}\right). \tag{14}$$

By insertion of (14) into (5) and (11) and by the use of (13), points in the diagram have been calculated. The curve dm is drawn through these points. It is interesting to note that in the limit of large $v_d(T_e/m)^{-1/2}$ this curve approaches $T'/T_e = \frac{2}{3}$ asymptotically. The physical explanation of this is as follows: Owing to the large expansion in the sheath at the hot plate the longitudinal temperature drops almost to zero. As the thermal energy in the

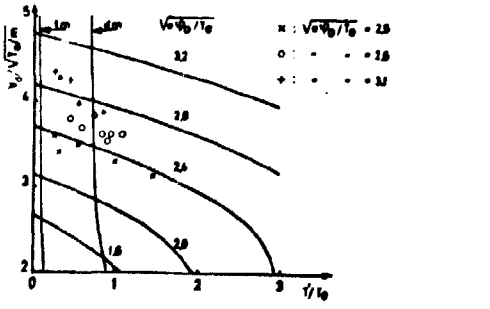

FIG. 6. Diagram showing the evolution along the column of the ion-flow parameters T' and v_d. Full curves (parabolas) show solutions to (13) for different values of $(e\varphi_0/T_e)^{1/2}$. Curves tm and dm represent $[T'/T_e, v_d(T_e/m)^{-1/2}]$ values for truncated Maxwellians and drifting Maxwellians, respectively. Points with the same signature are obtained by moving the analyzer along the column.

two perpendicular degrees of freedom is shared between all three degrees of freedom, the resulting temperature will be ⅔ of the original perpendicular temperature.

In an experiment where density and plate temperature are kept constant, i.e., $e\varphi_0/T_e$ is constant, we would expect to find values of $[T'/T_e, v_d(T_e/m)^{-1/2}]$ near the line tm in Fig. 6 when the analyzer is close to the hot plate where the distribution function is close to a truncated Maxwellian. As the analyzer is moved along the column, the distribution function will eventually change into a drifting Maxwellian. In the diagram we therefore expect to follow a parabola and, when full Maxwellization is obtained, to find points at the line dm.

Experiments were performed for three values of $e\varphi_0/T_e$. From characteristics like the one shown in Fig. 3, T'/T_e and $v_d(T_e/m)^{-1/2}$ were calculated on a digital computer. The value of φ_0 is determined from the characteristics taken nearest to the hot plate in the same way as indicated in Fig. 3. The experimentally obtained values are shown as points in Fig. 6. For each value of $e\varphi_0/T_e$ it is found that the points move in the direction of larger T'/T_e when the analyzer moves away from the hot plate. In the figure we notice that no points are found on the curve tm. This can be explained by the fact that the distribution functions near the hot plate are not truncated Maxwellians, but smooth functions as already discussed in Sec. IIIA. In the same way we can understand that points are found on the right-hand side of line dm. When we start with an effective temperature higher than that of a truncated Maxwellian near the hot plate, there is an excess of thermal energy present in the flow. This will give rise to increased temperature at the point where complete Maxwellization is reached.

We find agreement between theory and experiments in this medium-density region satisfactory. However, it should be pointed out that our measurements do not follow the theoretical calculations so closely as to permit us to exclude that part of the change in the distribution function is caused by instabilities.

C. High-Density Region ($n \gtrsim 5 \times 10^9$ cm^{-3})

This region is characterized by ion–ion mean free paths short compared with the length of the plasma column. The distribution function is, therefore, always very close to a Maxwellian.

In the low- and medium-density regions the plasma potential was determined by means of a few ions formed by charge exchange in the neutral Cs cloud in the copper tube. Such charge-exchange processes are also expected to take place in the neutral Cs cloud formed by oven A in front of the hot plate even when the copper tube and oven B are kept cold or removed. The approximate number of charge-exchange processes occurring in this cloud can be estimated as follows: The flux of neutrals from oven A is given approximately by

$$F_n \approx n_n\left(\frac{2T_{oven}}{m}\right)^{1/2}, \tag{15}$$

where n_n is the neutral density. Similarly, the plasma flux is given by

$$F_{pl} \approx n\left(\frac{2e\varphi_0}{m}\right)^{1/2}. \tag{16}$$

The neutrals from the oven hit the hot plate at an angle of about 45°, and it is known that only about half the neutrals become ionized on the hot plate; therefore, $F_n \approx 3F_{pl}$. By combining (15) and (16) and using $T_{oven} \approx 0.05$ eV and $\varphi_0 \approx 1.3$ V (see Fig. 5) we get $n_n \approx 15n$. The charge-exchange cross sections, σ_{ce}, at low energies have been measured by Dreicer *et al.*[12] to be $\sim 3 \times 10^{-15}$ cm^2. The length L of the neutral cloud is about 10 cm. The probability for an ion to pass through the neutral cloud without undergoing charge exchange is

$$P(n) = \exp(-n_n\sigma_{ce}L)$$

$$\approx \exp(-n/2 \times 10^{15}). \tag{17}$$

It is seen that for plasma densities lower than about 10^{10} cm^{-3} very few ions will undergo charge exchange in the neutral cloud at the hot plate. In the experiments with low and medium densities described in Secs. IIIA and B no sign of such charge exchange was seen. For densities $n \gtrsim 10^{10}$ cm^{-3}, where according to (17) charge-exchange processes are of importance, the mean free path for 90° deflection as a result of Coulomb collisions is short compared with the length of the plasma column ($L_{mfp} \approx 10$ cm at $n = 10^{10}$ cm^{-3}). The distribution function for $n \gtrsim 10^{10}$ cm^{-3} is, therefore, always expected to be a Maxwellian.

The temperature and drift velocity of this resulting distribution function are determined by the following three processes: (a) production and acceleration of primary ions at the surface of the hot Ta plate; (b) production of slow charge exchange ions in the neutral Cs cloud in the vicinity of the Ta plate; and finally (c) Maxwellization through ion–ion collisions within a distance of a few ion–ion mfp from the Ta plate. If only processes (a) and (b) took place, we would expect a double-humped dis-

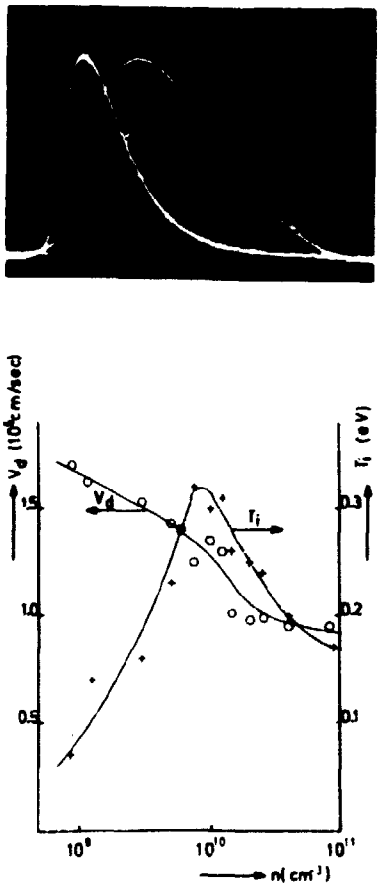

FIG. 7. (a) Examples of distribution functions measured at different densities. a, $n \approx 3 \times 10^9$ cm^{-3}; b, $n \approx 8 \times 10^9$ cm^{-3}; c, $n \approx 3 \times 10^{10}$ cm^{-3}. $T_{k_p} \approx 2400$°K. Analyzer positioned at $x = 62$ cm. Sweep 0.5 V/large div (amplitude gain varied from curve to curve). (b) Experimental values of drift velocity and ion temperature as functions of density.

tribution function similar to that shown in Fig. 3, where charge-exchange ions were produced artificially in the Cs cloud confined in the copper tube. In process (a) the acceleration of the primary ions is determined by the plate temperature and the flux of neutral Cs from oven A. In process (b) the production of slow charge-exchange ions is determined mainly by the Cs flux. We therefore expect the resulting distribution function to depend on the Ta plate temperature and especially on the density. For densities at which the production of charge exchange ions begins to be comparable to the production of primary ions one would expect the drift velocity to decrease; similarly, Maxwellization of the double-humped distribution function will lead to an increase in temperature. At very high densities, at which all ions undergo charge exchange, the distribution function is very narrow, and an ion temperature close to that of the neutral cloud is to be expected.

Experimentally, we have measured the velocity distribution function at different densities and constant plate temperature ($T_{k_p} \approx 0.21$ eV). As we expected, no variation in the distribution function is found when the energy analyzer is moved along the the column. Figure 7(a) shows a few examples of the distribution function (2) taken for different n values. From curves like the ones in Fig. 7(a), the drift velocity v_d and the temperature T_i have been deduced, and the result is shown in Fig. 7(b) as a function of n. We see that the drift velocity decreases with density, and that the temperature reaches a maximum around $n \approx 10^{10}$ cm^{-3}. This is in agreement with the qualitative discussion just given.

IV. SHAPING OF THE DISTRIBUTION FUNCTION

A few attempts to shape the ion velocity distribution function in Q machines have been reported in the literature. Andersen[11] introduced the copper tube shown in Fig. 1 in order to perform differential cooling of the plasma ions by collisions with the neutrals in the Cs cloud. He measured the propagation properties of an ion-acoustic wave launched in the downstream direction and found that the phase velocity and the damping of such a wave decreased with increasing density in the neutral cloud. This was indirect proof of the cooling since Landau's theory predicts that the phase velocity and the damping will decrease with decreasing ion temperature. For a plasma density ($n \sim 1.5 \times 10^9$ cm^{-3}) we have measured the ion velocity distribution on the downstream side of the tube at different neutral densities. The neutral density was varied by simply varying the temperature of Cs oven B. Figure 8 shows three examples; (a) is obtained at a rather low neutral density at which only a small part of the ions formed at the hot plate undergoes charge exchange in the tube. As the neutral density is increased, more charge-exchange processes take place, and distribution functions like the one in (b) are obtained. For very high neutral densities all ions undergo charge exchange, and we are left with a cold plasma with small drift velocities as shown in (c). Note that we are able to produce "double-humped" distribution functions as in (a) and (b). This kind of distribution function appears to be interesting because it should be suitable for the study of Landau growth.

In a few experiments attempts were made to cool the ions in a Q machine simply by introduc-

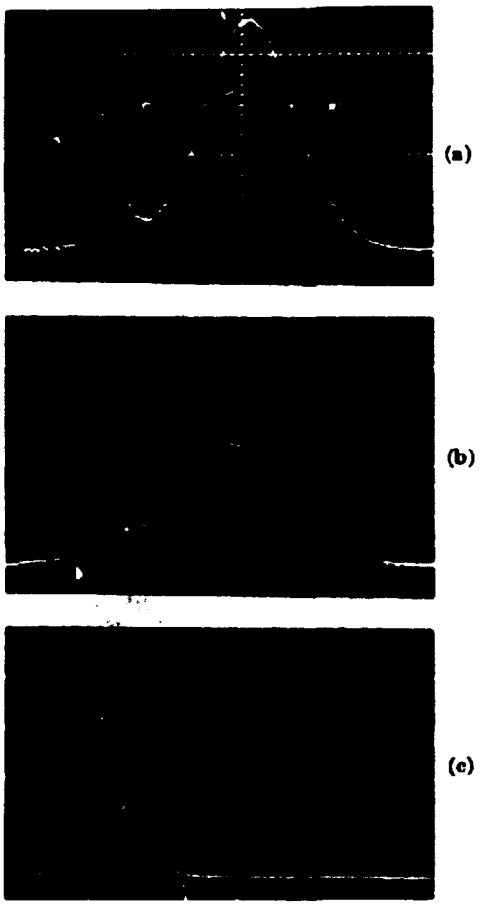

FIG. 8. Examples of distribution functions obtained at different neutral Cs pressures in the copper tube. a, Rather low Cs pressure; b, medium Cs pressure; c, high Cs pressure. $n \approx 1.5 \times 10^8$ cm^{-3}. Analyzer positioned at $x = 26$ cm. Sweep 0.5 V/large div.

ing a rather high pressure of an inert gas into the plasma.[1,14,15] We have examined this method of cooling with the analyzer. Figure 9 shows how the distribution function changes with distance in the case where $n \approx 10^9$ cm^{-3}, and $p_{neutral} = 2 \times 10^{-4}$ Torr of argon. In a similar way Fig. 10 shows the distribution functions obtained at a fixed position at three different argon pressures. We note that this method of cooling gives a distribution function which depends very much on distance from the hot plate and on argon pressure, and which is generally *not* a Maxwellian.

Finally, it should be mentioned that we have used the energy analyzer to check some earlier results obtained with a supersonic plasma wind tunnel.[16] This device is essentially a single-ended Q machine, where the magnetic field is reshaped to form a magnetic Laval nozzle.

FIG. 9. Distribution functions at three positions along the column in partly ionized plasma. a, $x = 26$ cm; b, $x = 56$ cm; c, $x = 106$ cm. Argon background pressure 2×10^{-4} Torr. Plate temperature 2400°K. Sweep 0.5 V/large div. $n \approx 10^9$ cm^{-3}.

The measurements were performed in a plasma that was cooled by charge exchange in the neutral cloud in the copper tube. The "throat" of the nozzle was about 5 cm from the downstream end of the tube shown in Fig. 1. The distribution function was measured with the analyzer placed 80 cm from the nozzle. The plasma potential at this position was determined by means of ions formed by charge exchange in a neutral Cs cloud from oven C (see Fig. 1). The measurements show that Mach numbers [$M = v_i(T_e m)^{-1/2}$] up to 3 and electron–ion temperature ratios, T_e/T_i, up to 4 are easily obtained. These measurements agree with our earlier results.

It should be noted that high Mach numbers ($M \sim 4$) and high temperature ratios ($T_e/T_i \sim 6$) are already present in the single-ended Q machine with a straight magnetic field at low and medium densities. These numbers can be deduced from Fig. 6. In this case the high Mach numbers are

FIG. 10. Distribution functions for three argon background pressures. a, $P_A = 5 \times 10^{-4}$ Torr; b, $P_A = 10^{-4}$ Torr; c, $P_A = 5 \times 10^{-4}$ Torr. Analyzer positioned at $x = 76$ cm. $n \approx 10^9$ cm^{-3}. Plate temperature 2400°K. Sweep 0.5 V/large div.

caused by acceleration through the potential drop, φ_0, at the hot plate.

V. CONCLUSION

In this paper we have described a low-energy electrostatic analyzer suitable for determination of ion velocity distribution functions in single-ended Q machines. The analyzer was used to measure the distribution function at different plate temperatures and densities. The measured functions agree reasonably well with predictions based on simple theoretical pictures.

From a theoretical point of view, knowledge of the distribution function is very important. Especially, all calculations based on the Vlasov equation require accurate knowledge of this function. For instance it is well known that the damping (Landau damping) of longitudinal waves is proportional to $df(v)/dv$ at v = the phase velocity of the wave. A weak point in many wave experiments reported in the literature has been lack of knowledge of the exact shape of the velocity distribution function. As seen from this paper, the distribution function varies greatly with density, plate temperature, and neutral pressure. In order that accurate knowledge of this function may be obtained in future experiments, we therefore suggest that the function be measured directly, for instance by means of a technique like the one described here, rather than deduced from our results.

Accurate measurements of the velocity distribution function as described here also raised the possibility of accurate density measurements. By combination of the velocity distribution function with the total ion flux, which can be determined by measuring the ion current to a negatively biased plate in the column, the density can be deduced. We believe that density measurements correct to within less than 10% can be obtained. Such measurements would seem to be very interesting for the calibration of other methods.

The analyzer described here can also be used for ac measurements, i.e., it also allows us to determine the ion velocity distribution as a function of time in different kinds of wave measurements. This opens the possibility of studying the very interesting concept of wave–particle interaction directly. Some preliminary work of this kind has already been performed.[6]

The "double-humped" distribution function obtained by means of the neutral cloud in the copper tube may make it possible to study Landau growth.

ACKNOWLEDGMENTS

The authors want to thank O. Rasmussen for discussions on the theoretical part of Sec. IIIB. Further, we thank K.-V. Weisberg for help with the electronic equipment, B. Reher for building the analyzer, and he and M. Nielsen for help in maintaining the Q device.

---

* Present address: The University of Texas at Austin, Austin, Texas 78712.

[1] H. J. Doucet and D. Gresillon, in *Plasma Physics and Controlled Nuclear Fusion Research* (International Atomic Energy Agency, Vienna, 1969), Vol. I, p. 659; Phys. Letters, 28A, 257 (1968); Phys. Fluids 13, 773 (1970).

[2] N. Sato, H. Ikezi, Y. Yamashita, and N. Takahashi, Phys. Rev. Letters 20, 837 (1968); N. Sato, H. Ikezi, N. Takahashi, and Y. Yamashita, Phys. Rev. 183, 278 (1969).

[3] H. Ikezi, N. Takahashi, and K. Nishikawa, Phys. Fluids 12, 853 (1969).

[4] D. R. Baker, N. R. Ahern, and A. Y. Wong, Phys. Rev. Letters 20, 318 (1968).

[5] H. K. Andersen, S. A. Andersen, V. O. Jensen, P. Michelsen, and P. Nielsen, in *Proceedings of the International Conference on Physics of Quiescent Plasmas*, Paris (Ecole Polytechnique, Paris, 1969), Vol. I, p. 55.

[6] S. A. Andersen, V. O. Jensen, P. Michelsen, and P. Nielsen, Phys. Letters 32A, 413 (1970).

[7] J. L. Hirshfield and J. H. Jacob, Phys. Fluids 11, 411 (1968).

[8] S. A. Andersen, V. O. Jensen, and P. Nielsen, Phys. Fluids 12, 2694 (1969).

[9] H. Ikezi and R. J. Taylor, Phys. Rev. Letters 22, 923 (1969); J. Appl. Phys. 41, 738 (1970).

[10] I. M. Buzzi, H. J. Doucet, and D. Gresillon, in *Proceedings of the International Conference on Physics of Quiescent Plasmas*, Paris (Ecole Polytechnique, Paris, 1969), Vol. III, p. 149.

[11] S. A. Andersen, Risö Report No. 188, Risö (1969).

[12] A. V. Gurevich, R. A. Salimov, and N. S. Buchel'nikova, Akademiya Nauk SSSR, Novosibirsk, Institut Yadernoi Fiziki, Preprint 208 (1968).

[13] H. Dreicer, D. B. Henderson, D. Mosher, F. E. Wittman, and K. Wolfsberg, in *Proceedings of the International Conference on Physics of Quiescent Plasmas*, Paris (Ecole Polytechnique, Paris, 1969), Vol. III, p. 11.

[14] F. P. Blau, E. Guilino, M. Hashmi, and N. D'Angelo, Phys. Fluids 10, 1116 (1967).

[15] H. K. Andersen, N. D'Angelo, V. O. Jensen, P. Michelsen, and P. Nielsen, Phys. Fluids 11, 1177 (1968).

[16] S. A. Andersen, V. O. Jensen, P. Nielsen, and N. D'Angelo, Phys. Fluids 12, 557 (1969).

THE PHYSICS OF FLUIDS VOLUME 14, NUMBER 5 MAY 1971

4. Measurements of Wave–Particle Interaction in a Single-Ended Q Machine

S. A. ANDERSEN, G. B. CHRISTOFFERSEN, V. O. JENSEN, P. MICHELSEN, AND P. NIELSEN*
Danish Atomic Energy Commission, Research Establishment Risö, Roskilde, Denmark
(Received 10 September 1970; final manuscript received 11 January 1971)

A Green-function technique is used to solve the linearized Vlasov equation for the perturbed ion velocity distribution function, $f(x, v, t)$, in a case where a short density pulse is released into a plasma. Some characteristic features in the calculated curves are caused by wave–particle interaction. Experimentally, short density pulses are generated in the plasma in a single-ended Q machine by application of electrical square pulses to a grid immersed in the plasma column. The perturbed ion velocity distribution function in the density pulse is measured by means of an electrostatic energy analyzer. The features showing the wave–particle interaction appear in the experimental results.

I. INTRODUCTION

The Vlasov equation is the basic tool used in dealing with theoretical problems in collisionless plasmas. For longitudinal disturbances propagating along the magnetic lines of force the equation is

$$\frac{\partial f_{i,e}(x, v, t)}{\partial t} + v \frac{\partial f_{i,e}(x, v, t)}{\partial x} - \frac{e_{i,e}}{m_{i,e}} \frac{\partial \varphi(x, t)}{\partial x} \frac{\partial f_{i,e}(x, v, t)}{\partial v} = 0. \quad (1)$$

All symbols have their normal meaning, and the potential φ is given by Poisson's equation

$$\frac{\partial^2 \varphi}{\partial x^2} = - \sum_{i,e} \frac{e_{i,e}}{\epsilon_0} \int f_{i,e}(x, v, t)\, dv. \quad (2)$$

The first two terms in (1) describe free streaming of noninteracting particles. The last term is the most interesting one as it takes into account the collective interaction between charged particles.

In recent years many experiments have been performed in Q machines in order to test the validity of the Vlasov equation, especially the significance of the last term. From the equation many interesting plasma phenomena can be deduced. Landau[1] damping of longitudinal waves and plasma wave echoes are famous examples of such phenomena which have been studied experimentally. Wong *et al.*[2,3] were the first to measure phase velocity and damping of ion acoustic waves in Q-machine plasmas. The results of their work were consistent with theoretical predictions based on the Vlasov equation; especially, their measurements seemed to confirm the existence of Landau damping. During the last few years many other experiments on phase velocity and damping characteristics of ion-acoustic waves in different Q-machine plasmas have been reported.[4–8]

Another interesting set of experiments performed in order to test the Vlasov equation are these on ion wave echoes. The echo phenomenon was first treated theoretically on the basis of the Vlasov equation by Gould *et al.*[9] and it has been investigated experimentally in Q-machine plasmas by many authors.[10–12]

When the results of the experiments mentioned above were compared with theoretical calculations based on the Vlasov equation, some difficulties arose:

(1) The shape of the undisturbed ion velocity distribution function which makes up part of the Vlasov equation, was not known. In most experiments this function was assumed to be a drifting Maxwellian with a temperature equal to that of the hot plate. In a recent work[13] we showed that this is generally not correct.

(2) In the above-mentioned experiments, the waves were generated by superimposing a small oscillating voltage on a negatively biased grid in the plasma. The detailed mechanism by which the grid perturbs the plasma and generates the wave has not been studied. It is very important to know the velocity distribution function of the perturbation at the grid because this function is also part of the solution to the Vlasov equation.[14]

(3) The density amplitudes of the waves in the experiments mentioned above were measured by means of the ion saturation current to Langmuir probes. The current to such probes is only a good measure for the density if the velocity distribution function is known.

Furthermore, some investigators have recently expressed doubt that the mentioned wave experiments do show collective interaction. Hirschfield and Jacob[15] showed that if the collective interaction contained in the Vlasov equation is neglected, then the phase mixing of the freely streaming ions in the density perturbation induced by the grid may result in a wave damping very similar to Landau damping. Similarly, the occurrence of ion wave echoes may also be explained physically by means of freely streaming particles only.[11,16]

It is, therefore, still of interest to perform detailed experiments whose results unambiguously show the effect of the last term in the Vlasov equation. In this paper we describe an experiment that clearly demonstrates the collective interaction predicted by the Vlasov equation. The Risö Q machine was operated single-ended with a grid at the floating potential immersed in the plasma column. Short, negatively going electrical pulses were applied to the grid, which thereby induces small density perturbations that propagate into the downstream plasma. The interaction between

these density pulses and ions with different velocities was measured by means of an electrostatic analyzer.[13] The problem is treated theoretically on the basis of the linearized Vlasov equation. Good agreement between the calculations and the experimental results is obtained. A characteristic feature seen in the experimental results as well as in the calculations clearly demonstrates the collective interaction. Preliminary results of this kind of measurement have been reported elsewhere.[17] In Ref. 17 a simplified physical picture of the interaction expected to take place is also given.

The above-mentioned difficulties encountered in wave and echo measurements were avoided in these experiments. The velocity distribution function of the undisturbed plasma and that of the density perturbations were measured with the electrostatic energy analyzer.[13] The analyzer was also used to measure accurately the density in the perturbations as a function of time and distance from the grid. Measurements were made at different velocity distribution functions of the main plasma obtainable in Q machines.[18]

In Sec. II of this paper we give the theoretical calculations. The experimental set-up is described in Sec. III and the results of the measurements are given in Sec. IV. The conclusions and discussion are found in Sec. V.

II. THEORY

In this section we present a calculation of the propagation properties of a short density pulse through a plasma with known ion velocity distribution function. Most of the work described in this section has been reported in more detail elsewhere.[18,19]

The experimental situation is as follows: The plasma is generated at the hot plate of a single-ended Q machine. It flows from the hot plate along a constant magnetic field through a biased grid at $x=0$. At grid potential φ_0 the one-dimensional ion velocity distribution function for the downstream plasma is $f_0(v)$, and at grid potential $\varphi_0+\Delta\varphi$ the velocity distribution function is $f_0(v)+g(v)$. The flux of ions with velocity v passing the grid when it is biased to φ_0 is, therefore, $vf_0(v)$, and when the grid is biased to $\varphi_0+\Delta\varphi$ the flux is $v[f_0(v)+g(v)]$. In the experiment the grid is kept at φ_0, but during short pulses, Δt, changed to $\varphi_0+\Delta\varphi$. During these pulses the flux of ions with velocity v passing the grid is therefore changed by $vg(v)$. In the experiments to be reported here $g(v)$ is small compared with $f_0(v)$. Therefore, we can solve the problem by using the linearized Vlasov equation. In the calculation we assume the electrons to behave as an isothermal fluid. Further, we shall assume that quasineutrality prevails at all times. With these assumptions the linearized Vlasov equation (1) and Poisson's equation (2) are reduced to

$$\frac{\partial f(x,v,t)}{\partial t}+v\frac{\partial f(x,v,t)}{\partial x}=c_s^2\frac{df_0(v)}{dv}\frac{\partial n(x,t)}{\partial x}, \quad (3)$$

where $f(x, v, t)$ is the perturbed ion distribution function, $n(x, t)$ is the relative density perturbation, $f_0(v)$ is the normalized zero-order velocity distribution, and $c_s^2=\kappa T_e/m_i$. A detailed discussion of the validity range for Eq. (3) is given by Mason.[20]

The short pulse, Δt, applied to the grid allows us to treat the problem as an initial-value problem with the initial condition

$$f(x,v,t=0)=\Delta t v g(v)\delta(x). \quad (4)$$

We can thus solve Eq. (3) by applying a Laplace transformation in time and Fourier transformation in space. Doing this we get the well-known result

$$n(k,\omega)=-\frac{\Delta t}{ik}\left(\int_{-\infty}^{\infty}\frac{vg(v)}{(\omega/k)-v}dv\Big/1+c_s^2\int_{-\infty}^{\infty}\frac{df_0(v)/dv}{(\omega/k)-v}dv\right)$$
$$=-\frac{\Delta t}{ik}H\left(\frac{\omega}{k}\right). \quad (5)$$

The usual way of solving Eq. (5) is to find the fundamental mode. As shown by Gould[14] there are certain shortcomings in the simple approach. We will use a more rigorous solution.

Instead of finding the inverse Laplace transform from (5) we follow the procedure used by Mason[20] and calculate

$$n(x,\omega)=\int_{-\infty}^{\infty}\frac{dk}{2\pi}n(k,\omega)\exp(ikx). \quad (6)$$

ω in (5) and (6) is a complex number with a positive imaginary part, given by the proper path of integration in the inverse Laplace transform. For $k<0$ the imaginary part of ω/k is negative, and the integration path along the real v axis runs above the pole at $v=\omega/k$. Similarly for $k>0$, where $\mathrm{Im}\,\omega/k>0$, the path of integration runs below the pole at $v=\omega/k$. We therefore split (6) up into two parts

$$n(x,\omega)=\int_{-\infty}^{0}\frac{dk}{2\pi}n_1(k,\omega)\exp(ikx)$$
$$+\int_{0}^{\infty}\frac{dk}{2\pi}n_2(k,\omega)\exp(ikx), \quad (7)$$

where

$$n_{1,2}(k,\omega)=-\frac{\Delta t}{ik}\left(\int_{1,2}\frac{vg(v)}{(\omega/k)-v}dv\Big/1+c_s^2\int_{1,2}\frac{df_0(v)/dv}{(\omega/k)-v}dv\right). \quad (8)$$

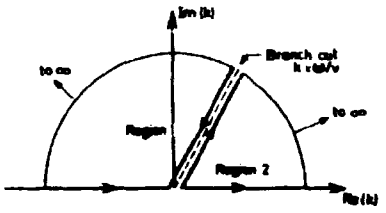

FIG. 1. Fourier inversion contour along branch cut.

The symbol $\int_1$ means that the integration path runs above the pole and $\int_2$ that it runs below.

$n_1(k, \omega)$ is defined for k values to the left of the line $k=\omega/v$ (v real) in the complex k plane shown as region 1 in Fig. 1. In this half-plane the numerator and the denominator in (8) are analytic functions. $n_2(k, \omega)$ is defined in region 2 to the right of $k=\omega/v$, and its numerator and denominator are analytic functions. Thus, n_1 and n_2 are analytic functions in their respective regions of definition except for possible k values for which their denominators equal zero.

The denominator in n_2 is the classical dielectric function for the plasma. A simple Nyquist analysis as performed, for instance, by Jackson[21] shows that for "well-behaved" distribution functions the dielectric function has no zeros for k values in the half-plane where $n_2(k, \omega)$ is defined. A similar Nyquist analysis of the denominator in $n_1(k, \omega)$ which makes use of the fact that

$$\int_1 \frac{h(v)}{x-v}\,dv=\left(\int_2 \frac{h(v)}{x-v}\,dv\right)^* \quad \text{for } x \text{ real},$$

shows that this denominator has no zeros in the half-plane where n_1 is defined. "Well-behaved" distribution functions in the sense used here are functions that have only a stable or damped solution to a normal Landau[1] treatment of wave propagation. Although unstable, not "well-behaved" functions can be produced in Q machines,[12,22] in this paper we shall restrict ourselves to treating "well-behaved" ones.

Because $n_1(k, \omega)$ is analytic to the left of the branch cut $k=\omega/v$ in Fig. 1, and $n_2(k, \omega)$ is analytic to the right of this cut, we can change the integration paths to run close to the cut as indicated in the figure. By introducing $k=\omega/v$ into (7) and (5) for $x>0$ we get

$$n(x, \omega) = \frac{\Delta t}{2\pi i}\int_0^\infty v^{-1}[H_1(v)-H_2(v)]\exp\left(\frac{i\omega x}{v}\right)dv. \quad (9)$$

The inverse Laplace transformation of $n(x, \omega)$ is easily performed. We get

$$n(x, t) = \frac{\Delta t}{2\pi i}\int_0^\infty v^{-1}[H_1(v)-H_2(v)]\beta\left(t-\frac{x}{v}\right)dv, \quad (10)$$

which may be integrated to give

$$n(x, t) = \frac{\Delta t}{2\pi i}\,t^{-1}\left[H_1\left(\frac{x}{t}\right)-H_2\left(\frac{x}{t}\right)\right] \quad (11)$$

or

$$n(x, t) = \frac{\Delta t}{\pi}\,t^{-1}\,\mathrm{Im}H_1\left(\frac{x}{t}\right)=\frac{\Delta t}{t}\,h\left(\frac{x}{t}\right). \quad (12)$$

In the last step we have used the already mentioned fact that $H_2(v)=H_1^*(v)$. From (12) we notice that the solution to $n(x, t)$ is of a self-similar type, a characteristic which may already be observed from Eq. (3).[23]

Instead of just knowing $n(x, t)$ it is more interesting to know the perturbed velocity distribution function $f(x, v, t)$, which can be measured by modern techniques.[17,24] To obtain $f(x, v, t)$ we integrate (3) over unperturbed orbits and obtain

$$f(x, v, t)=f(x', v, t'=0)+\int_0^t dt' c_s^2\,\frac{df_0(v)}{dv}\,\frac{\partial n(x', t')}{\partial x'}, \quad (13)$$

where x' and t' are related to x and t through $x'-x=v(t'-t)$. If we insert the density given by (12) and the initial condition given by (4), (13) yields

$$f(x, v, t)=\Delta t v g(v)\delta(x-vt)+\frac{\Delta t}{t}\,c_s^2\,\frac{df_0(v)}{dv}\,\frac{h(x/t)}{v-(x/t)}. \quad (14)$$

For this equation to be self-consistent we must require that

$$\int_{-\infty}^{\infty} f(x, v, t)\,dv=\frac{\Delta t}{t}\,h\left(\frac{x}{t}\right). \quad (15)$$

In order to satisfy this relation we must prescribe how to integrate over the singularity of the second term in (14). This we have done by replacing $vg(v)$ by some arbitrary function, $\lambda(v)$, and taking the principal value of the second term. $\lambda(v)$ is determined by solving (15). We then obtain as the final results

$$f(x, v, t)=\Delta t\lambda(v)\delta(x-vt)+\frac{\Delta t}{t}\,c_s^2 h\left(\frac{x}{t}\right)P\left(\frac{df_0(v)/dv}{v-(x/t)}\right), \quad (16)$$

where

$$\lambda\left(\frac{x}{t}\right)=h\left(\frac{x}{t}\right)\left(1-c_s^2 P\int_{-\infty}^{\infty}\frac{df_0(v)/dv}{v-(x/t)}\,dv\right). \quad (17)$$

Experimentally, $f(x, v, t)$ is measured with an electrostatic analyzer[18,17] with a finite resolution. The signal, $S_{v_a}(x, t)$, which we may obtain on the analyzer when it is adjusted to measuring at a velocity, v_a, is thus given by

$$S_{v_a}(x, t)=v_a^{-1}\int_0^\infty vf(x, v, t)\,T(v, v_a)\,dv, \quad (18)$$

where $T(v, v_a)$ is a transfer function taking into ac-

count the finite resolution of the experimental set-up. In the numerical calculations we have assumed this transfer function to be a Gaussian in v, i.e.,

$$T(v, v_a) \propto \exp\left[-\left(\frac{v-v_a}{v_r}\right)^2\right]. \qquad (19)$$

Equation (18) shows that we must insure a sufficiently narrow resolution, v_r, of the analyzer to prevent the second term of (16) from becoming embedded in the Gaussian term originating from the δ function.

Figure 2 shows the computed results for a situation where $f_0(v)$ is a drifting Maxwellian of the form

$$f_0(v) \propto \exp[-(v-v_{d0}/c_i)^2], \qquad (20)$$

and $g(v)$ a truncated, displaced Maxwellian of the form

$$g(v) \propto \exp[-(v-v_{d1}/c_i)^2] \quad \text{for } v \geq 0,$$
$$= 0 \quad \text{for } v<0, \qquad (21)$$

where $c_i^2 = 2\kappa T_i/m_i$.

In the special cases shown in Fig. 2 $T_i = T_e$, $v_r = \frac{1}{4}c_i$, $g(v)>0$ for $v>0$. In Fig. 2(a) $m_0 = v_{d0}/c_i = 1$ and $m_1 = v_{d1}/c_i = 1$, in Fig. 2(b) $m_0 = 0.5$ and $m_1 = 1.0$, and in Fig. 2(c) $m_0 = 1.0$ and $m_1 = 0.5$. The full curves shown in the figures represent the ion flux

$$\left(\int_0^\infty v f(v)\, dv\right)$$

or the ion-saturation current measured on a plate immersed perpendicularly to the plasma column. The four curves 1–4 represent S_{v_a} curves to be expected at four different v_a values.

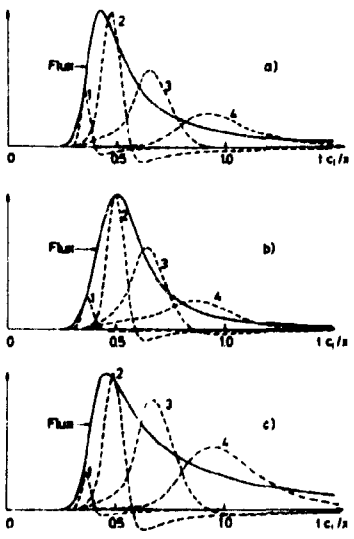

FIG. 2. Examples of calculated S_{v_a} and flux curves. (a) $m_0 = 1$, $m_1 = 1$; (b) $m_0 = 0.5$, $m_1 = 1$; (c) $m_0 = 1$, $m_1 = 0.5$. In all three cases $T_i = T_e$, $v_r = \frac{1}{4}c_i$. The full curves represent the flux. Curves 1–4 are S_{v_a} curves. For (1) $v_a = 8^{1/2}c_i$. For (2) $v_a = 2c_i$. For (3) $v_a = 2^{1/2}c_i$. For (4) $v_a = c_i$.

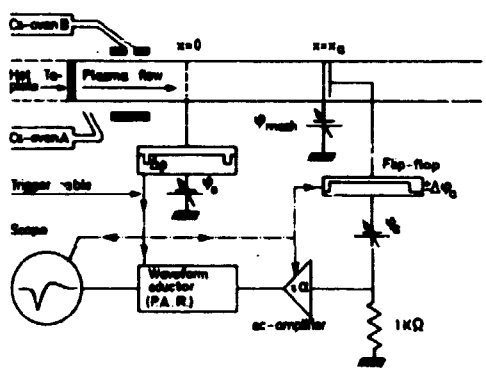

FIG. 3. Experimental set-up used for S_{v_a} measurements.

For experimental verification of wave–particle interaction the second term in (16) offers a very good opportunity. This term does not exist for a free-streaming situation ($T_e = 0$). It appears from curves 1 and 2 in Fig. 2 that a resolution of $v_r = \frac{1}{4}c_i$ is sufficiently good to reveal the undershoot originating from the wave–particle interaction.

A computer program has been developed that calculates curves such as the ones in Fig. 2 for $f_0(v)$ and $g(v)$ as drifting Maxwellians of the types (20) and (21). Input parameters that can be changed are T_e/T_i, m_0, m_1, and v_r.

III. EXPERIMENTAL SET-UP

A schematic drawing of the single-ended Q device used in this experiment is shown in Fig. 3. The plasma is produced by surface ionization of a beam of cesium atoms from Cs oven A on the hot tantalum plate (~2500°K.) and is confined radially by a uniform, axial, magnetic field of an intensity up to 1 T. The plasma column is 3 cm in diameter, and in the experiments to be described in this paper it ends at an ion-energy analyzer. A short copper tube, 5 cm in diameter, is placed around the plasma near the hot tantalum plate. This tube is connected with Cs oven B and indirectly heated from the hot plate and provides a spatially limited region with high neutral Cs pressure in the plasma column. The vacuum system consists of a stainless-steel tube (not shown in Fig. 3) which is cooled to −20°C in order to reduce the Cs background pressure. In operation the pressure is below 10^{-6} Torr.

The plasma perturbations studied in this paper were induced by a grid placed in the column at $x = 0$, 30 cm from the hot plate. The grid consists of a thin nickel mesh with 400 0.5×0.5 mm holes per cm². The optical transparency of the mesh is about 90%.

The ion velocity distribution function is measured

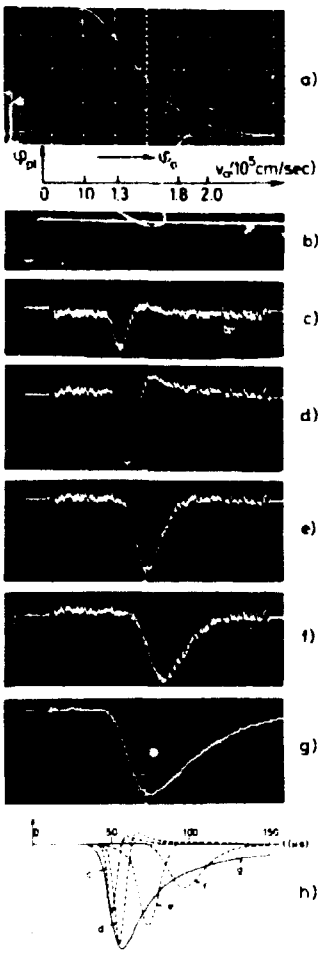

FIG. 4. (a) $f_0[v=(2e(\varphi_a-\varphi_{pl})/m_i)^{1/2}]$. 0.5 V large division. $n\approx 8\times10^8$ cm^{-3}. (b) Δt pulse applied to grid. 5 V/large division. (c–f) Measured $I(x_a, v_a, t)$ curves in arbitrary units. (c) $v_a=2.0\times10^5$ cm sec^{-1}. (d) $v_a=1.8\times10^5$; (e) $v_a=1.3\times10^5$, (f) $v_a=1.0\times10^5$; $x_a=10$ cm. (g) Measured total flux. (b)–(g) 20 μsec large division. (h) Calculated results. The letters on the curves correspond to experimental curves c–g.

with an electrostatic analyzer[13] placed at $x=x_a$. The analyzer consists of a fine copper mesh behind which a collector plate is placed. The mesh potential, φ_{mesh}, is negative with respect to the plasma potential, φ_{pl}, in order to reflect the electrons. The distribution of ion velocities parallel to the magnetic field lines is determined by measurement of the current voltage characteristic of the collector plate. As a function of the collector potential, φ_a, the collector current is given by

$$I(\varphi_a)=en_0A\int_{v_{min}}^{\infty} vf(v)\,dv, \qquad (22)$$

where A is the effective mesh area, n_0 is the ion density, and $f(v)$ is the ion velocity distribution function. The minimum velocity, v_{min}, accepted by the collector is given by $\frac{1}{2}mv_{min}^2=e(\varphi_a-\varphi_{pl})$.

When the analyzer was used for determination of the time-independent velocity distribution function $f_0(v)$ (see Sec. II), it was coupled to an electric circuit as described in Ref. 13. The circuit differentiates (22) with respect to φ_a and can thus display

$$f_0\left[v=\left(\frac{2e(\varphi_a-\varphi_{pl})}{m_i}\right)^{1/2}\right]$$

directly on a scope as a function of φ_a. In order to calculate $f_0(v)$ from oscilloscope trace, φ_{pl} has to be known.

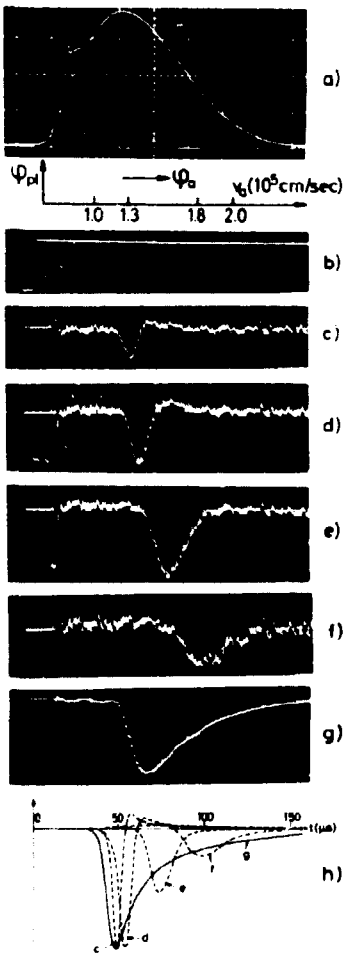

FIG. 5. (a) $f_0[v=(2e(\varphi_a-\varphi_{pl})/m_i)^{1/2}]$. 0.5 V/large division; $n\approx4\times10^8$ cm^{-3}. (b) Δt pulse applied to grid. 2 V/large division. (c)–(f) Measured $I(x_a, v_a, t)$ curves in arbitrary units. (c) $v_a=2.0\times10^5$ cm sec^{-1}. (d) $v_a=1.8\times10^5$. (e) $v_a=1.3\times10^5$. (f) $v_a=1.0\times10^5$. $x_a=10$ cm. (The curve in f is amplified by a factor of 2 with respect to curves c through e.) (g) Measured total flux. (b)–(g) 20 μsec/large division. (h) Calculated results. The letters on the curves correspond to experimental curves c–g.

In the present work we have used the same technique as in Ref. 13 for determination of φ_{pl}.

The experimental procedure is as follows: First, the undisturbed ion velocity distribution in which the experiment is to be performed is obtained by adjustment of the temperature of the hot plate and of Cs oven A.[13] The grid potential, φ_0, is chosen equal to the floating potential, and the velocity distribution function $f_0(v)$ is measured by means of the technique mentioned above (recordings in Figs. 4–6). The grid potential is then changed to $\varphi_0+\Delta\varphi(\Delta\varphi<0)$, and the corresponding velocity distribution function, $f_0(v)+g(v)$, is measured. The function $g(v)$ can now be obtained by subtraction of the first curve from the last one.

Now, the grid is connected to a pulse generator as shown in Fig. 3. The grid potential is φ_0, but during short time intervals, Δt, it is changed to $\varphi_0+\Delta\varphi$ whereby density perturbations are released. The velocity distribution function, $f(x, v, t)$, of the particles in the perturbations is measured by means of the analyzer which is now coupled to the circuit shown in Fig. 3. This circuit is designed in such a way that for a chosen velocity, v_a, the perturbed velocity distribution function, $f(x_a, v_a, t)$, is displayed on an oscilloscope as a function of time. v_a is related to φ_a through

$$v_a=[2e(\varphi_a-\varphi_{pl})/m_i]^{1/2}. \tag{23}$$

In detail the circuit works as follows: The generator runs continuously, applying the Δt pulses to the grid at a frequency of about 1 kc/sec. Each time a Δt pulse is applied, a flip-flop is triggered. The flip-flop adds or subtracts a small voltage, $\Delta\varphi_a(\approx 0.05$ V), to the plate potential, φ_a. Consider a case where the flip-flop is in the $+\Delta\varphi_a$ position after a pulse is released. The current to the analyzer plate is given by

$$I_+(t)=enA\int_{v_{min+}}^{\infty} vf(v, t)\,dv. \tag{24}$$

This current is measured by its voltage drop over the 1-kΩ resistor. This voltage signal is amplified by a factor $-\alpha$ by the ac amplifier and sent to the Princeton Applied Research waveform eductor. When the next Δt pulse is released, the flip-flop is triggered to the $-\Delta\varphi_a$ position and the amplifier to the $+\alpha$ position. The current to the plate is now given by

$$I_-(t)=enA\int_{v_{min-}}^{\infty} vf(v, t)\,dv. \tag{25}$$

In (24) and (25)

$$v_{min\pm}=[2e(\varphi_a\pm\Delta\varphi_a-\varphi_{pl})/m_i]^{1/2}. \tag{26}$$

The voltage drop over the 1-kΩ resistor corresponding to the current (25) is now amplified by a factor $+\alpha$ and sent to the waveform eductor. The signal stored in the eductor is therefore

$$S_{v_a}(t)\propto I_-(t)-I_+(t)\propto f(v_a, t). \tag{27}$$

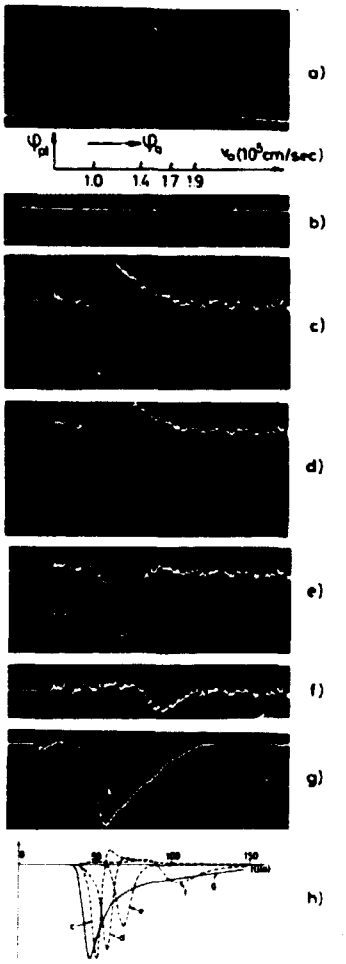

FIG. 6. (a) $f_0[v=(2e(\varphi_a-\varphi_{pl})/m_i)^{1/2}]$. 0.5 V/large division; $n\approx 10^6$ cm^{-3}. (b) Δt pulse applied to grid. 5 V/large division. (c)–(f) Measured $f(x_a, v_a, t)$ curves. (c) $v_a=1.9\times10^5$ cm/sec. 1 arbitrary unit/large division. (d) $v_a=1.7\times10^5$ cm/sec. 2 arbitrary units/large division. (e) $v_a=1.4\times10^5$ cm/sec. 4 arbitrary units/large division. (f) $v_a=1.0\times10^5$ cm sec. 4 arbitrary units/large division. (g) Measured total flux. (b)–(g) 20 μsec/large division. (h) Calculated results. The letters on the curves correspond to experimetal curves c–g.

For improvement of the signal/noise ratio many (10^4–10^5) pulses are analyzed, and the averaged signal is obtained by means of the waveform eductor. Examples of $S_{v_a}(t)$ curves are shown in Figs. 4–6.

Also the total flux of ions in the pulse was measured by the analyzer. This was simply done by setting $\varphi_a=\varphi_{pl}$ and measuring the current pulse to the analyzer plate with the flip-flop disconnected.

In the experiments reported here the grid potential, φ_0, was equal to the floating potential, and negative Δt pulses were applied to the grid. In choosing these conditions we found that the noise level in the plasma was minimized. With negative Δt pulses the grid releases

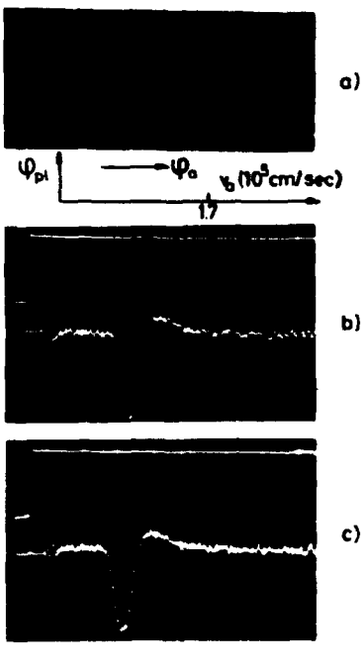

FIG. 7. (a) $f_0[v=(2e(\varphi_a-\varphi_{pl})/m_i)^{1/2}]$. 0.5 V/large division; $n\approx 3\times 10^9$ cm^{-3}. (b) Upper trace: Δt pulse applied to grid. 2 V/larger division. Lower trace: Measured $f(x_a=10$ cm, $v_a=1.7\times 10^5$ cm/sec, $t)$ curve. 20 μsec/large division. (c) Upper trace: Δt pulse applied to grid. 2 V/large division. Lower trace: Measured $f(x_a=25$ cm, $v_a=1.7\times 10^5$ cm/sec, $t)$ curve. 50 μsec/large division.

negative density perturbations. The theory based on the *linearized* Vlasov equation, of course, applies to negative as well as to positive perturbations. The theoretical curves showed in Fig. 2 are obtained for positive perturbations. In an earlier publication[17] where preliminary results were reported we used positive Δt pulses. A simple physical picture of the wave–particle interaction similar to the one discussed for positive density perturbations in Ref. 17 can be shown to apply to negative perturbations too.

IV. RESULTS

In this section we report measurements taken at three different velocity distribution functions, $f_0(v)$, and compare the results with calculations. In all three cases the analyzer position, x_a, was 10 cm and the width of the Δt pulses applied to the grid 10 μsec. The amplitude of the pulses in each case was chosen as small as possible; just large enough for the signal/noise ratio to be acceptable. In all three cases we found no change in the $f_0(v)$ functions when the grid was biased to $\varphi_0+\Delta\varphi(\Delta\varphi<0)$. For determination of the shape of $g(v)$ the grid potential was, therefore, lowered further until the amplitude of the distribution function began to decrease. It was found that the shape of the distribution was unchanged, and it was therefore concluded that $g(v)$ has the same shape as $f_0(v)$.

The results of the first series of measurements are shown in Fig. 4. The plasma density was $n_0\approx 8\times 10^8$ cm^{-3}. Figure 4(a) shows the undisturbed ion velocity distribution function,

$$f_0\{v=[2e(\varphi_a-\varphi_{pl})/m_i]^{1/2}\},$$

obtained with φ_0 being the floating potential. Figure 4(b) shows the Δt pulse applied to the grid, and Figs. 4(c)–(f) show $f(x_a, v_a, t)$ at four different v_a values. Finally, the measured total flux of ions in the pulse is shown in Fig. 4(g). From measurements on Fig. 4(a) it was observed that $f_0(v)$ and $g(v)$ correspond to displaced Maxwellians with a temperature ratio $T_e/T_i=0.74$ ($T_e=T_{\text{hot plate}}$ measured by a pyrometer) and with a drift velocity $m_0=m_1=1.7$. These numbers together with our best estimate of the analyzer resolution $v_r=c_s/4$ were inserted into the computer program. The results of the calculations for the four v_a values used in Figs. 4(c)–(f) are shown in Fig. 4(h).

Figure 5 shows results similar to those of Fig. 4, but obtained in a Maxwellian distribution function with a lower ion temperature and a higher drift velocity. This distribution function was obtained by lowering the density to $n_0\approx 4\times 10^8$ cm^{-3} and increasing the temperature of the hot Ta plate.[12] From Fig. 5(a) we deduce $T_e/T_i=0.87$ and $m_0=m_1=2.4$. The curves in Figs. 5(b)–(h) correspond to the curves in Fig. 4.

The third series of experiments was performed in the f_0 function shown in Fig. 6(a). This function was obtained by lowering the density to $n_0\approx 10^8$ cm^{-3} and by increasing the plate temperature even further. The plasma potential in this case was obtained as described in Ref. 13, namely, by ions formed by charge exchange in a neutral cloud in the copper tube in Fig. 3. The contribution of these ions is seen as the small peak on the left-hand side of the curve in Fig. 6(a). During the pulse measurements the copper tube was removed whereby the small peak disappears. Curves (b)–(g) correspond to the same curves in Figs. 4 and 5. Although f_0 is not a displaced Maxwellian in this case,[13] we have estimated from Fig. 6(a) that $T_e/T_i=1.3$ and $m_0=m_1=2.9$. With these figures used in the computer program we obtain the curves in Fig. 6(h).

The theory predicts that the density pulses and $f(x, v, t)$ propagate in a self-similar manner [see Eqs. (12) and (16)]. This property was tested experimentally in several cases. Figure 7 shows an example. The density was $n_0\approx 3\times 10^9$, and the f_0 function obtained with the analyzer is shown in Fig. 7(a). The upper trace in Fig. 7(b) shows the 10-μsec Δt pulse applied to the grid, and the lower trace shows $f(x_a, v_a, t)$ obtained with the analyzer in position $x_a=10$ cm and adjusted to the velocity $v_a=1.7\times 10^5$ cm/sec. The sweep in Fig. 7(b) is 20 μsec/large division. Figure 7(c) was obtained with the analyzer moved to $x_a=25$ cm, but still ana-

lyzing at $v_a = 1.7 \times 10^5$ cm/sec. Here, the sweep is 50 μsec large division. The length of the Δt pulse shown in this upper trace was increased to 25 μsec. Therefore, according to Eq. (16) we expect the picture of the analyzer signal to look exactly as the one in Fig. 7(b). This signal is shown in the lower trace in Fig. 7(c).

V. CONCLUSION AND DISCUSSION

The most interesting feature of the calculated curves is the overshoot seen, for instance on curves 1 and 2 in in Fig. 2. As shown in a simplified physical picture[17] this overshoot is caused by the acceleration of ions in the main plasma as they interact with the propagating density pulse. We take the general agreement between the calculated and experimentally obtained curves and especially the overshoot on the curves in Figs. 4–7 as clearcut experimental proof of the wave-particle interaction as described by the third term in the Vlasov equation (3). Also the self-similar pulses found in the experiment are in accordance with the Vlasov equation.

In connection with the discussion of whether earlier reported experiments[2–8] on propagation of ion-acoustic waves in Q machines do actually show Landau damping, i.e., collective interaction, or just phase mixing of freely streaming particles,[15] our results show that at least for pulses both are of importance. By comparing Figs. 2(a) and (c) we see the effect of changing of $g(v)$, i.e., the effect of changing the contribution of the freely streaming particle term. Similarly, comparison between Figs. 2(a) and (b) shows the effect of changing of $f_0(v)$, i.e., the effect of changing the contribution of the collective interaction. The fact that our results are self-similar shows the interesting feature that the ratio between the contribution of collective interaction and that of freely streaming particles is independent of the distance from the grid.

Experiments on propagation of short, grid-generated pulses through plasmas have been reported in two earlier publications.[12,24] In both publications it was concluded that the ions in the pulses move as freely streaming particles with no or negligible interaction with the main plasma. These conclusions are in agreement with our results because in both experiments the characteristic velocity of the ions in the pulse generated at the grid is very different from that of the ions in the main plasma (m_0 very different from m_1). For such cases our calculations show that the interaction is negligible, i.e., the ions move as freely streaming particles.

Some discrepancies between the calculated and experimental curves in Figs. 4–7 can be noted. We believe that these discrepancies can be explained by the following:

(1) For convenience $f_0(v)$ has been assumed to be a displaced Maxwellian in the calculations. This is an approximation which is permissible at high densities, but certainly not at lower densities as in the case of Fig. 6.[13] Performance of the calculations for the measured $f_0(v)$ functions in Fig. 6 would require tedious work, and we believe the change in the results would be minor.

(2) We have measured $g(v)$ as the difference between the distribution functions at the two grid potentials φ_0 and $\varphi_0 + \Delta\varphi$. It is well known that when the potential on a grid in a plasma is changed within a time that is short compared with the ion plasma period, a burst of high-velocity particles is generated.[24,25] The number of ions in the burst is essentially equal to the number of ions in a sheath with a thickness of a few Debye lengths. In the experiment we have kept the time interval, Δt, so long (10–100 ion plasma periods) that the predominant part of the ions in the pulse is released while the potential is $\varphi_0 + \Delta\varphi$. Therefore, we can neglect the relatively small number of ions released during the change in the grid potential. As a matter of fact, by shortening Δt to about one plasma period the signals received by the analyzer approach those discussed by Ikezi and Taylor.[24]

Another reason why the distribution function in the pulse might deviate from that obtained by our dc measurements is that when the potential on the grid is changed, a density pulse is reflected toward the hot plate.[12] This density pulse might interact with the plasma flow from the hot plate toward the grid and thus cause the distribution function in the downstream pulse to differ from that obtained by dc measurements. Because the interaction between the reflected pulse and the upstream plasma is very weak,[12,18,19] we believe that our dc measurements of $g(v)$ represent the distribution function in the pulse very well.

Finally, in the calculations we have approximated $g(v)$ to a displaced Maxwellian. We believe that this approximation is rather good [cf. the discussion of $f_0(v)$ in (1) above].

(3) In the calculation reported in this paper we assumed the analyzer resolution to be a Gaussian in velocity [see Eq. (19)]. We know of no direct way of measuring the resolution properties of the analyzer except at very low velocities.[13] In the preliminary publication[17] we assumed the resolution to be a Gaussian in energy rather than in velocity. Because we have obtained better agreement between experimental and calculated S_{v_a} curves, especially at low v_a values, in this paper than in Ref. 17, we now believe that the analyzer resolution is closer to a Gaussian in velocity than in energy. We have found that the calculated results are in best agreement with the experimental ones when we assume that $v_r = c_1/4$.

(4) Also the fact that the Δt pulse applied to the grid has a finite width may cause some of the discrepancies between the theoretical and the experimental curves. Especially at high v_a values, the experimental $S_{v_a}(t)$ curves would tend to broaden, and their am-

plitudes would decrease. This effect has been noted in many of our experimental data.

(5) In the derivation of (27) we have neglected the change in the plasma potential associated with the pulse. This change is given by

$$\Delta\varphi_{p1}(t) = (\kappa T_e/e)n(t), \tag{28}$$

where $n(t)$ is the relative density perturbation, and it causes an additional contribution to Eq. (27). Rigorously, the signal, $S_{\varphi_0}(t)$, displayed in Fig. 3 is written as

$$\begin{aligned} S_{\varphi_0}(t) &\propto \int_{v_{\min -}}^{v_{\min +}} v f(v,t)\, dv \\ &= \int_{\varphi_0-\Delta\varphi_0-[\varphi_{p1}+\Delta\varphi_{p1}(t)]}^{\varphi_0+\Delta\varphi_0-[\varphi_{p1}+\Delta\varphi_{p1}(t)]} [f_0(\varphi)+f(\varphi,t)]\, d\varphi \\ &\simeq 2\Delta\varphi_0 \Big(f_0(\varphi)+f(\varphi,t)-\frac{df_0(\varphi)}{d\varphi}\Delta\varphi_{p1}(t) \\ &\quad -\frac{df(\varphi,t)}{d\varphi}\Delta\varphi_{p1}(t)\Big)_{\varphi=\varphi_0-\varphi_{p1}}. \end{aligned} \tag{29}$$

The first term in the bracket is time-independent and thus not seen on the oscilloscope. The second term corresponds to the change in the velocity distribution function, i.e., it is the term given by Eq. (27). The third term is the additional signal caused by the change in the plasma potential. Finally, the last term is a second-order term which can be neglected.

From (28) and (29) we first notice that for φ values for which $df_0(\varphi)/d\varphi<0$ the third term has the same sign as $n(t)$. We can thus conclude that this term cannot cause the overshoot on the experimental curves.

To compare the magnitude of the second and third terms we use

$$f(\varphi,t)/f_0(\varphi)\approx n(t). \tag{30}$$

By means of (28) and (30) the third term is written

$$\frac{(d/d\varphi)f_0(\varphi)}{f_0(\varphi)}\,\frac{\kappa T_e}{e}f(\varphi). \tag{31}$$

From Figs. 4, 5, and 6 we see that

$$\frac{df_0(\varphi)/d\varphi}{f_0(\varphi)} \lesssim 1V^{-1}.$$

By using $T_e\approx 0.2$ eV we can calculate that the magnitude of the third term in (29) can at worst amount to 20% of that of the second term.

ACKNOWLEDGMENTS

The authors want to thank K. -V. Weisberg for help with the construction of the electronic equipment. Further we want to thank M. Nielsen and B. Reher for maintenance of the Q device. The numerical calculations were performed at the Northern Europe University Computing Center (NEUCC).

* Present address: The University of Texas at Austin, Austin, Texas 78712.
[1] L. D. Landau, J. Phys. (USSR) **10**, 25 (1946).
[2] A. Y. Wong, N. D'Angelo, and R. W. Motley, Phys. Rev. Letters **9**, 415 (1962).
[3] A. Y. Wong, R. W. Motley, and N. D'Angelo, Phys. Rev. **133**, A436 (1964).
[4] R. W. Motley and A. Y. Wong, in *Proceedings of the Sixth International Conference on Phenomena in Ionized Gases*, edited by T. Hubert and E. Crémien (Bureau des Editions, Centre d'Etudes Nucleaires de Saclay, Paris, 1964), Vol. 3, p. 133.
[5] H. K. Andersen, N. D'Angelo, V. O. Jensen, P. Michelsen, and P. Nielsen, Phys. Fluids **11**, 1177 (1968).
[6] N. Sato, H. Ikezi, N. Takahashi, and Y. Yamashita, Phys. Rev. **183**, 278 (1969).
[7] P. Korn, T. C. Marshall, and S. P. Schlesinger, Phys. Fluids **13**, 517 (1970).
[8] H. J. Doucet and D. Gresillon, Phys. Fluids **13**, 773 (1970).
[9] R. W. Gould, T. M. O'Neil, and J. H. Malmberg, Phys. Rev. Letters **19**, 219 (1967).
[10] H. Ikezi and N. Takahashi, Phys. Rev. Letters **20**, 140 (1963).
[11] D. R. Baker, N. R. Ahern, and A. Y. Wong, Phys. Rev. Letters **20**, 318 (1968).
[12] S. A. Andersen, V. O. Jensen, and P. Nielsen, Phys. Fluids **12**, 2694 (1969).
[13] S. A. Andersen, V. O. Jensen, P. Michelsen, and P. Nielsen, Phys. Fluids **14**, 728 (1971).
[14] R. W. Gould, Phys. Rev. **136**, A991 (1964).
[15] J. L. Hirschfield and J. H. Jacob, Phys. Fluids **11**, 411 (1968).
[16] S. Takamura, Phys. Letters **32A**, 254 (1970).
[17] S. A. Andersen, V. O. Jensen, P. Michelsen, and P. Nielsen, Phys. Letters **32A**, 413 (1970).
[18] P. Nielsen, Risö Report No. 190 (1969).
[19] P. Nielsen, in *Proceedings of the International Conference on Physics of Quiescent Plasmas*, Paris (Ecole Polytechnique, Paris, 1969), Vol. 1, p. 61.
[20] R. J. Mason, Phys. Fluids **13**, 1042 (1970).
[21] J. D. Jackson, J. Nucl. Energy, Pt. C **1**, 171 (1960).
[22] S. A. Andersen, V. O. Jensen, and P. Michelsen, Phys. Letters **31A**, 395 (1970).
[23] A. L. Gurevich, L. V. Parilskaya, and L. P. Pitaevskiĭ, Zh. Eksp. Teor. Fiz. **49**, 647 (1965) [Sov. Phys. JETP **22**, 449 (1966)].
[24] H. Ikezi and R. J. Taylor, J. Appl. Phys. **41**, 738 (1970).
[25] I. Alexeff, W. D. Jones, and M. Widner, Phys. Fluids **13**, 1519 (1970).

5. Investigation of ion acoustic waves in collisionless plasmas

G. B. Christoffersen, V. O. Jensen, and P. Michelsen

Danish Atomic Energy Commission, Research Establishment Risø, Roskilde, Denmark

(Received 6 February 1973; final manuscript received 9 October 1973)

The Green's functions for the linearized ion Vlasov equation with a given boundary value are derived. The propagation properties of ion acoustic waves are calculated by performing convolution integrals over the Green's functions. For T_e/T_i less than about 3 it is concluded that the collective interaction is very weak and that the propagation properties are determined almost completely by freely streaming ions. The wave damping, being due to phase mixing, is determined by the width of the perturbed distribution function rather than by the slope of the undisturbed distribution function at the phase velocity as concluded from normal mode calculations.

I. INTRODUCTION

During the last ten years many experiments on ion-acoustic waves propagating through steady state, collisionless plasmas have been performed[1-5]. The aim of most of this work has been to compare the results with calculations based on the linearized Vlasov equation and thereby verify the validity of that equation and the methods used to solve it. For the propagation of ion waves along the magnetic lines of force, the linearized Vlasov equation for the ions is

$$\frac{\partial f(x,v,t)}{\partial t} + v\frac{\partial f(x,v,t)}{\partial x} + \frac{E(x,t)q}{m_i}\frac{df_0(v)}{dv} = 0, \quad (1)$$

where $f_0(v)$ is the zero-order ion velocity distribution function, and $f(x,v,t)$ is the perturbed ion velocity distribution function. q and m_i are the charge and the mass of the ions, respectively.

By assuming that the electrons behave as an isothermal fluid and that quasi-neutrality prevails we get that the electric field is given by

$$E(x,t) = -\frac{\kappa T_e}{q}\frac{1}{n_0}\frac{\partial n(x,t)}{\partial x}. \quad (2)$$

Here, κ is Boltzmann's constant, and T_e is the electron temperature. n_0 is the zero-order density given by $n_0 = \int_{-\infty}^{\infty} f_0(v)\,dv$.

Combining (1) and (2) gives the ion Vlasov equation in the form

$$\frac{\partial f(x,v,t)}{\partial t} + v\frac{\partial f(x,v,t)}{\partial x} = c_i^2\frac{1}{n_0}\frac{\partial n(x,t)}{\partial x}\frac{df_0(v)}{dv}, \quad (3)$$

where

$$n(x,t) = \int_{-\infty}^{+\infty} f(x,v,t)\,dv, \quad c_i^2 = \kappa T_e/m_i. \quad (4)$$

The term on the right-hand side of Eq. (3) is the most interesting term since it describes the collective interaction between the electric field associated with a density perturbation [see Eq. (2)] and ions in the background plasma with the velocity distribution function $f_0(v)$. The two terms on the left-hand side alone describe ions streaming freely through space without any interaction with the plasma. The collective interaction term is peculiar to plasmas; a similar term is not found in the Boltzmann equation used to describe other many-body systems (normal gases, neutrons in a fission reactor, etc.).

The technique normally used in solving Eq. (3) for propagation of ion acoustic waves was given by Landau.[6] In this technique the dielectric function, $\epsilon(k,\omega)$, is calculated from the Vlasov equation, and the dispersion relation is then given by the equation $\epsilon(k,\omega) = 0$. From Eqs. (3) and (4)[7] we obtain

$$\epsilon(k,\omega) = 1 - c_i^2\frac{1}{n_0}\int_{-\infty}^{+\infty}\frac{f_0'(v)}{v-\omega/k}dv, \quad (\mathrm{Im}\,\omega/k > 0). \quad (5)$$

A solution (ω', k') to the dispersion relation indicates that the plasma can transmit a wave which is often called a natural mode or normal mode of the type $\exp[i(\omega' t - k' x)]$. This wave is damped (Landau damping) or grows depending on the sign of the imaginary part of ω' or k'.

Quantitative agreements between experiments with grid excited ion-acoustic waves in a Q machine and calculations based on the procedure mentioned here were first reported by Wong *et al.*[1] Because $\epsilon(k,\omega)$, as given in (4), depends on $f_0(v)$, a quantity which only appears in the collective term in the Vlasov equation, the results of these experiments were taken as indications of the importance of this term.

Calculations of the propagation properties of waves based on the technique just mentioned have been criticized by various authors.[8-12] Hirschfield and Jacob[13] showed that "the interpretation of experiments on the spatial Landau damping is complicated by the contribution of the free-streaming, initially perturbed particles". They considered an electrostatic wave excited by a grid in a steady-state plasma. By assuming a simple interaction mechanism between grid and plasma they calculated the velocity distribution function in the density perturbation at the grid. With this distribution as the boundary value they solved the Vlasov equation without the collective interaction term and found that the wave propagates and damps away very much the same way as when calculated by the normal mode method described above. In this case the damping is caused by phase mixing of the freely streaming particles in the perturbation excited at the grid. The normal mode technique ignores this effect [the boundary value does not appear in the expression for $\epsilon(k,\omega)$]. Therefore, the experimental results cannot be taken as proof of collective interaction.

The difference between the normal mode method and that of Hirschfield and Jacob can most readily be clarified as follows: A formal solution of Eqs. (3) and (4) for a case where a wave is excited at $x = 0$ can be obtained by using the "method of characteristics", i.e., by integrating along the unperturbed orbits $x' - x = v(t' - t)$ in an (x', t') diagram. For the perturbed velocity distribution function we get

$$f(x, v, t) = g(x' = 0, v, t') + c_i^2 \frac{1}{n_0} \frac{1}{v} f_0(v) \int_0^x \frac{\partial n(x', t')}{\partial x'} dx', \quad (v > 0), \tag{6}$$

$$f(x, v, t) = c_i^2 \frac{1}{n_0} \frac{1}{v} f_0(v) \int_\infty^x \frac{\partial n(x', t')}{\partial x'} dx', \quad (v < 0).$$

The perturbed density is obtained by inserting Eq. (6) into Eq. (4). In Eq. (6), $g(x' = 0, v, t')$ is the distribution function in the perturbation generated by the exciter at $x = 0$. The particles in the g function move freely in the x direction and, therefore, also contribute to the perturbation for $x > 0$. The integral terms in Eq. (6) clearly stem from collective interaction.

The normal mode technique neglects the g function and only considers the collective interaction terms in Eq. (6). Hirschfield and Jacob neglect the last terms and show that the g term alone gives results very similar to those obtained from a normal mode treatment. Offhand, one cannot say which term is the most important one in an actual experimental situation. In the limit of very low electron temperature ($c_e \to 0$), the integral terms disappear and the normal mode technique is evidently incorrect. At high electron temperature the collective forces become strong [see Eq. (2)]and the g term will become unimportant. For an actual case one has to calculate solutions to Eqs. (3) and (4); such calculations require knowledge of $f_0(v)$ as well as of $g(x = 0, v, t)$.

In this paper we report on exact calculations of wave properties obtained for situations realizable in single-ended Q machines and some other steady-state plasmas.

We also present experimental results which agree with theory. The work presented here is essentially a continuation of an earlier work[12] in which we solved Eqs. (3) and (4) for an initial value where the perturbed velocity distribution function at $t = 0$ has the form $g(v)\delta(x)$; i.e., we found the Green's function for the equations with a given initial value. This situation was approximated experimentally by applying short pulses to a grid in a single-ended Q machine. Measurements of $f(x, v, t)$ and $n(x, t)$ showed very good agreement with the calculations. It was concluded that in Q machines where $T_e \approx T_i$, the freely streaming g term is much more important than the collective term; a clear-cut signature of the last term for $v > 0$ in Eq. (6) could only be seen in measurements of the perturbed velocity distribution function, $f(x, v, t)$.

In the case of waves treated in this paper, $g(x = 0, v, t)$ is an oscillating function of the type $g(v)\exp(i\omega t)$.[14] We obtain the solution to the wave problem by calculating the Green's functions for Eqs. (3) and (4) with a given boundary value and then by performing a normal convolution integration over time. The solutions of the equations for Q machine plasmas ($T_e \approx T_i$) again show that the contribution from the collective term is very weak and scarcely noticeable in any experiment. Only if $T_e \gtrsim 3T_i$, can collective effects be expected to be seen in measurements of $f(x, v, t)$, and not in density measurements. Our experimental results agree with the calculations.

The paper is organized as follows. In Sec. II we present the mathematical procedure used to solve the equations. A few theoretical results are shown in Sec. III, where we also give a brief discussion of the physical mechanisms explaning these results. Section IV describes the experimental setup and the results obtained. Finally, in Sec. V we give a general discussion and present our conclusions.

Fragments of the work described in this paper have been described elsewhere.[14,15]

II. THEORETICAL RESULTS

The experimental situation is as follows: The plasma is generated at the hot plate of a single-ended Q machine. It flows from the plate along a constant magnetic field through a biased grid at $x = 0$. At grid potential, ϕ_0, the one-dimensional ion velocity distribution function for the downstream plasma, as measured by an electrostatic energy analyser,[16] is $f_0(v)$. When the grid potential is changed by a small amount, $\Delta\phi$, the velocity distribution function is $f_0(v) + g(v)$. For sufficiently small values of $\Delta\phi$, the shape of $g(v)$ is independent of $\Delta\phi$ while the amplitude is proportional to $\Delta\phi$.[14] Therefore, it is clear that both $f_0(v)$ and $g(v)$ equal zero for $v < 0$. In our case, then the integral term for $v < 0$ in Eq. (6) vanishes. However, from a mathematical point of view it simplifies the analysis if $g(v)$ and $f_0(v)$ are analytic functions in the whole complex v plane. This means, of course, that $g(v)$ and $f_0(v)$ cannot be equal to zero for all negative v's, but we assume that the values of the two functions for v negative are so small that for physical reasons they can be neglected. Drifting Maxwellians of the type $\exp[-(v - v_d)^2/c_i^2]$ with $v_d \gtrsim 2.5c_i$ fulfill this requirement. The numerical calculations reported in the next section are performed for such $f_0(v)$ and $g(v)$ functions.

At this point we would point out that we cannot specify $g(v)$ for $v < 0$ because we also have to satisfy the condition that no particles are coming from infinity [$f(x \to \infty, v < 0, t) = 0$]. If however $f_0(v)$ is small for $v < 0$, it follows that $g(v)$ must also be small for negative v's.

In the experiment the wave is generated by superimposing an oscillating potential $\Delta\phi\exp(-i\omega t)$ on the dc voltage ϕ_0 of the grid. The boundary value for which we have to solve Eqs. (3) and (4) is therefore,

$$f(x = 0, v, t) = g(v)\exp(-i\omega t) \tag{7}$$

and

$$n(x = 0, t) = \exp(-i\omega t) \int_{-\infty}^{\infty} g(v)\, dv. \tag{8}$$

Here, we integrate from $-\infty$ to ∞ but in accordance with the preceding remarks the contribution to the density from particles moving with negative velocity is negligible. In this way the calculation is reduced to a pure boundary

value problem. The general case wher· $f_0(v) \neq 0$ for $v < 0$ is more complicated, but can, for instance, be solved as a mixed initial value-boundary value problem as done by Weitzner.[10]

The use of the linearized equation is justified by the fact that in the experiment $n(x = 0, t) \ll n_0$.

In the calculations we use a Green's function technique and first calculate the time and space dependence of perturbations generated by short pulses, $[\delta(t)]$, applied to the grid, and then perform a convolution integration over time to obtain the response to an oscillating potential on the grid.

We introduce the δ function as follows

$$\delta(t) = \lim_{\alpha \to 0} \frac{1}{\pi} \frac{\alpha}{\alpha^2 + t^2}. \tag{9}$$

To find the Green's function for the density, $n_G(x, t)$, and that for the distribution function, $f_G(x, v, t)$, we solve Eqs. (3) and (4) with the boundary conditions

$$f_G(x = 0, v, t) = g(v) \frac{1}{\pi} \frac{\alpha}{\alpha^2 + t^2} \tag{10}$$

and

$$n_G(x = 0, t) = \int_{-\infty}^{\infty} g(v) \frac{1}{\pi} \frac{\alpha}{\alpha^2 + t^2} dv \equiv \eta \frac{1}{\pi} \frac{\alpha}{\alpha^2 + t^2}, \tag{11}$$

and let $\alpha \to 0$ in the solutions. In solving the equations we apply a Laplace transformation in space, $f(k) = \int_0^{\infty} \exp(ikx) f(x) dx$, and a Fourier transformation in time, $f(\omega) = \int_{-\infty}^{\infty} \exp(-i\omega t) f(t) dt$. Doing this we find the results

$$\begin{aligned} n_G(k, \omega) &= \frac{1}{ik} \exp(-\alpha|\omega|) \left(\frac{\eta c_e^2}{n_0} \int_{-\infty}^{\infty} \frac{f_0'(v)}{v - \omega/k} dv - \int_{-\infty}^{\infty} \frac{v g(v)}{v - \omega/k} dv \right) \left(1 - \frac{c_e^2}{n_0} \int_{-\infty}^{\infty} \frac{f_0'(v)}{v - \omega/k} dv \right)^{-1} \\ &= -\frac{1}{ik} \exp(-\alpha|\omega|) \left[\eta + \frac{\omega}{k} \int_{-\infty}^{\infty} \frac{g(v)}{v - \omega/k} dv \left(1 - \frac{c_e^2}{n_0} \int_{-\infty}^{\infty} \frac{f_0'(v)}{v - \omega/k} dv \right)^{-1} \right] \\ &\equiv \frac{1}{ik} \exp(-\alpha|\omega|) N\left(\frac{\omega}{k}\right), \end{aligned} \tag{12}$$

and

$$\begin{aligned} f_G(k, v, \omega) &= \frac{1}{ik} \exp(-\alpha|\omega|) \left(\frac{c_e^2}{n_0} N\left(\frac{\omega}{k}\right) \frac{f_0'(v)}{v - \omega/k} - \frac{v g(v)}{v - \omega/k} + \frac{c_e^2 \eta}{n_0} \frac{f_0'(v)}{v - \omega/k} \right) \\ &= \frac{1}{ik} \exp(-\alpha|\omega|) \left(-\frac{v g(v)}{v - \omega/k} - \frac{c_e^2}{n_0} \frac{f_0'(v)}{v - \omega/k} \frac{\frac{\omega}{k} \int_{-\infty}^{\infty} \frac{g(v)}{v - \omega/k} dv}{1 - (c_e^2/n_0) \int_{-\infty}^{\infty} dv f_0'(v)/[v - (\omega/k)]} \right) \\ &\equiv \frac{1}{ik} \exp(-\alpha|\omega|) M\left(v, \frac{\omega}{k}\right). \end{aligned} \tag{13}$$

To transform $n_G(k, \omega)$ and $f_G(k, v, \omega)$ back to time and space variables we have to perform the integrations

$$n_G(x, t) = \frac{1}{4\pi^2} \int_{-\infty + i\delta}^{+\infty + i\delta} \exp(-ikx) \times \int_{-\infty}^{\infty} \exp(i\omega t) n_G(k, \omega) \, d\omega \, dk \tag{14}$$

and

$$f_G(x, v, t) = \frac{1}{4\pi^2} \int_{-\infty + i\delta}^{+\infty + i\delta} \exp(-ikx) \times \int_{-\infty}^{\infty} \exp(i\omega t) f_G(k, v, \omega) \, d\omega \, dk, \tag{15}$$

where δ is a positive number assuring that the integration path in the k plane runs above all singularities in $n_G(k, \omega)$ and in $f_G(k, v, \omega)$. Since ω only takes real values in the integrations in Eqs. (14) and (15), it is clear that $n_G(k, \omega)$ and $f_G(k, v, \omega)$ are singular on the real k axis. However, by defining $n_G(k, \omega)$ and $f_G(k, v, \omega)$ for real k values by the analytic continuation of the functions, we can avoid the singularities on the real axis. Furthermore, $n_G(k, \omega)$ and $f_G(k, v, \omega)$ also have singularities in the positive imaginary part of the k plane if there exist k values in this plane for which the denominator of $N(\omega/k)$ equals zero. We assume that the denominator of $N(\omega/k)$ has no zero for $\mathrm{Im}\, k > 0$; later, we shall show that this assumption holds as long as we confine ourselves to treat $f_0(v)$ functions which only have stable solutions in a normal mode treatment of the wave problem.[6,12]

The v integrations in $N(\omega/k)$ have poles for $v = \omega/k$. For $\mathrm{Im}\, k > 0$, the pole lies above the real v axis if $\omega < 0$ and below if $\omega > 0$. Therefore, the analytic continuation

of $n_G(k,\omega)$ and $f_G(k,v,\omega)$ for real k is obtained by prescribing that the v integration path shall run below the pole for $\omega < 0$ and above for $\omega > 0$. We therefore define

$$N(\omega\, k) = \begin{cases} N_b(\omega/k) & \text{for } \omega < 0 \\ N_a(\omega/k) & \text{for } \omega > 0 \end{cases} \tag{16}$$

and

$$M(v,\omega/k) = \begin{cases} M_b(v,\omega/k) & \text{for } \omega < 0 \\ M_a(v,\omega/k) & \text{for } \omega > 0, \end{cases} \tag{17}$$

where the subscript b indicates that the v integration path runs below the pole and the subscript a indicates that it runs above the pole.

Having defined the analytic continuations of $n_G(k,\omega)$ and $f_G(k,v,\omega)$, we can go to the limit $\delta = 0$ in Eqs. (14) and (15) and rewrite Eq. (14) in the form

$$\begin{aligned} n_G(x,t) = {} & \frac{1}{4\pi^2 i} \\ & \times \left[\int_{-\infty}^{0} \int_{\infty}^{0} \frac{1}{k} \exp(i\omega t + \alpha\omega - ikx) N_b\left(\frac{\omega}{k}\right) d\omega\, dk \right. \\ & + \int_{-\infty}^{0} \int_{0}^{\infty} \frac{1}{k} \exp(i\omega t - \alpha\omega - ikx) N_a\left(\frac{\omega}{k}\right) d\omega\, dk \\ & + \int_{0}^{\infty} \int_{-\infty}^{0} \frac{1}{k} \exp(i\omega t + \alpha\omega - ikx) N_b\left(\frac{\omega}{k}\right) d\omega\, dk \\ & \left. + \int_{0}^{\infty} \int_{0}^{\infty} \frac{1}{k} \exp(i\omega t - \alpha\omega - ikx) N_a\left(\frac{\omega}{k}\right) d\omega\, dk \right]. \end{aligned} \tag{18}$$

By substituting $k = \omega/u$ after some simple algebra we get

$$\begin{aligned} n_G(x,t) = {} & -\frac{1}{4\pi^2 i} \left\{ \int_{-\infty}^{\infty} \frac{1}{u} N_b(u) \right. \\ & \times \int_{-\infty}^{0} \exp\left[-i\omega\left(\frac{x}{u} + i\alpha - t \right) \right] d\omega\, du \\ & \left. - \int_{-\infty}^{\infty} \frac{1}{u} N_a(u) \int_{0}^{\infty} \exp\left[-i\omega\left(\frac{x}{u} - i\alpha - t \right) \right] d\omega\, du \right\}. \end{aligned} \tag{19}$$

Performing the ω integration we immediately get

$$\begin{aligned} n_G(x,t) = {} & \frac{1}{4\pi^2} \left(\frac{1}{t + i\alpha} \int_{-\infty}^{\infty} N_a(u) \left(u - \frac{x}{t + i\alpha} \right)^{-1} du \right. \\ & \left. + \frac{1}{t - i\alpha} \int_{-\infty}^{\infty} N_b(u) \left(u - \frac{x}{t - i\alpha} \right)^{-1} du \right). \end{aligned} \tag{20}$$

To proceed we note that $N_a(u)$ is analytic in the half-u plane in which $\operatorname{Im} u \leq 0$ and $N_b(u)$ is analytic for $\operatorname{Im} u \geq 0$. This is assured by the analytic continuation of the function as described here and because the denominators in N_a and N_b are assumed to have no zeros in the half-planes where the two functions are defined. The denominator in N_b is the classical dielectric function for the plasma [see Eq. (5)]. This function is known[12] to have no zeros in the half-plane in which it is defined for $f_0(v)$ functions which are stable in a normal mode treatment.

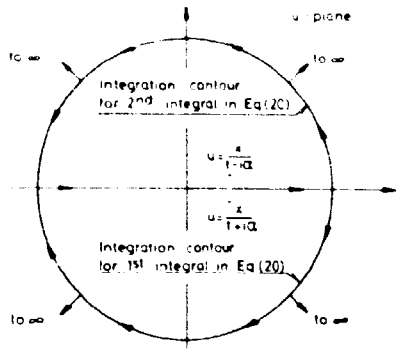

FIG. 1. Integration contours.

Similarly, as also shown in Ref. 12, the denominator of N_a has no zeros in the half-plane where it is defined as long as we only consider Landau-stable $f_0(v)$ functions. Finally, it is clear from the definitions of the N functions in Eq. (12) that $N_{a,b}(u) \to 0$ for $|u| \to \infty$ in the two half-planes where the N functions are defined. Thus in calculating the integrals in (20) we can use Jordan's lemma and change the integration paths to closed half-circles as indicated in Fig. 1. The integrand in the first integral in (20) has a pole at $u = x/t + i\alpha$, i.e., within the integration contour; similarly, the integrand in the last integral has a pole at $u = x/t - i\alpha$ within the integration contour for this integral. Using residue calculations we thus get

$$n_G(x,t) = \frac{1}{2\pi i} \left[\frac{1}{t + i\alpha} N_a\left(\frac{x}{t + i\alpha} \right) - \frac{1}{t - i\alpha} N_b\left(\frac{x}{t - i\alpha} \right) \right]. \tag{21}$$

By going to the limit $\alpha \to 0$ we get

$$n_G(x,t) = \frac{1}{2\pi i} \frac{1}{t} \left[N_a\left(\frac{x}{t} \right) - N_b\left(\frac{x}{t} \right) \right] \tag{22}$$

and because $N_a(x/t) = N_b^*(x/t)$ for real x/t we get

$$n_G(x,t) = -\frac{1}{\pi} \frac{1}{t} \operatorname{Im} N_b\left(\frac{x}{t} \right). \tag{23}$$

Equation (23) is the Green's function for the perturbed density obtained from Eqs. (3) and (4) with the boundary conditions (10) and (11). Equation (23) differs from the corresponding function [Eq. (12)] in Ref. 12 only by the term

$$\frac{\eta c_r^2}{n_0} \int_{-\infty}^{\infty} \frac{f_0'(v)}{v - \omega/k}\, dv$$

in the definition of N in Eq (12). This difference is caused by the fact that in Ref. 12 the Green's function was found for an initial value problem, while here it is for a boundary value problem. The case treated here is more relevant to grid-excited perturbations in Q machines.

To calculate $f_G(x,v,t)$ from (15) we proceed in a way similar to that used in the $n_G(x,t)$ calculations. Thus, we obtain, in analogy with Eq. (21)

$$f_G(x,v,t) = \frac{1}{2\pi i} \left[\frac{1}{t + i\alpha} M_a\left(v, \frac{x}{t + i\alpha} \right) \right.$$

$$- \frac{1}{t - i\alpha} M_b\left(v, \frac{x}{t - i\alpha}\right)\Bigg]. \tag{24}$$

By inserting the M functions given by Eqs. (17) and (13) into Eq. (24) we get

$$f_G(x,v,t) = \frac{1}{2\pi i}\frac{c_e^2}{n_0} f_0'(v)\left(\frac{N_e(x/t + i\alpha)}{vt + i\alpha v - x} - \frac{N_b(x/t - i\alpha)}{vt - i\alpha v - x}\right)$$
$$- \frac{vg(v)}{2\pi i}\left(\frac{1}{vt + i\alpha v - x} - \frac{1}{vt - i\alpha v - x}\right)$$
$$+ \frac{1}{2\pi i}\frac{c_e^2}{n_0}\eta f_0'(v)\left(\frac{1}{vt + i\alpha v - x} - \frac{1}{vt - i\alpha v - x}\right). \tag{25}$$

After some simple algebra we go to the limit $\alpha = 0$ and use the definition of the δ function in Eq. (9) and the well-known definition of the principal value

$$P\frac{1}{y - a} = \lim_{\alpha \to 0} \frac{y - a}{(y - a)^2 + \alpha^2}. \tag{26}$$

Doing this we get

$$f_G(x,v,t) = \left\{vg(v) - \frac{c_e^2}{n_0} f_0'(v)\left[\mathrm{Re}\ N_b\left(\frac{x}{t}\right) + \eta\right]\right\}$$
$$\times \delta(x - vt) + \frac{c_e^2}{n_0} f_0'(v)\,\mathrm{Im}\ N_b\left(\frac{x}{t}\right)\frac{1}{\pi} P\frac{1}{x - vt}. \tag{27}$$

Equation (27) is the Green's function for the perturbed ion velocity distribution function. The difference between this function and the corresponding one derived in a somewhat different way in Ref. 12 is again caused by different choices of initial conditions.

Having the Green's function for the perturbed density and ion velocity distribution function, it is simple to calculate the response for any signal applied to the grid. Here, we consider the case where an oscillating potential as $\exp(-i\omega t')$ is applied to the grid and calculate the propagation properties of the wave generated thereby.

The density, $n(x,t)$, in the wave as a function of x and t is given by

$$n(x,t) = \int_{-\infty}^{t} \exp(-i\omega t') n_G(x, t - t')\,dt', \tag{28}$$

which, with the substitution $t - t' = \tau$ and with the use of (23), can be rewritten

$$n(x,t) = -\exp(-i\omega t)\int_0^\infty \frac{1}{\pi\tau}\exp(i\omega\tau)\,\mathrm{Im}\ N_b\left(\frac{x}{\tau}\right)d\tau$$
$$= \exp(-i\omega t)\frac{1}{\pi}\int_0^\infty \frac{1}{v}\exp\left(i\omega\frac{x}{v}\right)\mathrm{Im}\ N_b(v)\,dv. \tag{29}$$

To obtain the last term in Eq. (29) we have introduced $v = x/\tau$. Inspection of Eq. (12) shows directly that $N_b(v) \to 0$ for $v \to 0$; therefore, there is no problem at the lower limit of the integral in Eq. (29). The same expression for $n(x,t)$ was derived by using different arguments elsewhere.[15] The modulus of the complex integral in Eq. (29) gives the amplitude of the density in a wave as a function of x. Similarly, the argument of the integral is the phase of the wave measured with respect to the phase of the wave exciter.

A similar calculation of the perturbed ion velocity distribution in a wave gives

$$f(x,v,t) = \exp(-i\omega t)\Bigg(\exp\left(i\omega\frac{x}{v}\right)$$
$$\times\left\{g(v) - \frac{c_e^2}{n_0}\frac{1}{v} f_0'(v)[\mathrm{Re}\ N_b(v) + \eta]\right\}$$
$$- \frac{c_e^2}{n_0} f_0'(v)\frac{1}{\pi} P\int_0^\infty \frac{1}{v}\frac{\mathrm{Im}\ N_b(v)}{v - v}\exp\left(i\omega\frac{x}{v}\right)dv\Bigg). \tag{30}$$

Again, the modulus of the complex term in the large parenthesis in Eq. (30) represents the amplitude of the perturbed ion velocity distribution function and the argument gives the phase. The same formula for $f(x,v,t)$ was obtained in Ref. 15.

A computer code has been produced which allows us to calculate the Green's functions (23) and (27) and the amplitude and phase of the wave function (29) and (30). The code calculates the quantities mentioned for cases where $f_0(v)$ and $g(v)$ are drifting Maxwellians of the form

$$f_0(v) \propto \exp[-(v - v_d)^2/c_i^2] \tag{31}$$

and

$$g(v) \propto \exp[-(v - v_{d_e})^2/c_{i_e}^2]. \tag{32}$$

c_i is related to the ion temperature through $c_i^2 = 2\kappa T_i/m_i$ and similarly $c_{i_e}^2 = 2\kappa T_{i_e}/m_i$. The propagation properties can be calculated for various values of the parameters T_e/T_i, v_d/c_i, v_{d_e}/c_i, and T_i/T_{i_e}.

III. DISCUSSION OF NUMERICAL RESULTS

In this section we show and discuss a few results obtained from calculating the Green's functions given in Eqs. (23) and (27), and the wave propagation properties in Eqs. (29) and (30). We have chosen to present the calculations for a situation where the parameters in Eqs. (31) and (32) have the following values: $v_d/c_i = 3$, $v_{d_e}/c_i = 3$, and $T_i/T_{i_e} = 1$. Such values can be obtained in single-ended Q machines.[19] To show the effect of changing the electron to ion temperature ratio we have performed the calculations for various values of T_e/T_i. In an experiment performed in order to check the Green's functions[12] one can apply short pulses to a grid and measure the response as a function of time from a probe at some fixed position. We therefore present the calculated Green's function as a function of the dimensionless time, tc_i/x, rather than as a function of distance. The Green's functions, $f_G(x,v,t)$, as given in Eq. (27) are singular for $x = vt$. Experimentally, these functions can be measured by means of an electrostatic energy analyzer[12] which necessarily has a finite resolution. The signal $S_G(x,v_a,t)$ which we obtain from the analyzer when it is adjusted to measure a velocity v_a is therefore given by

$$S_G(x,v_a,t) \propto \frac{1}{v_a}\int_0^\infty v f_G(x,v,t)\exp[-(v - v_a)^2/v_r^2]\,dv. \tag{33}$$

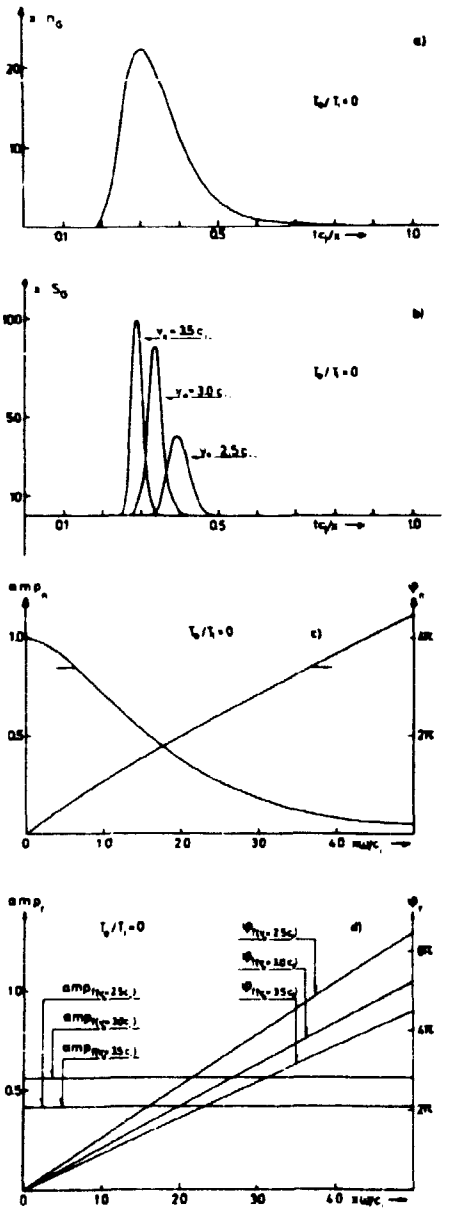

FIG. 2. Propagation through plasma with cold electrons, $T_e/T_i = 0$. (a) The Green's function for the density. (b) The analyzer signal $S_G(x, v_a, t)$ [see Eq. (33)] calculated for various v_a values. (c) Amplitude and phase of wave density. (d) Amplitude and phase of perturbed ion velocity distribution function in a wave.

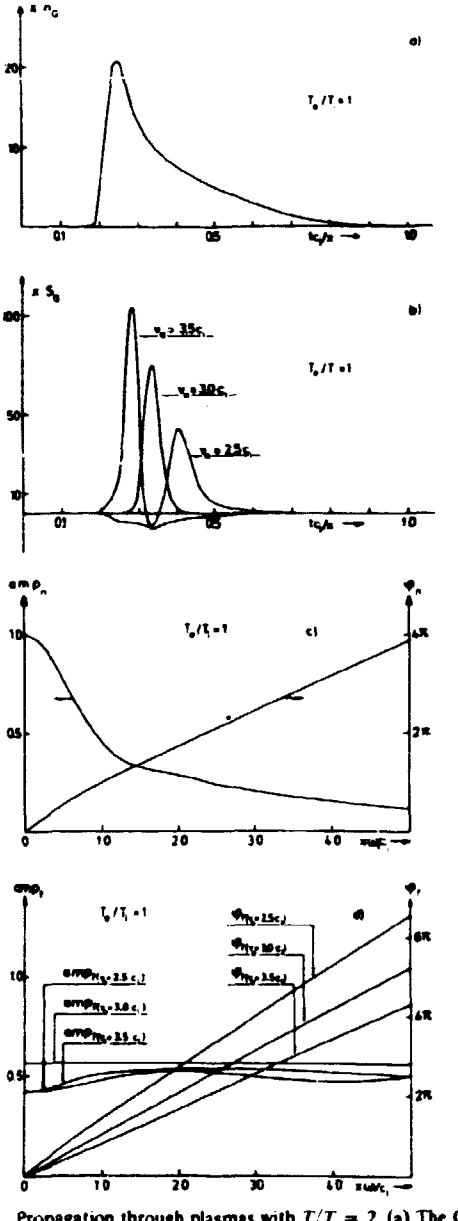

FIG. 3. Propagation through plasmas with $T_e/T_i = 2$. (a) The Green's function for the density. (b) The analyzer signal $S_G(x, v_a, t)$ [see Eq. (33)]calculated for various v_a values. (c) Amplitude and phase of wave density. (d) Amplitude and phase of perturbed ion velocity distribution function in a wave.

This equation is obtained under the assumption that the resolution of the analyzer is a Gaussian of the type $\exp[-(v - v_a)^2/v_r^2]$. The functions, S_G, shown in Figs. 2–4 are obtained for the case where $v_r = c_i/4$.

The curves amp$_n$ and ϕ_n showing the amplitude and the phase of the density, respectively, are calculated directly from Eq. (29) as functions of the dimensionless parameter $\omega x/c_i$. Similarly, the amplitude amp$_f$ and the phase ϕ_f of the perturbed distribution function in a wave are calculated from Eq. (30), also as functions of $\omega x/c_i$.

Figure 2 shows the results obtained for the case of freely streaming ions where $T_e/T_i = 0$. In Fig. 2(a) we present the Green's function, n_G, for the density and in Fig. 2(b) the S_G function calculated for three v_a values. Figures 2(c) and (d) show the amplitude and the phase of the density and of the distribution function in a wave, respectively. The wave damping in this case is clearly caused by phase-mixing of freely streaming ions.

In Fig. 3 we show the corresponding curves obtained for the case $T_e/T_i = 1$. We notice that the most significant difference between the curves in Fig. 2 and the ones in Fig. 3 is the undershoot seen on the S_G curves in Fig. 3(b). This undershoot, which is a clear-cut signature of the collective interaction term in Eq. (3), was demonstrated experimentally in Ref. 12 and a physical explanation was

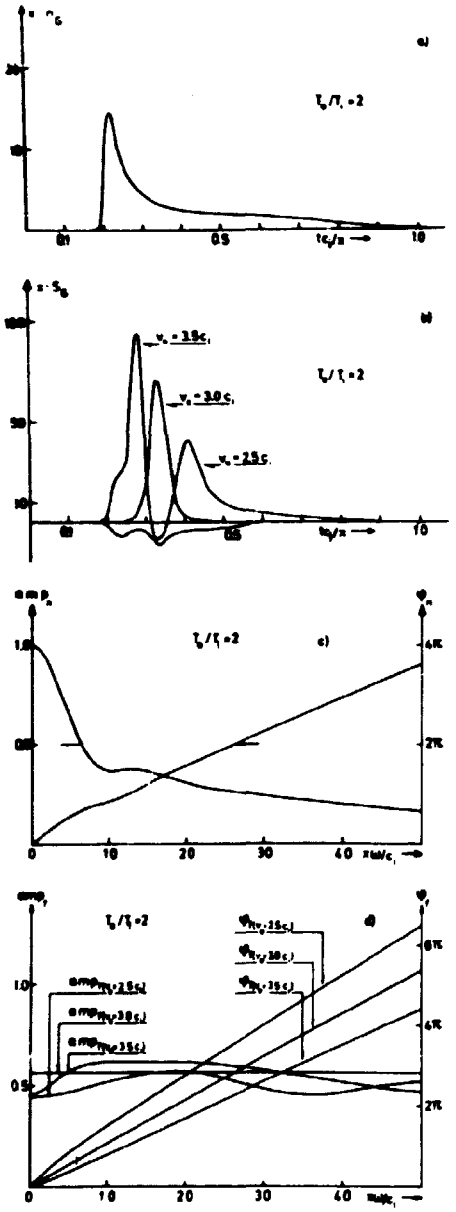

FIG. 4. Propagation through plasmas with $T_e/T_i = 2$. (a) The Green's function for the density. (b) The analyzer signal $S_G(x, v_a, t)$ [see Eq. (33)] calculated for various v_a values. (c) Amplitude and phase of wave density. (d) Amplitude and phase of perturbed ion velocity distribution function in a wave.

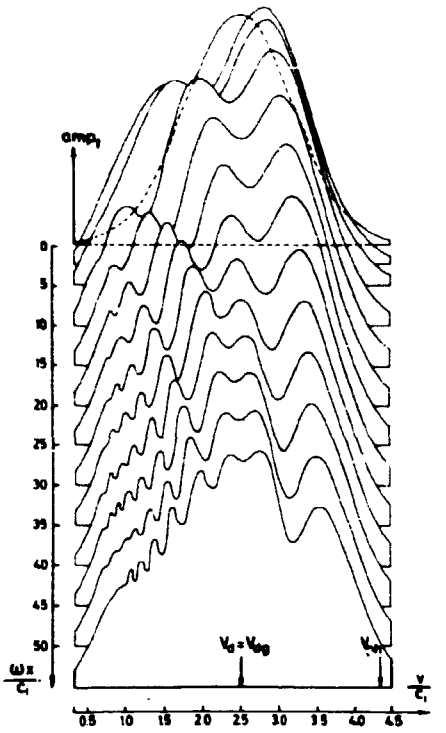

FIG. 5. Curves showing the amplitude of the perturbed ion velocity distribution function at various positions calculated for a plasma where $T_e/T_i = 3$, $v_d = v_{dg} = 2.5c_i$, and $T_i/T_g = 1$.

given in Ref. 20. The curves in Fig. 3(c) and (d), showing the wave characteristics, are so similar to the corresponding ones in Figs. 2(c) and (d) that it seems unlikely that collective interaction in ion-acoustic waves can be demonstrated experimentally if $T_e \lesssim T_i$. The damping is, in this case, of course, partly due to phase mixing and partly to collective interaction.

The curves in Fig. 4 are calculated for $T_e/T_i = 2$. Here, we note a tendency in the n_G curve to show two maxima. This is a significant change in comparison with the corresponding results in Fig. 2(a) and 3(a). The physical reason for this splitting up has been discussed in some detail in Ref. 16. The two maxima in the n_G curve are responsible for the tendency of the amp$_n$ curve in Fig. 4(c) to oscillate with distance. This oscillation can be understood physically as a beating between two damped waves propagating with velocities corresponding to the velocity of the two maxima in the n_G curve.[16,17] We also note a clear difference between the amp$_f$ curve in Fig. 4(d) and that in Fig. 2(d). This difference is also a clear sign of collective interaction. In Fig. 5 we show examples of amp$_f$ curves calculated as functions of v/c_i at various $\omega x/c_i$ values for the case where $T_e/T_i = 3$, $v_d = v_{dg} = 2.5c_i$, and $T_i/T_g = 1$. The very characteristic oscillations of the curves are explained physically in Refs. 17 and 18. An experimental observation of these oscillations would constitute a clear-cut sign of collective interaction in ion acoustic waves.

More extensive discussions of the physical mechanism explaining the results obtained by calculating the Green's functions and the wave characteristics are given in Refs. 15–18, and 20. It should be noted that the calculations in Refs. 16 and 20 are based on the Green's functions of Ref. 12 which were obtained for an initial value problem. A comparison between the Green's functions of Ref. 12 and those obtained for a boundary value problem in this paper shows that the functions are very similar and that they have the same characteristic dependences of the parameters. Therefore, the discussions given in Refs. 16 and 20 are also valid for waves treated as a boundary value problem.

IV. EXPERIMENTAL RESULTS

In this section we describe measurements of the perturbed ion velocity distribution in ion waves in a single-ended Q machine. The experimental setup is shown

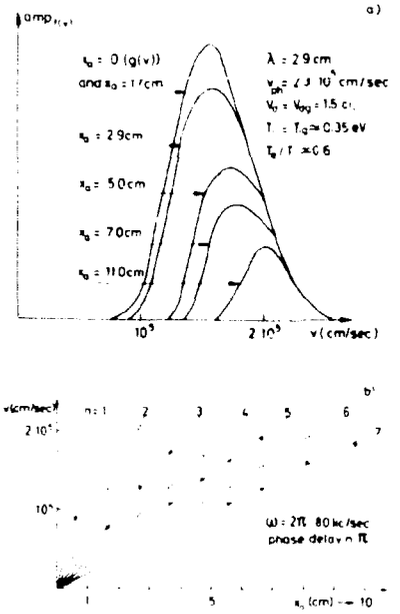

FIG. 6: Experimental set up.

schematically in Fig. 6. The plasma is produced by surface ionization of a beam of cesium atoms from the Cs oven on the hot tantalum plate ($\approx 2500°K$) and is radially confined by a uniform, magnetic field of an intensity up to 1 T. The plasma column is 3 cm in diameter and it ends at an electrostatic ion energy analyzer[19] at $x = x_a$. In the experiments to be described here the plasma density, n_0, is less than $10^9 cm^{-3}$, i.e., the plasma can be considered as being collisionless. The vacuum system consists of a stainless steel tube (not shown in Fig. 6) which is cooled to $-20°C$ to reduce the Cs background pressure. In operation the pressure is below 10^{-5} Torr. The plasma waves studied in this work were excited by a grid at $x = 0$. The grid consists of a thin nickel mesh with 400 0.5×0.5 mm² holes per cm².

The experimental procedure is as follows: First, the desired undisturbed ion velocity distribution function, $f_0(v)$, is obtained by adjusting the temperature of the hot plate and the density of the Cs beam. The grid is biased to a potential ϕ_0 which is close to the floating potential and $f_0(v)$ is measured by the analyzer by using the technique described in Ref. 19. The grid potential is now changed by a small amount $\Delta\phi$ to $\phi_0 + \Delta\phi$ and the velocity distribution $f_0(v) + g(v)$ is measured. The function $g(v)$ can then be obtained by using the technique described in Ref. 14.

Now the grid is connected to the oscillating signal $[\exp(i\omega t)]$ of a lock-in amplifier as shown in Fig. 6. Thereby a wave with frequency ω is launched; this wave is analyzed by the electrostatic analyzer. For the measurements of the perturbed velocity distribution function, the circuit shown in Fig. 6 was used. The analyzer grid is biased negatively with respect to the plasma potential ϕ_{pl} in order to reflect all electrons. The collector plate is connected to a sweep-box which varies the plate potential ϕ_a slowly and linearly with time as indicated in the figure. The time varying part of the ion current to the collector plate, when biased to ϕ_a, is given by

$$I(\phi_a, t) = qA \int_{v_{min}}^{\infty} v f(x_a, v, t)\, dv, \tag{34}$$

where $\frac{1}{2}mv_{min}^2 = q(\phi_a - \phi_{pl})$ and A is the effective mesh area. By changing the variable: $v^2 = (2q/m)(\phi - \phi_{pl})$. Eq. (34) becomes

$$I(\phi_a, t) = \text{const} \int_{\phi_a}^{\infty} f(x_a, \phi, t)\, d\phi; \tag{35}$$

this is the signal led from the sweep-box to the lock-in amplifier in Fig. 6. The lock-in amplifier amplifies the part of this signal which oscillates with the frequency ω and thus produces a signal

$$S(\phi_a) = \frac{1}{\Delta T}\int_0^{\Delta T} I(\phi_a, t) \exp[i(\omega t - \theta_0)]\, dt$$

$$= \frac{\text{const}}{\Delta T}\int_0^{\Delta T} \exp[i(\omega t - \theta_0)]\, dt \int_{\phi_a - \phi_{pl}}^{\infty} f(x_a, \phi, t)\, d\phi. \tag{36}$$

θ_0 is a phase angle adjustable on the amplifier. $S(\phi_a)$ is led to the differential unit and differentiated with respect to time. The output signal, which is led to the y plates of the scope and displayed as a function of ϕ_a, is

$$\frac{dS(\phi_a)}{dt} = \frac{dS(\phi_a)}{d\phi_a}\frac{d\phi_a}{dt}$$

$$= -\frac{\text{const}}{\Delta T}\frac{d\phi_a}{dt}\int_0^{\Delta T} \exp[i(\omega t - \theta_0)]\, f(x_a, \phi_a - \phi_{pl}, t)\, dt$$

$$\propto \left| f\left[x_a, v = \left(\frac{2q(\phi_a - \phi_{pl})}{m}\right)^{1/2}\right] \right|$$

$$\times \exp\{i[\theta(\phi_a - \phi_{pl}) - \theta_0]\}. \tag{37}$$

$d\phi_a(t)/dt$ is a constant because $\phi_a(t)$ as generated by the sweep-box is proportional to time. The electric circuit only works the way discussed if the time constants for differentiation, integration, voltage sweeping, and for the wave are chosen properly.

Experimental measurements of $\text{amp}_f = |f(x_a, v = (2q(\phi_a - \phi_{pl})/m)^{1/2})|$ and of $\phi_f = \theta(\phi_a - \phi_{pl})$ are obtained by varying θ_0 on the lock-in amplifier until amp_f as displayed on the oscilloscope reaches its maximum value for a given ϕ_a. As seen from Eq. (37) it is possible to convert the measured quantities, amp_f and ϕ_f, into functions of velocity only if the effective analyzing potential, $\phi_a - \phi_{pl}$, is known. Experimentally, we have determined ϕ_{pl} by utilizing the technique described in Ref. 19.

In Fig. 7 we show experimental results obtained for a situation where $f_0(v)$ and $g(v)$ were found to be close to Maxwellian distribution functions with drift velocities $v_d = v_{dg} = 1.5c_i$, $T_i = T_g \simeq 0.35$ eV, and $T_i/T_i \simeq 0.6$. The density $n_0 \simeq 10^9 cm^{-3}$ and the frequency, $\omega/2\pi$, applied to the exciting grid was 80 kc/sec. The phase velocity and

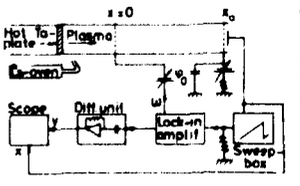

FIG. 7. Experimental results obtained in measurements on an ion acoustic wave with frequency 80 kc/sec. (a) The amplitude of the perturbed ion velocity distribution function measured at various positions. (b) The phase delay of $f(x_a, v)$ measured at various positions.

the damping of the wave density were determined in the conventional way by measuring the amplitude and the phase of the ion saturation current ($\phi_a = \phi_{pl}$) to the analyzer collector at various positions. The phase velocity was found to be $v_{ph} = 2.3 \times 10^5$ cm/sec corresponding to a wavelength $\lambda = 2.9$cm. The wave amplitude damps with an e^{-1} – folding length of approximately one wavelength.

In Fig. 7(a) we present measurements of $\text{amp}_{f(v)}$ as functions of v obtained at various analyzer positions. Figure 7(b) shows experimentally obtained phase relations. At different x_a positions we have found those v values for which $f(x_a, v)$ is delayed $n \times \tau$ with respect to the phase of the exciter (n is an integer). The results shown in the figure constitute an experimental verification of the phase relation $\exp(i\omega x_a/v_a)$, which is obtained directly from Eq. (30) by going to the limit $c_r = 0$, i.e., in the limit where collective interaction can be ignored. The small discrepancy ($\approx 10\%$) between the phase relation obtained from Eq. (30) and the experimental points can be explained by the uncertainty in the experimental determination of ϕ_{pl}, which causes an uncertainty in the calculation of v [see Eq. (37)].

According to Eq. (30), $\text{amp}_{f(v)}$ should be equal to $g(v)$ and independent of x_a if $c_r = 0$. The experimental results in Fig. 7(a) show a strong damping of $\text{amp}_{f(v)}$ with distance x_a especially for low v values. By using the following arguments based on freely streaming ions this damping can be explained by the finite resolution of the analyzer The ions are released from the grid with the velocity distribution function $g(v)\cos\omega t$. At $x = x_a$ the analyzer measures $\text{amp}_{f(v_a)}$ at the time $t_a = x_a/v_a$. At this time however, there are also ions present at x_a with the velocity v, and they are partly accepted by the analyzer because of its finite resolution expressed by $\exp[-(v - v_a)^2/v_r^2]$. The ions with velocity v were released from the grid at $t = t_a - x_a/v$. Therefore, the analyzer adjusted to measure at the velocity v_a gives a signal

$$S_{v_a} \propto \int_0^\infty v g(v) \cos\left[\omega\left(\frac{x_a}{v_a} - \frac{x}{v}\right)\right] \exp[-(v - v_a)^2/v_r^2]\, dv. \tag{38}$$

By assuming v_r to be small compared with c_r, $vg(v)$ can be considered as a constant and $v_a^{-1} - v^{-1} \simeq (v - v_a)/v_a^2$. After some simple algebra one gets

$$S_{v_a} \propto \exp\left[-\left(\frac{\omega x_a v_r}{2v_a^2}\right)^2\right]. \tag{39}$$

This expression explains the very strong damping measured at low v_a values.

Measurements such as the ones described here have been performed at various frequencies and densities, and with different $f_0(v)$ and $g(v)$ functions. The conclusions from all the measurements are that *no* sign of collective interaction could be demonstrated. This is what would be expected from the theoretical work of Secs. II and IV. It should be mentioned that similar measurements leading to the same conclusions were reported by Ikezi and Taylor.[21,22]

Further, we have heated the electrons in order to reach a T_e/T_i value around 3. The heating technique used has been described by Christoffersen and Prahm.[23] At these high-temperature ratios the characteristic oscillation in $\text{amp}_{f(v)}$ shown in Fig. 5 can be expected. We were not able to detect these oscillations experimentally. We believe that the reason is that the resolution of the analyzer is not sufficiently good.

V. DISCUSSION AND CONCLUSIONS

In this paper we have calculated the Green's functions for the linearized ion Vlasov equation for a known boundary value problem. The Green's functions for the density as well as for the perturbed velocity distribution function are obtained, and they are always found to take the self-similar form, $n_a, f_a = (1/t)h_{n_a,f_a}(x/t)$. The functions, $h_{n_a,f_a}(x/t)$, depend on the boundary value, $g(v)$, and on the dielectric properties of the plasma, which in turn depend on T_e and on the undisturbed ion velocity distribution function $f_0(v)$.

The Green's function for the density, $n_G(x,t)$, varies weakly with T_e/T_i as long as $T_e/T_i \lesssim 3$ (see Figs. 2, 3, and 4). Furthermore, it should be noted that the Green's function for the density obtained for the case where $T_e \neq 0$ could also be obtained for $T_e = 0$ if another $g(v)$ was assumed. The $g(v)$ function needed in order to produce a $n_G(x,t)$ function of a given form for a case without collective interaction can be calculated from Eqs. (12), (16), and (23) with $T_e = 0$. It is therefore clear that to demonstrate collective effects in a measurement of $n_G(x,t)$ would require a detailed knowledge of the boundary value function $g(v)$. In an actual experimental situation such knowledge is very difficult to obtain and it can, therefore, be concluded that it is very unlikely that collective effects can be demonstrated in measurements of $n_G(x,t)$.

For $T_e \neq 0$, the Green's functions for the perturbed velocity distribution function, $f_G(x,v,t)$ show the same characteristic features [the undershoots seen in Figs. 3(b) and 4(b)] which are clearly caused by collective interaction. The experimental observations of these features reported in Ref. 12 are therefore a clear demonstration of collective effects.

The propagation characteristics for locally excited ion acoustic waves were calculated by performing convolution integrals of the Green's functions. The calculations show that waves are, in general, damped. For $T_e = 0$, the damping is clearly caused solely by phase mixing of freely streaming ions and therefore the ratio, δ/λ, between the damping length and the wavelength is roughly given by $v_{ph}/\Delta v$ where Δv is the width of the $g(v)$ function. For $T_e \neq 0$, collective interaction plays a role in the wave damping. It should, however, be noted that by assuming the proper $g(v)$ function, one can get the same Green's function for the density for $T_e = 0$ as the one we get for $T_e \neq 0$. We can also obtain the same amp_n curve for the case where $T_e = 0$ as the one we obtain for $T_e \neq 0$. We may therefore conclude that density measurements in a wave are equally unlikely to demonstrate collective interaction as are measurements of $n_G(x,t)$. We can further point out that for the case $T_e \neq 0$, the damping ratio, δ/λ, is roughly determined by the width of the $n_a(x,t)$ function divided by the phase velocity of the wave. This

statement is in contradiction to the results obtained in a normal mode treatment where it is found that the damping is determined by the slope of the $f_0(v)$ function at $v = v_{ph}$. Our results suggest that some calculations of stability problems based on a normal mode treatment probably ought to be reconsidered. In this respect it should be noted that by using the Green's functions obtained in this work it has been possible to show rigorously that an exponentially damped wave of the normal mode form $\exp[-i(\omega t - kx)]$(Im $k > 0$) is *not* a possible solution to the Vlasov equation (3) for all values of x.[24] Further, it should be noted that Estabrook and Alexeff[25] have recently integrated the Vlasov equation numerically and found results that confirm our statement that collective interaction in ion acoustic waves is negligible.

Our calculations of the perturbed velocity distribution function in a wave show that the effect of collective interaction is very weak unless $T_e \gtrsim 3T_i$. At these relatively high values of the electron temperature, characteristic oscillations in $\text{amp}_{f(\omega)}$, as seen in Fig. 5, occur. These oscillations have not been seen experimentally, but the observations of them would constitute a clear signature of the collective effect in ion acoustic waves.

As a last remark it should be emphasized that in our treatment we have assumed the perturbed velocity distribution function at the boundary to take the form $g(v)\exp(-i\omega t)$. We believe that this assumption holds for grid-excited waves in single-ended Q machines as long as $\omega \ll \omega_{pi}^{12}$. At higher frequencies the potential around the grid varies significantly during the transit time for an ion moving through the sheath around the grid. Therefore, the g function will most likely also become a function of time, i.e., take the form $g[v, \exp(i\omega t)]$, which means that higher harmonics are generated. As long as we are only concerned with the fundamental mode this will not change the main features of our results.

The experimental results reported in this paper are in agreement with our statement that collective effects are negligible in ion-acoustic waves if $T_e \lesssim 3T_i$.

ACKNOWLEDGMENTS

The authors want to thank A. S. Jensen for pointing out the possibility of using the technique in Sec. II for performing the inverse Laplace–Fourier transformations. The helpful discussions and assistance with the numerical computations of H. C. S. Hsuan, H. Pécseli, P. I. Petersen, and L. P. Prahm are acknowledged. Finally, we would like to thank M. Nielsen and B. Reher for help in the experiments and for maintaining the Q device.

[1] A. Y. Wong, R. M. Motley, and N. D'Angelo, Phys. Rev. 133, A436 (1964).
[2] N. Sato, H. Ikezi, N. Takahashi, and Y. Yamashita, Phys. Rev. 183, 278 (1969).
[3] P. Korn, T. C. Marshall, and S. P. Schlesinger, Phys. Fluids 13, 517 (1970).
[4] H. J. Doucet and D. Gresillon, Phys. Fluids 13, 773 (1970).
[5] G. Joyce, K. Lonngren, I. Alexeff, and W. D. Jones, Phys. Fluids 12, 2592 (1969).
[6] L. D. Landau, J. Phys. USSR 10, 25 (1946).
[7] V. O. Jensen, Risø Report No. 54 (1962).
[8] R. W. Gould, Phys. Rev. 136, A991 (1964).
[9] H. Weitzner, Phys. Fluids 6, 1123 (1963).
[10] H. Weitzner and D. Dobrott, Phys. Fluids 11, 152 (1968).
[11] H. Weitzner, in *Magnetic-Fluid and Plasma Dynamics*, edited by H. Grad (American Mathematical Society, Providence, Rhode Island 1967) p. 127.
[12] S. A. Andersen, G. B. Christoffersen, V. O. Jensen, P. Michelsen, and P. Nielsen, Phys. Fluids 14, 990 (1971).
[13] J. L. Hirschfield and J. H. Jacob, Phys. Fluids 11, 411 (1968).
[14] G. B. Christoffersen, in *Proceedings of the Third International Conference on Quiescent Plasmas* (Danish Atomic Energy Commission, Risø, Denmark, 1971), p. 55.
[15] G. B. Christoffersen, V. O. Jensen, and P. Michelsen, in *Proceedings of the Third International Conference on Quiescent Plasmas* (Danish Atomic Energy Commission, Risø, Denmark, 1971) p. 63.
[16] V. O. Jensen, in *Proceedings of the Third International Conference on Quiescent Plasmas* (Danish Atomic Energy Commission, Risø, Denmark, 1971), p. 87.
[17] V. O. Jensen and P. Michelsen, Risø Report No. 257, 1972.
[18] G. B. Christoffersen, V. O. Jensen, and L. P. Prahm, in *Proceedings of the Fifth European Conference on Controlled Fusion and Plasma Physics* (Euratom CEA, Grenoble, 1972), Vol. 1, p. 175
[19] S. A. Andersen, V. O. Jensen, P. Michelsen, and P. Nielsen, Phys. Fluids 14, 728 (1971).
[20] S. A. Andersen, V. O. Jensen, P. Michelsen, and P. Nielsen, Phys. Lett. A32, 413 (1970).
[21] H. Ikezi and R. J. Taylor, Phys. Lett. 22, 923 (1969).
[22] H. Ikezi and R. J. Taylor, Phys. Fluids 13, 2348 (1970).
[23] G. B. Christoffersen and L. P. Prahm, Plasma Phys. 14, 1140 (1972).
[24] H. C. S. Hsuan and V. O. Jensen, Phys. Fluids 16, 1776 (1973).
[25] K. Estabrook and I. Alexeff, Phys. Rev. Lett. 29, 573 (1972).

6. Absolute and convective ion beam instability studied through Green's function

V. O. Jensen and P. Michelsen
Association Euratom-AEK, Danish Atomic Energy Commission, Research Establishment Risø, Roskilde, Denmark

Hulbert C. S. Hsuan*
Department of Electrical Engineering, University of Iowa, Iowa City, Iowa 52240

(Received 27 December 1973; final manuscript received 3 June 1974)

A Vlasov plasma with a double-humped, unstable ion velocity distribution function is considered. A δ function in space is assumed as the initial perturbation and the plasma response to this perturbation is calculated, i.e., the Green's function for the problem is found. The response can be divided into two parts: a self-similar, damped part of the form $t^{-1}h(x/t)$, and an unstable, exponentially growing part. The conditions for absolute and convective growth of the latter are discussed.

I. INTRODUCTION

During the past fifteen years great interest has been shown in the problem of growing waves in unstable plasmas. Sturrock[1,2] has performed pioneer work in this field by classifying the possible types of instabilities as evanescent, convective, or nonconvective (absolute) and by discussing the conditions under which the various types can be expected. Many authors[3–7] have considered unstable waves and described in detail various mathematical techniques used to treat the problem. In a recent paper, Rognlien and Self[8] include a review chapter on most of the work in this field; in their work references to many other interesting papers can be found.

Our interest in this problem is caused by the possibility of creating, in Q machines, a plasma with a double-humped ion velocity distribution function which is unstable to the ion acoustic wave mode.[9] This plasma provides the unique experimental possibility of following in detail the development in time and space of an instability which started as a narrow perturbation at $(x, t) = (0, 0)$. In this paper we present calculations based on the linearized Vlasov equation of the development of such a perturbation in an unstable plasma of the type obtainable in Q machines, i.e., we calculate the Green's function for the equations describing wave propagation through the plasma.

As is often found in this kind of treatment, some parts of the wavelength or frequency spectrum of the wave mode under consideration are unstable (growing) and other parts are stable (damped). In most treatments only the growing waves are considered because they are argued to be the predominant ones in the limit of large times or distances where experiments are most readily performed. We show that in a Q machine plasma it should be possible to detect the contribution from the stable waves and that from the unstable waves separately. The contribution from the stable waves dies away in a self-similar fashion as $t^{-1}h(x/t)$ as described elsewhere.[10,11] The contribution from the unstable waves is found to be absolutely unstable in some frames of reference and convective in others, and normally convective in the frame which follows the bulk of the self-similar stable wave contribution, as well as in the laboratory frame. We show that our results are in qualitative agreement with the experimental results of Baker[12,13] and that they therefore constitute an alternative explanation of his observations.

II. ANALYSIS

As in previous calculations[10,11] we describe the ions by their linearized Vlasov equation. We choose to model the electrons by a massless isothermal fluid. The electrons and the ions are coupled through the Poisson equation, and we consider a one-dimensional situation. Thus, our starting equations are

$$\frac{\partial f(x, v, t)}{\partial t} + v\frac{\partial f(x, v, t)}{\partial x} = \frac{c_s^2}{n_0}\frac{\partial n_e(x, t)}{\partial x}\frac{df_0(v)}{dv}, \tag{1}$$

$$\lambda_D^2\frac{\partial^2 n_e(x, t)}{\partial x^2} = n_e(x, t) - n_i(x, t), \tag{2}$$

and

$$n_i(x, t) = \int_{-\infty}^{\infty} f(x, v, t)dv. \tag{3}$$

Here,

$$c_s^2 = \kappa T_e/m_i, \quad n_0 = \int_{-\infty}^{\infty} f_0(v)dv$$

is the uniform unperturbed density for both ions and electrons, $\lambda_D = (\epsilon_0\kappa T_e/n_0e^2)^{\frac{1}{2}}$ is the electron Debye length, and $n_e(x, t)$ is the perturbed electron density.

Let us consider the response of the system to an initial perturbation with an ion velocity destribution

$$f(x, v, t = 0) = g(v)\frac{1}{\pi}\frac{\alpha}{x^2 + \alpha^2}, \tag{4}$$

where α is a scale length representing the size of the initial perturbation. This form of the initial perturbation is chosen for mathematical convenience since $\pi^{-1}\alpha(\alpha^2 + x^2)^{-1}$ is a normal representation of a delta function, $\delta(x)$, in the limit of α going to zero.

We use a standard Laplace-Fourier transform technique to solve (1)–(3) with initial condition (4). The transform is defined so that

$$F(k, \omega) = \int_{-\infty}^{\infty}\exp(-ikx)\int_0^{\infty}\exp(i\omega t)F(x, t)\,dt\,dx$$

and

$$F(x,t) = (2\pi)^{-2}\int_{-\infty}^{\infty}\exp(ikx)\int_{a}\exp(-i\omega t)F(k,\omega)d\omega\,dk,$$

where $F(x,t)$ can be any of the three functions: $f(x,v,t)$, $n_e(x,t)$, or $n_i(x,t)$. The integral contour in the ω plane indicated by the index a runs above any of the poles of $F(k,\omega)$. The following relation can be shown, in general, from the reality condition, i.e., from the condition that $F(x,t)$ has to be a real quantity.

$$F(-k^*,-\omega^*) = [F(k,\omega)]^*,$$

where the asterisk (*) denotes the complex conjugate. With this relation it is easy to prove that

$$F(x,t) = \frac{1}{2\pi^2}\,\mathrm{Re}\int_0^{\infty}\int_{a}F(k,\omega)\exp(-i\omega t+ikx)d\omega\,dk.$$

Re stands for the "real part of."

Straightforward algebra leads to the relation

$$n_e(k,\omega) = -\frac{i}{k}\left(\frac{I(\omega/k)}{1+(k\lambda_D)^2-P(\omega/k)}\right)e^{-\alpha|k|},$$

where $I(\omega/k)$ is related to the initial condition through

$$I\left(\frac{\omega}{k}\right) = \int_{-\infty}^{\infty}\frac{g(v)}{v-(\omega/k)}dv, \tag{5}$$

and where $P(\omega/k)$ is related to the plasma properties through

$$P\left(\frac{\omega}{k}\right) = \frac{c_s^2}{n_0}\int_{-\infty}^{\infty}\frac{f_0'(v)}{v-(\omega/k)}dv. \tag{6}$$

For $n_e(x,t)$ we get

$$n_e(x,t) = \frac{1}{2\pi^2}\,\mathrm{Im}\int_0^{\infty}\int_{a}\frac{1}{k}\frac{I(\omega/k)}{1+(k\lambda_D)^2-P(\omega/k)} \times\exp(-i\omega t+ikx-\alpha k)d\omega\,dk, \tag{7}$$

where Im represents the "imaginary part of."

In Ref. 10 we obtained an expression similar to (7) except for the $(k\lambda_D)^2$ term. This term only enters here because of our use of the Poisson equation (2) rather than the quasineutrality condition assumed in the former work. In Ref. 10 we considered stable plasmas, i.e., plasmas for which the equation

$$1+(k\lambda_D)^2-P(\omega/k) = 0 \tag{8}$$

has no solutions in the complex ω plane for which $\mathrm{Im}\omega > 0$. By using this we could move the ω integration path down to the real axis, and we found that the density always took the self-similar form $t^{-1}h(x/t)$. In this paper we consider unstable plasmas for which (8) has only one solution, $\omega(k)$, with $\mathrm{Im}\omega > 0$ for a fixed k. This solution is found for k values in the interval $0 < k < k_m$ and $\mathrm{Im}\omega(0) = \mathrm{Im}\omega(k_m) = 0$.[3] Using this we can write (7) in the form

$$n_e(x,t) = n_{es}(x,t) + n_{eu}(x,t), \tag{9}$$

where

$$n_{es}(x,t) = \frac{1}{2\pi^2}\,\mathrm{Im}\int_0^{\infty}\int_{-\infty}^{\infty}\frac{1}{k}\frac{I(\omega/k)}{1+(k\lambda_D)^2-P(\omega/k)} \times\exp(-i\omega t+ikx-\alpha k)d\omega\,dk \tag{10}$$

and

$$n_{eu}(x,t) = \mathrm{Re}\frac{1}{\pi}\int_0^{k_m}\left[\frac{I(\omega/k)}{k[\partial P(\omega/k)/\partial\omega]}\right]_{\omega=\omega(k)} \times\exp[-i\omega(k)t+ikx-\alpha k]dk. \tag{11}$$

In (11) the function $\omega(k)$ is to be determined by (8). The stable contribution, $n_{es}(x,t)$, is essentially of the form obtained in Ref. 10. The unstable contribution, $n_{eu}(x,t)$, is of the general type treated by several authors.[1-8] In the following we discuss the two contributions separately.

A. The stable contribution

Since $P(\omega/k)$ and $I(\omega/k)$ are known functions as given by (5) and (6), $n_{es}(x,t)$ can be calculated by numerical computation from (10). This computation, however, is rather involved because we have to perform a triple integration over k, ω, and v for each (x,t) value for which we want to calculate n_{es}. Rather than performing such integrations, we show that in the limit of large t, where experiments are most likely to be possible, the $(k\lambda_D)^2$ term in the denominator is of no importance and can therefore be neglected, which simplifies (10) considerably. To neglect the $(k\lambda_D)^2$ term is equivalent to assuming quasineutrality rather than using (2).[10]

In (10) we substitute $v_p = \omega/k$ and find

$$n_{es}(x,t) = \frac{1}{2\pi^2}\,\mathrm{Im}\int_0^{\infty}\int_{-\infty}^{\infty}\frac{I(v_p)}{1+(k\lambda_D)^2-P(v_p)} \times\exp\left[-ikt\left(v_p-\frac{x+i\alpha}{t}\right)\right]dv_p\,dk. \tag{12}$$

This form suggests an asymptotic expansion of $n_{es}(x,t)$ in terms of t^{-1}. We substitute $y = kt$ and expand $n_{es}(k,v_p) = I(v_p)[1+(k\lambda_D)^2-P(v_p)]^{-1}$ in terms of t^{-1} as follows:

$$n_{es}(k,v_p) = n_{es}(0,v_p) + \left(\frac{y}{t}\right)^2\left.\frac{\partial n_{es}}{\partial(k^2)}\right|_{k^2=0} + O\left(\frac{1}{t^4}\right)$$

$$= \frac{I(v_p)}{1-P(v_p)} - \left(\frac{y}{t}\right)^2\lambda_D^2\frac{I(v_p)}{[1-P(v_p)]^2} + O\left(\frac{1}{t^4}\right).$$

Equation (12) can now be rewritten as

$$n_{es}(x,t) = \frac{1}{2\pi^2 t}\,\mathrm{Im}\int_0^{\infty}\int_{-\infty}^{\infty}\frac{I(v_p)}{1-P(v_p)} \times\exp\left[-iy\left(v_p-\frac{x+i\alpha}{t}\right)\right]dv_p\,dy + \frac{1}{2\pi^2}\frac{\lambda_D^2}{t} \times\mathrm{Im}\left\{\frac{\partial^2}{\partial x^2}\int_0^{\infty}\int_{-\infty}^{\infty}\frac{I(v_p)}{[1-P(v_p)]^2} \times\exp\left[-iy\left(v_p-\frac{x+i\alpha}{t}\right)\right]dv_p\,dy\right\} + O\left(\frac{1}{t^4}\right). \tag{13}$$

In writing the second term in (13) we made use of the fact that

$$\int_0^\infty (y/t)^2 \exp(iyx/t)dy$$

can be replaced by

$$-\partial^2/\partial x^2 \int_0^\infty \exp(iyx/t)dy.$$

Performing the y integration we obtain

$$n_{es}(x,t) = \frac{1}{2\pi^2 t} \times \mathrm{Im}\int_{-\infty}^{\infty} \frac{I(v_p)}{[1-P(v_p)]i\{v_p - [(x+i\alpha)/t]\}} dv_p + \frac{1}{2\pi^2}\frac{\lambda_D^2}{t}\mathrm{Im}\left(\frac{\partial^2}{\partial x^2} \times \int_{-\infty}^{\infty} \frac{I(v_p)}{[1-P(v_p)]i\{v_p - [(x+i\alpha)/t]\}} dv_p\right) + O\left(\frac{1}{t^3}\right). \tag{14}$$

By closing the v_p integration paths around the upper half of the v_p plane we get, by means of residue calculations,

$$n_{es}(x,t) = \frac{1}{t}F_1\left(\frac{x}{t}\right) + \frac{\lambda_D^2}{t^3}F_2\left(\frac{x}{t}\right) + O\left(\frac{1}{t^5}\right),$$

where

$$F_1\left(\frac{x}{t}\right) = \lim_{\alpha\to 0}\frac{1}{\pi}\mathrm{Im}\left(\frac{I[(x+i\alpha)/t]}{1-P[(x+i\alpha)/t]} - \frac{I(u_p)}{\{u_p - [(x+i\alpha)/t]\}P'(u_p)}\right),$$

and

$$F_2\left(\frac{x}{t}\right) = \lim_{\alpha\to 0}\frac{1}{\pi}\mathrm{Im}\left\{\frac{d^2}{d(x/t)^2}\left[\frac{I[(x+i\alpha)/t]}{\{1-P[(x+i\alpha)/t]\}^2} + \left(\frac{1}{P'^2(u_p)}\frac{d}{dv_p}\frac{I(v_p)}{\{v_p - [(x+i\alpha)/t]\}}\right)_{v_p=u_p}\right]\right\}.$$

In these equations u_p is defined by the solution to the equation $1 - P(u_p) = 0$.

It is seen that in the limit of long time ($t \gg \omega_{pi}^{-1}$), the first term in (14) is the predominant one. Since we shall only be interested in this limit, we write

$$n_{es}(x,t) = \frac{1}{t}\lim_{\alpha\to 0}\frac{1}{\pi}\mathrm{Im}\left(\frac{I[(x+i\alpha)/t]}{1-P[(x+i\alpha)/t]} - \frac{I(u_p)}{\{u_p - [(x+i\alpha)/t]\}P'(u_p)}\right). \tag{15}$$

This equation, which will be used for numerical calculations, is identical to what we would have obtained if we had assumed quasineutrality rather than introduced the Poisson equation, (2). We have thus shown that the quasineutrality assumption is good in the limit where $t \gg \omega_{pi}^{-1}$.

$n_{es}(x,t)$ as given by (15) takes a self-similar form as t^{-1} times some function of (x/t); this is a property which was found for stable distribution functions in Ref. 10. The first term in the large parentheses of (15) is equal to the expression obtained in Ref. 10. The last term is an extra contribution caused by the pole in the upper half of the v_p plane. It could be argued that this contribution should rather be included in the unstable part of $n_e(x,t)$ [Eq. (9)]. We decided to keep it as part of $n_{es}(x,t)$ because of its self-similar form.

B. The unstable contribution

In order to calculate $n_{eu}(x,t)$ from (11) we need to find the spectrum of unstable waves, $\omega(k)$, from (8). The wavenumber, k_m, of the marginally stable wave is determined by

$$1 + (k_m\lambda_D)^2 - \frac{c_e^2}{n_0}\int_{-\infty}^{\infty}\frac{f_0'(v)}{v - [\omega(k_m)/k_m]}dv = 0. \tag{16}$$

We introduce $v_0 = \omega(k_m)/k_m$, which is the phase velocity of the marginally stable wave. As v_0 is a real number we have, directly from (16),

$$f_0'(v_0) = 0. \tag{17}$$

An appropriate formula for $\omega(k)/k$ can be obtained by a Taylor expansion of (8) around v_0

$$\frac{\omega(k)}{k} = v_0 + z \tag{18}$$

$$1 + (k\lambda_D)^2 - \frac{c_e^2}{n_0}\int_{-\infty}^{\infty}\frac{f_0'(v)}{v - v_0}dv - z\frac{c_e^2}{n_0}\int_{-\infty}^{\infty}\frac{f_0''(v)}{v - v_0}dv = 0. \tag{19}$$

From (16), (18), and (19) we get

$$\omega(k) = k\left[v_0 + \frac{k_m^2 - k^2}{\omega_{pi}^2}A(v_0)\right], \tag{20}$$

where ω_{pi} is the ion plasma frequency and where $A(v_0)$ is defined by

$$A(v_0)^{-1} \equiv -\lim_{\epsilon\to 0+} n_0^{-1}\int_{-\infty}^{\infty}\frac{f_0''(v)}{v - v_0 - i\epsilon}dv. \tag{21}$$

Equations (11) and (20) constitute the basis for the numerical calculations of $n_{eu}(x,t)$ reported in the next section.

The instability under consideration is triggered at $(x,t) = (0,0)$. An observer moving through the plasma with a velocity within a certain interval, v_- to v_+, will find that the instability grows at all times, i.e., that the instability is absolute. For velocities outside this interval the instability is convective. In finding v_+ and v_- we roughly follow the procedure given by Baldwin and Rowlands.[7]

We insert (20) into (11) and get

$$n_{sw}(x,t) = \frac{1}{\pi}\,\mathrm{Re}\frac{I(v_0)}{P'(v_0)} \times \int_0^{k_m} \exp\left\{ikx - ikt\left[v_0 + \frac{k_m^2 - k^2}{\omega_{pi}^2}A(v_0)\right]\right\}dk. \quad (22)$$

Equation (22) is obtained by going to the limit $\alpha = 0$ and by assuming that the quantity in the bracket in (11) varies insignificantly with k in the interval 0 to k_m; this assumption certainly holds for weakly unstable plasmas where $k_m \ll \lambda_D^{-1}$. We want to calculate $n_{sw}(x,t)$ as felt by an observer moving through the plasma with the velocity, v, i.e., at the position $x(t) = vt$. Thus, we get

$$n_{sw}(x(t),t) = \mathrm{Re\ const}\int_0^{k_m} \exp\left\{ik\left[v - v_0 - \frac{k_m^2 - k^2}{\omega_{pi}^2}A(v_0)\right]t\right\}dk \equiv \mathrm{Re\ const}\int_0^{k_m} \exp[S(k)t]dk. \quad (23)$$

To determine for which velocities v the instability is absolute and for which it is convective we look for a curve in the complex k plane which connects $k = 0$ with $k = k_m$ and on which $\mathrm{Re}S(k) = 0$. If such a curve exists, we can change the integration contour into this curve; it is then clearly seen from Riemann's lemma that n_{sw} goes to zero for large t, i.e., that the instability is convective. If such a curve does not exist, the instability is absolute. For further discussion of this procedure, see Ref. 7.

In the appendix we describe a relatively simple procedure to determine for which v values we have absolute instability, and for which the instability is convective. We find that for v close to v_0 the instability is absolute, while v values very different from v_0 lead to convective instability. The limiting values, v_+ and v_-, are shown to be determined by the condition that $\mathrm{Re}S(k_s) = 0$. k_s are the k values for which $S(k)$ has saddle points.

III. NUMERICAL RESULTS AND DISCUSSION

Most authors who consider unstable waves are interested in growth rates and asymptotic expansions. Our Eq. (11) can also be used for this kind of analysis by leading to an expression for the density growth. Such an expansion, however, is of limited value because in an experiment a growing perturbation will soon reach a level where nonlinearities are important and an asymptotic expansion based on the results from the linear equations (1) to (3) becomes invalid. We study the initial linear growth of perturbations by performing numerical calculations of the stable as well as the unstable contribution discussed in the previous section.

We first consider the growing part of the solution, i.e., the expression in (11) which with the assumption $(k_m\lambda_D)^2 \ll 1$ can be reduced to (22). For simplicity, we shall assume that the ion velocity distribution functions $f_0(v)$ and $g(v)$ are symmetrical around $v = 0$ in some frame of reference. We shall solve the equations in this frame where from (17) we get $v_0 = 0$.

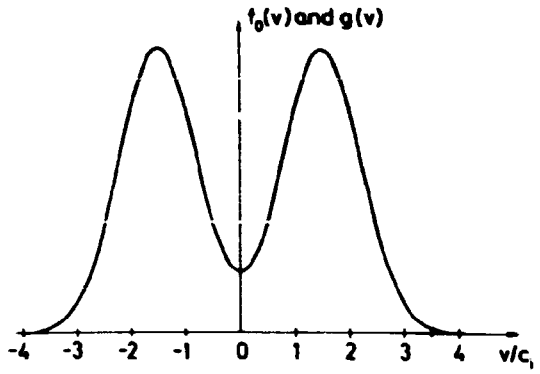

FIG. 1. The shape of the ion velocity distribution functions, $f_0(v)$ and $g(v)$, used in the numerical calculations.

$$f_0(v) \propto g(v) \propto \exp[-(v - v_d)^2/c_i^2] + \exp[-(v + v_d)^2/c_i^2]$$

is an example of such a distribution function; this function, which is shown in Fig. 1 for $v_d = 1.5c_i$ is used in the numerical calculations. From (21) we get that $A(0)$ is a purely imaginary quantity. From (22) we obtain the simplified integral

$$n_{sw}(x,t) = \frac{1}{\pi}\frac{I(0)}{P'(0)} \times \int_0^{k_m} \cos kx \exp\left[t\frac{\mathrm{Im}A(0)}{\omega_{pi}^2}k(k_m^2 - k^2)\right]dk. \quad (24)$$

Because the integrand has a maximum for $k = 3^{-\frac{1}{2}}k_m$, the wave with this wavenumber will have the largest growth rate, which can be found to be $3^{-\frac{1}{2}}2k_m^3\,\mathrm{Im}A(0)\omega_{pi}^{-2}$. This growth rate is in agreement with our numerical calculations of the expression (24) presented in Fig. 2. In the figure we show $n_{sw}(x)$ calculated for various values of the dimensionless time parameter, $\tau = \mathrm{Im}A(0)k_m^2\omega_{pi}^{-2}t$. For $t = 0$, we notice that $n_{sw}(x,t) \propto \sin k_m x/k_m x$ which is not the initial condition given by (4). This is, of course, because we have not included the term giving the stable contribution.

Using the procedure mentioned at the end of Sec. II on our simplified case we get, after straightforward algebra, $v_\pm = \pm\sqrt{3}k_m^2\,\mathrm{Im}A(0)\omega_{pi}^{-2}$. Also, this is in agreement with the numerical results shown in Fig. 2. From these results we get that an observer moving with a velocity in the interval between v_- and v_+ will see a growing perturbation, i.e., an absolute instability, while an observer with a velocity out-

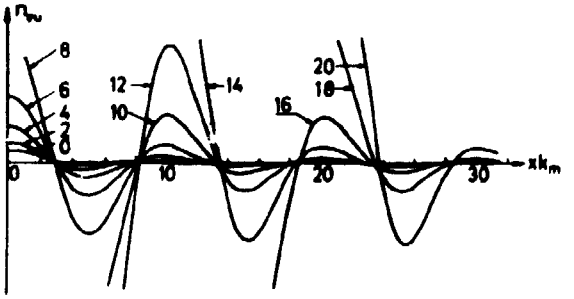

FIG. 2. Unstable contribution, $n_{sw}(x)$, at various times, versus distance xk_m. The dimensionless time τ written on the curves is given by $\tau = tk_m^2\,\mathrm{Im}A(0)\omega_{pi}^{-2}$.

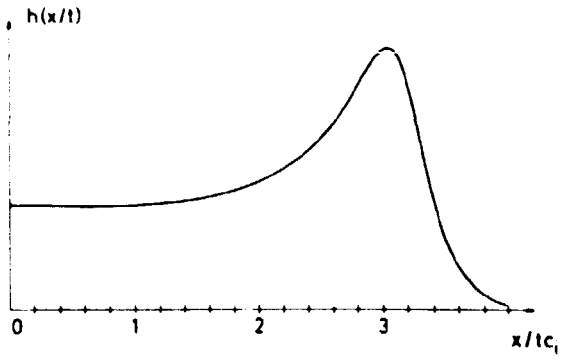

FIG. 3. The stable contribution, $h(x/t)$, for the case where $T_e/T_i = 4$ plotted as a function of $x/c_i t$.

side this interval will see a damped perturbation for sufficiently large t, i.e., a convective instability.

Let us now consider the stable part of the solution. This part is given by (15) and it can be written in the self-similar form $n_{es}(x, t) = t^{-1}h(x/t)$. We have calculated $h(x/t)$ numerically for a case where the ion velocity distribution functions, $f_0(v)$ and $g(v)$, again are the double-humped, symmetrical functions shown in Fig. 1. In order to insure that the plasma is unstable we have chosen $T_e/T_i = 4$.[14] In Fig. 3 we show the results as a function of $x/c_i t$, where $c_i^2 = 2\kappa T_i/m_i$.

We note that the stable contribution contains a positive pulse whose maximum moves through the plasma with a velocity about equal to $v_d + c_s$. Since in most cases this velocity is greater than v_+, which is the characteristic velocity of the front of the unstable contribution, it should be possible to experimentally observe the two contributions separately. Therefore, if the instability is observed at a fixed position in that frame of reference where $v_0 = 0$, the fast self-similar pulse from the stable contribution will arrive first and then the growing contribution from the unstable part will arrive and eventually dominate. The relative strength between $n_{eu}(x, t)$ and $n_{es}(x, t)$ depends on all the plasma parameters involved: $f_0(v), g(v), T_e/T_i$, and also on time and position of observation [see Eqs. (15) and (22)]. Since $n_{eu}(x, t)$ normally starts at a low level and $n_{es}(x, t)$ goes as t^{-1}, the latter term will in many cases be the predominant one at small times.

Baker[13] has examined the propagation of pulses excited by a grid in an unstable Q machine plasma with an ion velocity distribution function of the kind considered here. He actually sees two contributions: a fast damped pulse followed by a slower growing one. The main features of his observations are in agreement with our calculations. In order to claim that the Baker work constitutes an experimental verification of our theoretical results more detailed experimental work has to be performed. One feature that is likely to complicate such work is the fact that the propagation of the stable part of the pulse, $n_{es}(x, t)$, is independent of plasma density, while the unstable part, $n_{eu}(x, t)$, propagates in a way that depends on n_i [n_0 enters into (22) through ω_{pi}^2]. Therefore, in a Q machine plasma where there is necessarily a radial density gradient, the propagation of the unstable part will depend on radius, while the stable part propagates independently of radius.

The solution to Eqs. (1) to (3) with another initial condition, e.g., a wave, can, in principle, be found from our results by performing a convolution of the Green's function with the given initial condition. Although this method may be unnecessarily complicated, it can give us some information about the propagation of waves from our knowledge of the Green's function. For stable plasmas, the Green's function only contains the self-similar part, and a wave is known to be damped.[11] We may therefore conclude that in cases where we consider unstable plasmas and find that the self-similar part of the Green's function predominates over the unstable part, a wave will decay. It has been discussed that for small times the self-similar part can predominate ; in such cases a wave will start out as a decaying wave and only begin to grow when the unstable part of the Green's function becomes the predominant one. An effect of this kind, but for a boundary value problem, was observed experimentally by Christoffersen and Prahm.[15] Physically, the damping can be interpreted as a phase mixing of the particles in the initial density perturbation with the distribution function $g(v)$; only that part of $g(v)$ which corresponds to the distribution function in an unstable wave will grow.

To summarize, in this paper we have reported on a calculation of the development of a narrow perturbation in a plasma, unstable to an ion beam instability, i.e. we have found the Green's function for this problem. Our results are valid in a time period from a few times ω_{pi}^{-1} until the instability reaches a nonlinear level. We have determined in which frames of reference the instability is absolute and in which it is convective. In many cases a damped pulse will propagate faster than the region of instability, and this pulse can in the initial phase, depending on the excitation, have a considerable amplitude.

APPENDIX

We consider the complex function $S(k)$ of the complex variable, k [see Eq. (23)]

$$S(k) = i\left[k(v - v_0) - \frac{A(v_0)}{\omega_{pi}^2}k(k_m^2 - k^2)\right]$$

and want to discuss for which v values there exists a curve connecting $k = 0$ with $k = (\pm k_m, 0)$ on which $\mathrm{Re}S(k) = 0$.

We substitute

$$u = v - v_0$$

and

$$\beta = iA(v_0)/\omega_{pi}^2 \tag{A1}$$

and get

$$S(k) = k[\beta(k^2 - k_m^2) + iu]. \tag{A2}$$

The equation

$$\mathrm{Re}S(k) = \mathrm{Re}\{k[\beta(k^2 - k_m^2) + iu]\} = 0, \tag{A3}$$

being of third order in k, describes three curves in the complex $k = k_r + ik_i$ plane; these curves are obviously sym-

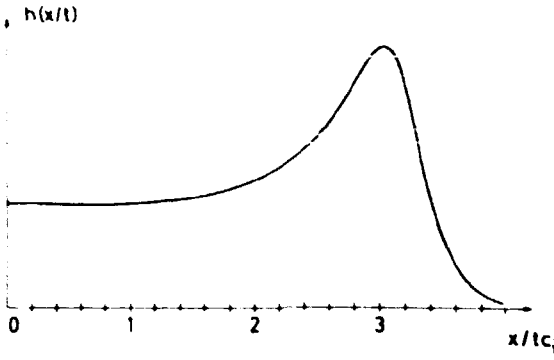

FIG. 3. The stable contribution, $h(x/t)$, for the case where $T_e/T_i = 4$ plotted as a function of $x/c_i t$.

side this interval will see a damped perturbation for sufficiently large t, i.e., a convective instability.

Let us now consider the stable part of the solution. This part is given by (15) and it can be written in the self-similar form $n_{es}(x, t) = t^{-1}h(x/t)$. We have calculated $h(x/t)$ numerically for a case where the ion velocity distribution functions, $f_0(v)$ and $g(v)$, again are the double-humped, symmetrical functions shown in Fig. 1. In order to insure that the plasma is unstable we have chosen $T_e/T_i = 4$.[14] In Fig. 3 we show the results as a function of $x/c_i t$, where $c_i^2 = 2\kappa T_i/m_i$.

We note that the stable contribution contains a positive pulse whose maximum moves through the plasma with a velocity about equal to $v_d + c_e$. Since in most cases this velocity is greater than v_+, which is the characteristic velocity of the front of the unstable contribution, it should be possible to experimentally observe the two contributions separately. Therefore, if the instability is observed at a fixed position in that frame of reference where $v_0 = 0$, the fast self-similar pulse from the stable contribution will arrive first and then the growing contribution from the unstable part will arrive and eventually dominate. The relative strength between $n_{eu}(x, t)$ and $n_{es}(x, t)$ depends on all the plasma parameters involved: $f_0(v), g(v), T_e/T_i$, and also on time and position of observation [see Eqs. (15) and (22)]. Since $n_{es}(x, t)$ normally starts at a low level and $n_{eu}(x, t)$ goes as t^{-1}, the latter term will in many cases be the predominant one at small times.

Baker[13] has examined the propagation of pulses excited by a grid in an unstable Q machine plasma with an ion velocity distribution function of the kind considered here. He actually sees two contributions: a fast damped pulse followed by a slower growing one. The main features of his observations are in agreement with our calculations. In order to claim that the Baker work constitutes an experimental verification of our theoretical results more detailed experimental work has to be performed. One feature that is likely to complicate such work is the fact that the propagation of the stable part of the pulse, $n_{es}(x, t)$, is independent of plasma density, while the unstable part, $n_{eu}(x, t)$, propagates in a way that depends on n_0 [n_0 enters into (22) through ω_{pi}^2]. Therefore, in a Q machine plasma where there is necessarily a radial density gradient, the propagation of the unstable part will depend on radius, while the stable part propagates independently of radius.

The solution to Eqs. (1) to (3) with another initial condition, e.g., a wave, can, in principle, be found from our results by performing a convolution of the Green's function with the given initial condition. Although this method may be unnecessarily complicated, it can give us some information about the propagation of waves from our knowledge of the Green's function. For stable plasmas, the Green's function only contains the self-similar part, and a wave is known to be damped.[11] We may therefore conclude that in cases where we consider unstable plasmas and find that the self-similar part of the Green's function predominates over the unstable part, a wave will decay. It has been discussed that for small times the self-similar part can predominate; in such cases a wave will start out as a decaying wave and only begin to grow when the unstable part of the Green's function becomes the predominant one. An effect of this kind, but for a boundary value problem, was observed experimentally by Christoffersen and Prahm.[15] Physically, the damping can be interpreted as a phase mixing of the particles in the initial density perturbation with the distribution function $g(v)$; only that part of $g(v)$ which corresponds to the distribution function in an unstable wave will grow.

To summarize, in this paper we have reported on a calculation of the development of a narrow perturbation in a plasma, unstable to an ion beam instability, i.e., we have found the Green's function for this problem. Our results are valid in a time period from a few times ω_{pi}^{-1} until the instability reaches a nonlinear level. We have determined in which frames of reference the instability is absolute and in which it is convective. In many cases a damped pulse will propagate faster than the region of instability, and this pulse can in the initial phase, depending on the excitation, have a considerable amplitude.

APPENDIX

We consider the complex function $S(k)$ of the complex variable, k [see Eq. (23)]

$$S(k) = i\left[k(v - v_0) - \frac{A(v_0)}{\omega_{pi}^2}k(k_m^2 - k^2)\right]$$

and want to discuss for which v values there exists a curve connecting $k = 0$ with $k = (\pm k_m, 0)$ on which $\mathrm{Re}S(k) = 0$.

We substitute

$$u = v - v_0$$

and

$$\beta = iA(v_0)/\omega_{pi}^2 \tag{A1}$$

and get

$$S(k) = k[\beta(k^2 - k_m^2) + iu]. \tag{A2}$$

The equation

$$\mathrm{Re}S(k) = \mathrm{Re}\{k[\beta(k^2 - k_m^2) + iu]\} = 0, \tag{A3}$$

being of third order in k, describes three curves in the complex $k = k_r + ik_i$ plane; these curves are obviously sym-

metrical around $k = 0$. In the general case where $\mathrm{Re}S(k_s) \neq 0$ [k_s being those k values for which (A2) has saddle points] the three curves cannot cut each other.

Before proceeding we note:

(a) k_m^2 is a real positive number depending only on the properties of the plasma under consideration.

(b) β is a complex number depending only on the plasma properties. From (21) and (A1) it follows that for unstable distribution functions where $f_0''(v_\phi) > 0$, the real part of β is negative, i.e., if we write $\beta = |\beta| \exp(i\theta_\beta)$, then

$$(\pi/2) + 2n\pi < \theta_\beta < (3\pi/2) + 2n\pi, \quad n = 0, 1, 2, \ldots.$$

(c) u is a real parameter to be varied from $-\infty$ to $+\infty$.

For $|k| \to \infty$ the curves described by (A3) asymptotically approach the straight lines through $k = 0$ which are determined by $\mathrm{Re}(\beta k_s^2) = 0$. In a polar system of coordinates this equation is written

$$|\beta|\,|k_s^3|\cos(3\theta_s + \theta_\beta) = 0$$

and is satisfied for

$$\theta_s = (\pi/6) - (\theta_\beta/3) + p(\pi/3), \quad p = 0, 1, 2, \ldots. \quad \text{(A4)}$$

We note that for $p = n = 0$ we have $-\pi/3 \leq \theta_s \leq 0$, and we further note that θ_s only depends on the plasma properties and not on the chosen u value.

Because the left-hand side of (A3) is a third-order polynomial, any straight line in the k plane can only cut the curves defined by this equation in three points. From this it follows that the only point of intersection between the asymptotes and the curves is the origin of the k plane. Therefore, in the general case we can only have the three situations shown in Fig. 4. In situation (a) the three points, $k = (0, 0)$ and $k = (\pm k_m, 0)$ lie on three different curves, which corresponds to absolute instability. In situations (b) and (c) the three points lie on the same curve, which guarantees that the instability is convective. It is clear that a shift from one situation to another which can be obtained by varying u, will only occur for u values for which $\mathrm{Re}S(k_s) = 0$.

To determine which situation holds for an actual case we only have to determine the slope at $k = (0, 0)$ of the curve which passes through this point. If the slope is such that the curve falls within that 60° angle between the asymptotes in which the real k axis is situated, then we have situation (b) or (c). If it falls outside this angle, we have situation (a).

Around $|k| = 0$ (A3) can be approximated by

$$\mathrm{Re}(-\beta k_m^2 k + iuk) = 0.$$

From this we get that the slope at $k = 0$ is determined by

$$\frac{dk_i}{dk_r} = \frac{\beta_r k_m^2}{\beta_i k_m^2 - u},$$

which for $u = 0$ is written

$$\frac{dk_i}{dk_r} = \frac{\beta_r}{\beta_i}. \quad \text{(A5)}$$

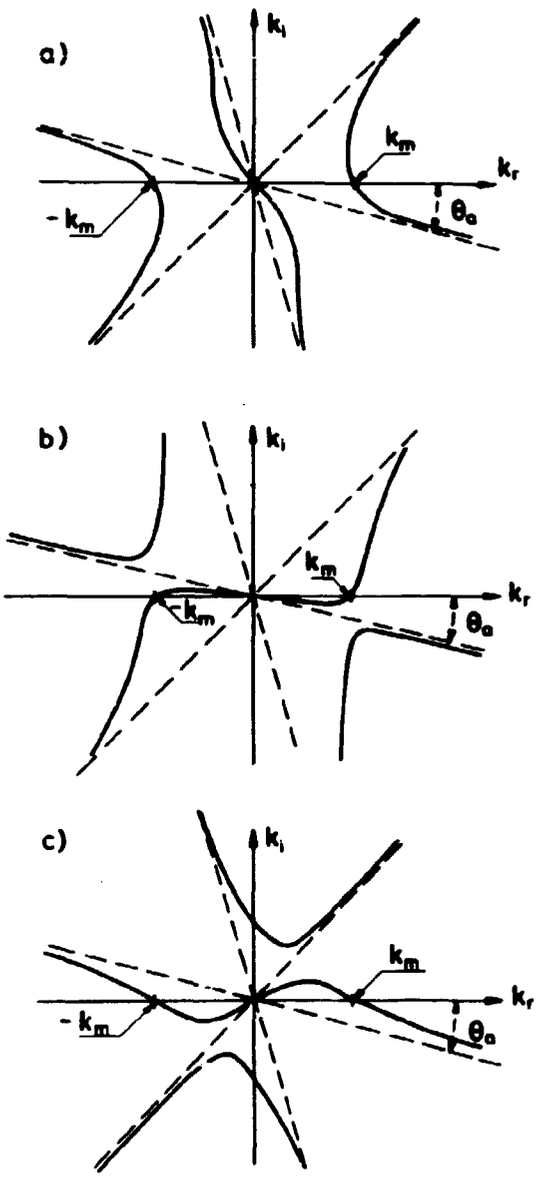

FIG. 4. The three drawings show the three possible general shapes of the curves which are described by $\mathrm{Re}S(k) = 0$. In situation (a) the three points $k = 0$ and $k = \pm k_m$ do not lie on the same curve; this corresponds to absolute instability. In situations (b) and (c) the three points lie on the same curve and, therefore, the instability is convective.

Simple analysis based on (A4) and (A5) shows that the line given by $k_r = k_i\beta_i/\beta_r$ falls outside that 60° angle between asymptotes in which the real k axis is situated. Therefore we have, as expected, an absolute instability for $u = 0$. To find the limiting value, u_+ and u_-, between absolute and convective instability we only have to find that u value for which $\mathrm{Re}S(k_s) = 0$. The saddle points are determined by

$$3\beta k_s^2 - \beta k_m^2 + iu = 0.$$

Inserting k_s determined by this equation into (A3) allows us to determine for which values of u $\mathrm{Re}S(k_s) = 0$.

* Present address: Plasma Physics Laboratory, Princeton University, Princeton, N.J. 08540.

[5] P. Sturrock, Phys. Rev. 112, 1488 (1958).
[6] P. Sturrock, *Plasma Physics*, edited by J. E. Drummond (McGraw-Hill, New York, 1961), Chap. 4.

[5] M. Feix, Nuovo Cimento **27**, 1130 (1963).
[6] R. N. Sudan, Phys. Fluids **8**, 1899 (1965).
[7] L. S. Hall and W. Heckrotte, Phys. Rev. **166**, 120 (1968).
[8] D. A. Lee and G. K. Soper, Phys. Fluids **13**, 995 (1970).
[9] D. E. Baldwin and G. Rowlands, Phys. Fluids **13**, 2036 (1970).
[10] T. D. Rognlien and S. A. Self, J. Plasma Phys. **7**, 13 (1972).
[11] S. A. Andersen, V. O. Jensen, P. Michelsen, and P. Nielsen, Phys. Fluids **14**, 728 (1971).
[12] S. A. Andersen, G. B. Christoffersen, V. O. Jensen, P. Michelsen, and P. Nielsen, Phys. Fluids **14**, 990 (1971).
[13] G. B. Christoffersen, V. O. Jensen, and P. Michelsen, Phys. Fluids **17**, 390 (1974).
[14] D. R. Baker, C. Bartoli, and M. Ritter, in *Proceedings of the Third International Conference on Quiescent Plasmas* (Danish Atomic Energy Commision, Risø, Denmark, 1971), p. 111.
[15] D. R. Baker, Phys. Rev. Lett. **28**, 1189 (1972); and Phys. Fluids **16**, 1730 (1973).
[16] P. Michelsen and L. P. Prahm, in *Proceedings of the Third International Conference on Quiescent Plasmas* (Danish Atomic Energy Commission, Risø, Denmark, 1971), p. 103.
[17] G. B. Christoffersen and L. P. Prahm, Phys. Fluids **16**, 708 (1973).

7. ADDITIONAL REMARKS ON CHAPTERS THREE THROUGH SIX

The papers presented as reprints in the four previous chapters differ in notation. To facilitate reading a few remarks about notation are given in the following subsection, which also contains a list of misprints found in the articles.

The four reprint chapters all contain discussions. However, after publication a few further problems arose concerning details of the Green's functions. In the latter part of this chapter we discuss these details. A general discussion and conclusions concerning the entire work, seen in the light of the list of problems mentioned in chapter 2, are left to the next chapter.

7.1. Notation, Corrections and Misprints

Essentially the same notation is used in the four preprint chapters as in the rest of the present treatise. The following two exceptions are mentioned here in order to facilitate reading.

1) Throughout this report except in chapter 3 the unperturbed ion velocity distribution function is denoted $f_o(v)$; in chapter 3 this function is called $f(v)$.

   In all chapters except chapter 4, $f_o(v)$ is defined so that the unperturbed density is given by $n_o = \int_{-\infty}^{\infty} f_o(v)dv$. In chapter 4 $f_o(v)$ is normalized so that $1 = \int_{-\infty}^{\infty} f_o(v)dv$. Therefore, if all terms containing $f_o(v)$ in chapter 4 are divided by n_o we obtain consistency concerning this point throughout the present report.

2) The temperature is denoted by T and measured in K in all chapters except chapter 3, where it is measured in energy units. Therefore in order to obtain consistency T in chapter 3 should be replaced by κT, where κ is the Boltzmann constant.

In the four reprint chapters there are a number of inaccuracies and misprints, and the following corrections should be made (the page numbers in the list below refer to the pagination of the journal in question):

Chapter 4

Page 992, line 11 below Fig. 1:

This paragraph should start: Except for a factor $(k\lambda_D)^{-2}$, where λ_D is the Debye-length, the denominator in the parenthesis of the expression for n_2 in Eq. (8) is the classical ... etc.

Page 993, line 4 below Fig. 3:

For (16) read (14)

Page 998, first column, last line:

For T_e read κT_e.

Chapter 5

Page 390, Eq. (5):

For $\varepsilon(k,\omega)$ read $(k\lambda_D)^2\ \varepsilon(k,\omega)$.

Page 390, second column, line 3 below Eq. (5):

For $\exp[i(\omega' t - k' x)]$ read $\exp[-i(\omega' t - k' x)]$

Page 390, second column, line 11 below Eq. (5):

For (4) read (5).

Page 395, Fig. 3, in the figure caption:

For $T_e/T_i = 2$ read $T_e/T_i = 1$.

Page 397:

The drawings in Figs. 6 and 7 should be interchanged.

Page 398, formula (38):

For $\cos\left[\omega\left(\frac{x_a}{v_a} - \frac{x}{v}\right)\right]$ read $\cos\left[\omega\left(\frac{x_a}{v_a} - \frac{x_a}{v}\right)\right]$.

7.2. Comments on the Green's Functions

In chapter 4 the Green's functions for Eqs. (1.11) and (1.12) are derived for the initial condition

$$f(x,v,t=0) = \Delta t\ v\ g(v)\ \delta(x)\ . \qquad (7.1)$$

The experimental situation is, however, such that it is the boundary condition

$$f_G(x=0,v,t) = g(v)\ \delta(t) \qquad (7.2)$$

which is known. Although the arguments in chapter 4 for interpreting the situation as an initial value problem seem reasonable, it is beforehand not clear how similar are the Green's functions obtained with condition (7.1) to those obtained with condition (7.2). In chapter 5 the Green's functions derived from the basic equation with the boundary condition (7.2) are obtained. Numerical calculations of the Green's functions obtained with the two conditions have been compared, and it is found that the difference between them is scarcely noticeable. Therefore no errors of any importance are introduced by solving the equations with the initial condition (7.1) rather than with the boundary condition (7.2), and all conclusions drawn in chapter 4 hold good.

Arguments may also be put forward against the mathematical procedure used to obtain the Green's functions (12) and (16) in chapter 4 because of the use of δ-functions. It is, however, relatively easy to show that, if we introduce the δ-functions in the traditional and mathematically more correct way as

$$\delta(y) = \lim_{\alpha \to 0} \frac{1}{\pi} \frac{\alpha}{\alpha^2+y^2}$$

and perform the analysis in a manner similar to that used in chapter 5, then we recover the Green's functions (12) and (16) of chapter 4.

The Green's functions in the previous chapters were derived from experimental situations, such as in single-ended Q-machines, where no particles move in the negative x-direction. Only because the mathematical procedure requires the distribution functions to be analytic for all v, have we approximated the measured $f_o(v)$ and $g(v)$ functions by drifting Maxwellians of the type $\exp[-(v-v_d)^2/c_i^2]$. Obviously such functions do not vanish for $v < 0$, but if v_d is sufficiently large compared to

c_i then there are so few particles moving in the negative direction that, based on physical reasons, we can argue that they are of very little importance for the phenomenon under consideration. For the cases presented in the previous chapters, where $v_d \geq 2c_i$, such arguments certainly apply.

It is of interest to discuss to what extent the Green's function technique developed in this work can be used for the general case where the distribution function does contain particles with negative velocities. For the initial value problem treated in chapters 4 and 6 there is no problem in calculating the Green's functions, also for cases where $f_o(v)$ and $g(v)$ are non-vanishing for $v < 0$. These Green's functions can then be used to calculate the propagation properties of a wave set up at $t = 0$ in an infinite plasma. Such a problem is, of course, only academic in the sense that it cannot be examined experimentally.

The problem is more difficult for the experimentally realizable situation of a finite plasma perturbed by an oscillating exciter at some position. If, in this case, there are particles moving towards the exciter their contribution to the perturbation will depend on the position and on the condition of the end of the plasma column. Therefore, the problem is not determined alone by the boundary conditions at the exciter; and the Green's function technique developed in this report can only solve the problem approximately.

8. GENERAL DISCUSSION AND CONCLUSIONS

A list of the problems and deficiencies that remained for a detailed understanding of ion acoustic waves around the year 1970 was given in the introduction. The aim of the study described in this report was to contribute to a clarification of these problems. In this chapter an attempt is made to discuss to what extent this study has succeeded in improving the situation. Emphesis is placed upon presenting simple physical arguments explaining the various phenomena under discussion.

The discussion and conclusions in this chapter contain material which has been published earlier by the author and collaborators. Part of this material is only of limited interest for the main purpose of the study as described above and in more detail in the introduction. This part of the work has been performed mainly in order to improve on various details of the studies presented in the preprint chapters, or it constitutes by-products of these studies. This material is described very shortly here and it is only included in this treatise in order to make the present description of the work performed by the author in the Q-machine field more complete. Details of this part of the work can be found in the publications.

There are two main features in the work described in this paper which are new in the study of the ion acoustic wave problem. The one is the development and use of the electrostatic ion energy analyzer for determination of the unperturbed and the perturbed ion velocity distribution function. The other is the use of Green's functions in the theoretical as well as in the experimental study of the ion acoustic wave problem.

8.1. The Analyzer

The development and construction of the electrostatic ion energy analyzer made it possible to measure $f_o(v)$, $g(v)$, and the time and space dependence of the distribution function $f(x,v,t)$ in a propagating density perturbation. Within the limitations of the performance of the analyzer we have therefore contributed to rectifying the deficiencies under points 3), 4) and 5) in the list given in chapter 1.

One of the two most serious limitations of the analyzer performance is that it can only measure the velocity distribution function of particles moving in one direction. This implies that the plasma column must be terminated at the analyzer. Because all ions move away from the hot plate in a single-ended Q-machine operated in the collisionless regime, this limitation is of no consequence for the work described in this paper. In the more general case one would be interested in measuring the velocity distribution function for ions moving in both directions at various positions within the plasma. The analyzer cannot be used for this purpose.

The other serious limitation is that the energy resolution of the analyzer cannot be determined with satisfactory accuracy. As mentioned when describing the experimental set-up in chapter 3, an indication of the resolution can be obtained from the positive slope of the charge-exchange peak on the analyzer characteristics. This procedure, however, only gives an indication of the resolution at very low energies. There is no direct way to determine the resolution around 2 eV corresponding to the energy of most of the ions. Only the shapes of the measured characteristics can give some idea of the upper limit of the resolution. It is clear from the results of chapter 4 that the resolution is good enough to reveal the undershoot on the $f(x_a,v_a,t)$ curves, i.e. to demonstrate the existence of collective interaction in propagating pulses. It is, however, also clear from the results of chapter 5 that better resolution is needed to demonstrate collective effects in ion acoustic waves.

Simultaneously with the development of our analyzer a somewhat similar analyzer was constructed by the French group[15]. The main difference between the two analyzer techniques is that the French group determines the position of ϕ_{pl} on the abcissa of the analyzer characteristics by calculations based on work functions and contact potentials of the various conductors in the electrical system connected to the analyzer. As the work functions and the contact potentials are poorly known, our direct method using the charge exchange technique gives a more accurate determination of ϕ_{pl}.

A shortcoming of the charge exchange technique for determination of ϕ_{pl}, as described in chapter 3, is that it requires

that the plasma potential is constant over the volume occupied by the neutral Cs-cloud; i.e. the spatial resolution of this method is rather limited. In order to increase this resolution another technique, essentially based on the same idea, was developed[16]. This technique utilizes an electrically heated molybdenum wire immersed in the plasma column at the place where ϕ_{pl} is to be determined. The potential of the wire can be varied with respect to the plasma potential. When the wire potential is close to the plasma potential a small peak similar to the charge exchange peak seen in Fig. 3 of chapter 3 appears on the analyzer characteristic. This peak is believed to be caused by ions which have hit the wire and which are then re-emitted into the plasma. Since some of these ions are re-emitted with very low parallel velocity they are accepted by the analyzer when $\phi_a = \phi_{pl}$. If the wire potential is above the plasma potential, no ions can penetrate up to its surface and the peak therefore disappears. At wire potentials below the plasma potential none of the ions that have hit the wire have enough energy to penetrate back into the plasma, and the peak disappears again. The procedure in determining the plasma potential by this method is thus: the potential of the wire is varied until the small peak reaches its maximum value. The left-hand side of this peak then determines the plasma potential in exactly the same way as for the charge exchange case described in chapter 3.

As a by-product of the work with the method used for determination of the plasma potential by means of the charge exchange peak on the analyzer characteristics, a new technique for measurements of charge exchange cross sections at low energies ($\sim$ 2 eV) was developed. The technique was used to measure the cross section for the process $Cs^+ + Cs \rightarrow Cs + Cs^+$ at 2 eV[17]. The idea behind this technique is to let the plasma column pass through a neutral cloud of Cs with known length, l, and with known density, n_n, and use the analyzer to measure the ratio of the flux, I, of ions which have passed through the cloud to the flux, ΔI, of ions having suffered charge exchange in the cloud. When conditions are arranged such that $\Delta I \ll I$ the charge exchange cross section is simply determined by

$$\sigma_{c.e} \approx \frac{\Delta I}{n_n \, l \, I} \quad .$$

The result of the measurements described in [17] is

$$\sigma_{c.e} = 0.6 \cdot 10^{-13} \text{ cm}^2 \pm 20\% \ .$$

8.2. The Green's Function Technique

To the best of our knowledge the Green's technique has not been used for a comprehensive study of the ion acoustic wave problem before. The result of our Green's function study adds to the clarification of the five problems mentioned in the introduction.

One of the main objectives of the work described in this report was to evaluate the importance of the collective interaction described by the term on the right-hand side of the Vlasov equation (1.11) as compared to freely streaming effects described solely by the left-hand side terms of Eq. (1.11). It would be of special interest to demonstrate experimentally some clear-cut features which can only be explained by the collective interaction term. It was hoped that such a demonstration would clarify some of the questions raised by Hirschfield and Jacob[13], and mentioned under point 2) in the introduction.

As described in chapter 4 the overshoot on the calculated S_{v_a}-curves and the demonstration of this overshoot on the experimental curves in Figs. 4 through 7 in chapter 4 constitute an obvious sign of collective interaction. In chapter 4 the argumentation that the overshoot is caused by collective effects is based on an inspection of Eq. 14 that shows that the last collective term in this equation changes sign for $t = x/v$. It is also possible to base the argumentation on simple physical reasoning[18]. Before these arguments are presented a few remarks about the linearized Vlasov equation are helpful.

In the nonlinear forms (1.1) and (1.5) the Vlasov equation expresses Liouville's theorem, which states that for a conservative system $F_{i,e}(x,v,t)$ is constant along a dynamical trajectory. If, however, we prefer to consider $F_{i,e}$ on a line

$$x-x' = v(t-t') \tag{8.1}$$

(1.5) can be written

$$\frac{dF_{i,e}(x,v,t)}{dt} = - \frac{e_{i,e}}{m_{i,e}} E(x,t) \frac{\partial F_{i,e}(x,v,t)}{\partial v} , \qquad (8.2)$$

i.e. we can consider the collective interaction term as a source or a sink for $F_{i,e}(x,v,t)$ as we move through the plasma with velocity v.

Derived from the linearized form (1.8), Eq. (8.2) is written

$$\frac{df_{i,e}(x,v,t)}{dt} = - \frac{e_{i,e}}{m_{i,e}} E(x,t) f'_{o_{i,e}}(v) . \qquad (8.3)$$

From this equation it is evident that the linearization implies that we neglect the collective interaction between particles in the perturbation distribution function $f_{i,e}(x,v,t)$ and the electric fields in the plasma. It is also clear that the requirement that the linearization be acceptable is that $|df_{o_{i,e}}(v)/dv| >> |\partial f_{i,e}(x,v,t)/\partial v|$ for all v. This last requirement is somewhat more rigorous than the more commonly used requirement that $f_{o_{i,e}}(v) >> |f_{i,e}(x,v,t)|$, which is stated in connection with Eq. (1.7).

By writing Eq. (1.11) in the same form as Eq. (8.2) and (8.3) we get

$$\frac{df(x,v,t)}{dt} = \frac{c_e^2}{n_o} \frac{\partial n(x,t)}{\partial x} f'_o(v) . \qquad (8.4)$$

Eq. (13) in chapter 4 was obtained by integrating Eq. (8.4) along the line given by (8.1).

To understand the physical mechanism causing the overshoots on the S_{v_a}-curves in chapter 4, we consider the (x,t)-diagram shown in Fig. 2. A density pulse of the type discussed in chapter 4 is released at (x,t) = (0,0) and it propagates in the x-direction with the self-similar form $t^{-1}h(x/t)$. The ion energy analyzer is placed at $x = x_a$ and is adjusted to measure the perturbed ion velocity distribution function at $v = v_a$ as a function of time, i.e. it measures a signal proportional to $f(x_a,v_a,t)$.

The broken line through (0,0) in Fig. 2 represents the pos-

ition of the maximum of the density pulse as a function of time. The velocity of this maximum is denoted v_{max}, therefore the slope of the broken line is v_{max}^{-1}. It follows from Eq. (1.10) that the E-field associated with the density pulse is positive in front of the density pulse and negative behind the pulse. The small arrows in Fig. 2 indicate the direction and the magnitude of the E-field.

Since the analyzer is adjusted to measure $f(x_a,v_a,t)$ it is only sensitive to particles whose orbits in the (x,t)-diagram have the slope v_a^{-1} when they cross the line $x = x_a$. At $t = t_a = x_a/v_a$ those particles with velocity v_a, which were part of the pulse released at (x,t) = (0.0), will appear at x_a and be detected by the analyzer. This contribution corresponds to the first term on the right-hand side of Eq. (13) in chapter 4, and it is clearly a free-streaming contribution. As a function of time the output signal $S_{v_a}(t)$ corresponding to this contribution is determined by the analyzer resolution and it will presumably take a Gaussian-like form around $t = t_a$, as indicated by the dotted curve in Fig. 3.

At times $t \neq t_a$ the analyzer will only receive contributions caused by collective interaction in the plasma and given by the last term on the right-hand side of Eq. (13) in chapter 4. The physical mechanism causing these contributions is simple: Let us consider a case where $v_a > v_{max}$. Particles which arrive at $x = x_a$ with velocity v_a at times earlier than t_a have been running in front of the pulse all the time from $t = 0$, and thus they have been accelerated by the E-field. Hence their orbits are curved as that labelled a in Fig. 2. Since these particles were in the background plasma with velocity distribution function $f_o(v)$ at $t = 0$, and as they had a velocity smaller than v_a at that time, they will cause a positive contribution to the analyzer signal if $f_o'(v_a) < 0$ and a negative one if $f_o'(v_a) > 0$. In most experimental cases $f_o'(v_a) < 0$, and we therefore get a positive signal from the analyzer as indicated by the broken curve in Fig. 3. For times $t > t_{max} = x_a/v_{max}$ similar arguments show that the particles that appear at x_a with velocity v_a have been decelerated by the E-field in the plasma and have followed orbits curved as that labelled b in Fig. 2. These particles

cause negative signals from the analyzer if $f_o'(v_a) < 0$ and positive ones if $f_o'(v_a) > 0$. Again in most cases $f_o'(v_a) < 0$, and we therefore expect a negative signal as also indicated by the broken curve in Fig. 3. In the time interval between t_a and t_{max} the analyzer receives particles that have crossed the maximum of the pulse and have therefore been subjected to an acceleration as well as a deceleration. Thus the collective contribution in this time interval is more difficult to predict, but it is clear that the curve drawn for $t < t_a$ must join the one for $t > t_{max}$ approximately as shown in Fig. 3. The final signal, $S_v(x_a,v_a,t)$, from the analyzer is the sum of the free-streaming contribution and the collective contribution; this sum is indicated in Fig. 3 by a full line. It is clear that the undershoot on the $S(x_a,v_a,t)$ curves for $t > t_a$ is a characteristic feature that is caused by collective interaction. Our claim to have demonstrated collective interaction is based on our experimental verification of this undershoot, as seen in Figs. 4-7 of chapter 4.

In Sec. V of chapter 4 the effects of various possible sources of error were discussed, especially regarding the problem of whether these sources could produce such overshoots as seen on the S_{v_a}-curves in plasmas without collective interaction, thus invalidating our claim to have demonstrated collective interaction experimentally.

After the publication of the paper in chapter 4, some further questions were raised about the problems discussed under point (2) in Sec. V. One question was: Could the real g(v)-function deviate so much from the results of the static measurements described at the beginning of Sec. II of chapter 4 that the overshoot could be explained by freely streaming effects alone? Especially, would a change in sign in g(v) cause an overshoot on the S_{v_a}-curves in a freely streaming case? As a matter of fact, it has been demonstrated experimentally by G. Christoffersen (see ref. 14 in chapter 5) that g(v)-functions with a change in sign can be produced.

To discuss this question, we consider a positive density pulse with a velocity distribution proportional to vg(v) released at $t = 0$ into a plasma without collective interaction. We assume that $g(v) = 0$ for $v = v_o$, that $g(v > v_o) > 0$ and that $g(v < v_o) < 0$. Let the analyzer at $x = x_a$ be adjusted to measure

a $S_{v_a}(t)$-curve for a velocity, v_a, which is slightly greater than v_o. The analyzer starts to produce a positive signal at $t \simeq x_a/v_o+v_r$, where v_r is the width of the analyzer resolution function. The signal increases with time, runs through a maximum and decreases again. If $v_a-v_r < v_o$ the signal will pass through zero and produce a negative overshoot during the time interval $x_a/v_o \lesssim t \lesssim x_a/v_a-v_r$ because $g(v_a-v_r) < 0$. Thus an overshoot may be produced in a plasma without collective interaction if g(v) changes sign. This cannot, however, be the explanation of the overshoots seen in Figs. 4 through 7 in chapter 4, because it is clear from the above discussion that if v_a is decreased to below v_o then we get $S_{v_a}(t)$-curves that have negative values for all t. This is not seen in the figures in chapter 4; on the contrary, even the overshoot disappears for lower v_a-values. We may therefore conclude that a g(v)-function, which changes sign for some value of v, cannot be the explanation for the overshoots seen in the figures.

A further question that was raised again was whether the overshoot could be caused by the acceleration or deceleration of ions present within a few Debye-lenghts from the grid during the short time intervals when the grid potential is changed. Here we give a few arguments against this possibility in addition to those presented under (2) in Sec. V of chapter 4. If the overshoots were indeed produced by ions accelerated or decelerated by the changes in grid potential, the measured S_{v_a}-curves would depend strongly on the shape of the electrical pulses applied to the grid. To examine this point, we applied bell-shaped pulses of the form $(t^2+a^2)^{-1}$ to the grid rather than square pulses. With the area of the two kinds of pulse kept equal, there was no notable change in the measured S_{v_a}-curves. This shows that the deceleration or acceleration of ions as a result of changing grid potential is of little importance and not responsible for the overshoots.

Curves b) and c) in Fig. 7 of chapter 4 constitute another experimental indication that the acceleration or deceleration of ions during intervals when the grid potential is changed are not responsible for the overshoots. The similarity of the two curves shows that the amplitudes of the S_{v_a}-curves are proportional to the width of the square pulses applied to the grid. If the am-

plitude of the S_{v_a}-curves was determined by the intervals during which the grid potential is changed (the amplitude being equal for the two cases in Fig. 7), the amplitude of curve c) would only be 40% of that of curve b).

It should be stressed at this point that measurements of the perturbed density in a pulse can only demonstrate collective effects if the function g(v) is well known. Any shape of the density, $t^{-1}h(x/t)$, can be obtained by free-streaming contributions alone. For the initial value problem treated in chapter 4 a g function fulfilling the condition $\frac{x}{t}\, g(\frac{x}{t}) \propto h(x/t)$ would in the free-streaming case generate the density shape $t^{-1}h(x/t)$. The corresponding condition for the boundary value problem of chapter 5 is $g(x/t) \propto h(x/t)$. Therefore, in order to be able to claim to have seen collective effects in density measurements, one has to demonstrate deviations from the conditions for g(v) mentioned above. Such demonstrations have never been reported.

8.3. Collective Interaction in Ion Acoustic Waves

The propagation properties of ion acoustic waves are determined by integrals over the Green's functions as shown in Eqs. (29) and (30) of chapter 5. Therefore arguments about collective interaction contra free-streaming effects, similar to those raised for the pulses in Sec. 8.2, apply to the wave problem.

First of all it is evident that because any shape of the Green's function for the density can be obtained by a free-streaming contribution alone, we also know that any wave form obtained by performing integrals over such Green's functions can be explained by free-streaming effects alone. In the same way as for the pulse case discussed in Sec. 8.2, one can only claim to have seen collective effects in measurements of the wave density if one has measured the g(v)-functions and demonstrated that the corresponding free-streaming density deviates from the measured one.

Such demonstrations have never been reported. We base our claim that collective interaction has never been demonstrated experimentally in measurements of the density in ion acoustic waves on the arguments given above.

When discussing the perturbed ion velocity distribution function in a propagating pulse we found that this distribution

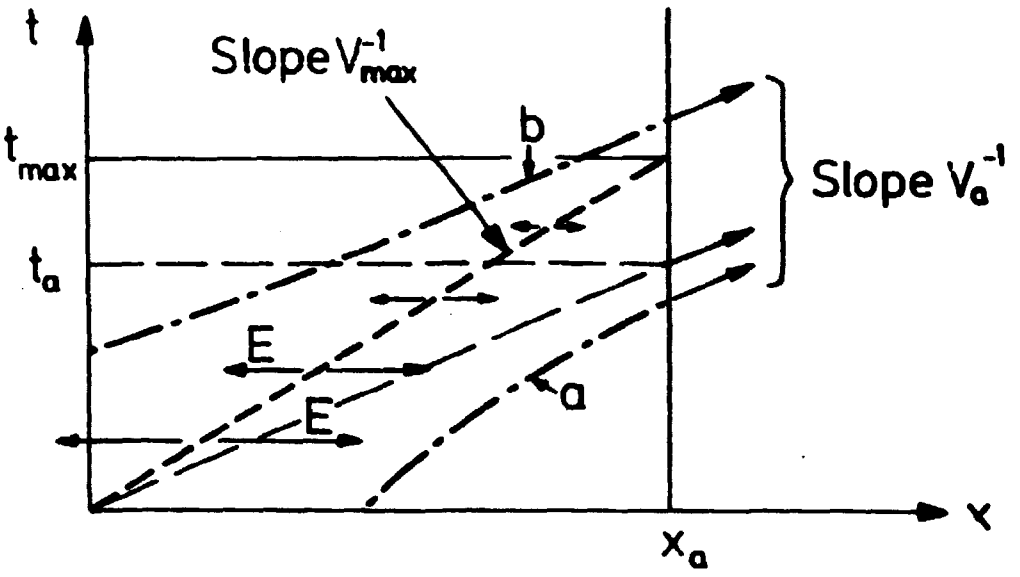

Fig. 2. Schematics of pulse propagation.

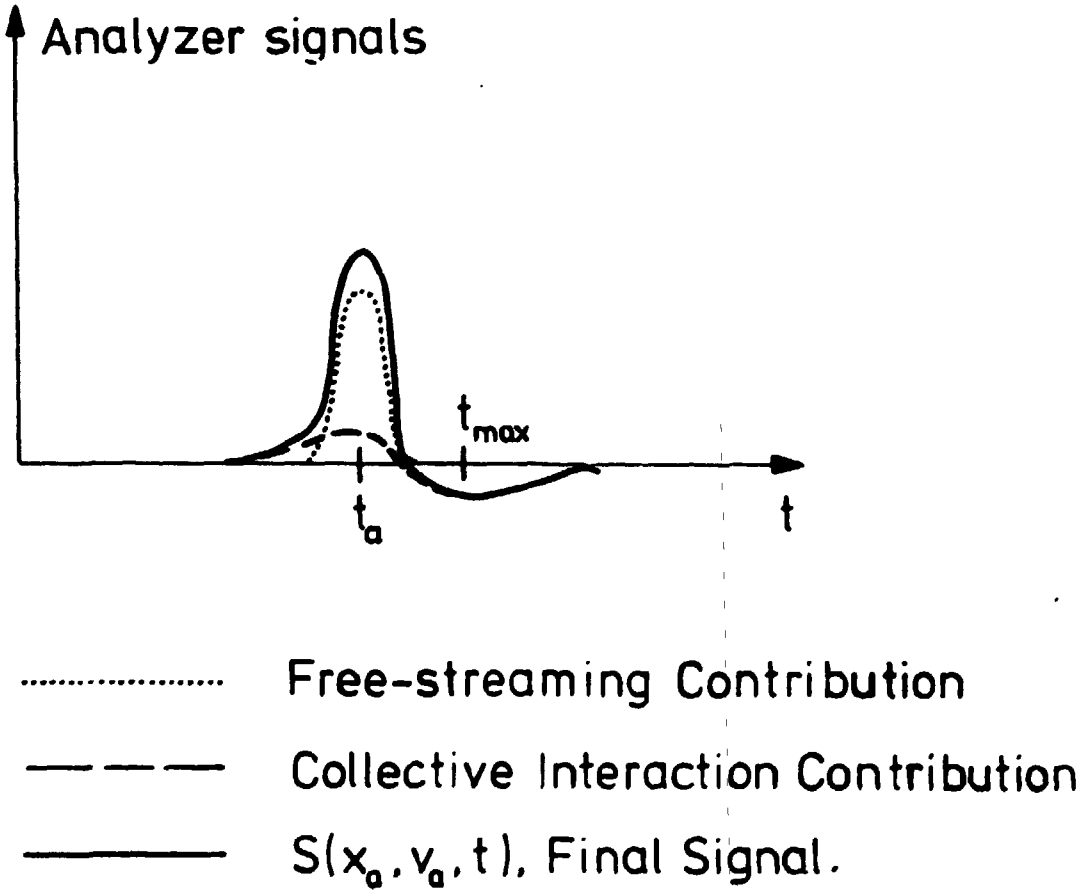

Fig. 3. Indications of the shapes of the various contributions to the analyzer signal, when measuring the velocity distribution in a pulse.

function exhibits a characteristic feature, the undershoot, which is an obvious sign of collective interaction. If we turn to the perturbed ion velocity distribution function in a wave we find a similar feature also caused by collective interaction.

Examples of the amplitude of the ion velocity distribution functions calculated from Eq. (30) of chapter 5 are shown in Fig. 5 of chapter 5. The amplitude of the perturbed distribution function is equal to g(v) at x = 0. As we move away from x = 0 we see that the amplitude deviates from g(v) by some characteristic oscillations. The wavelength in velocity space of these oscillations decreases with increasing distance from the exciter. From the following arguments it is easy to see that these oscillations are caused by collective effects[19,20]. In Fig. 4 a wave is generated by a signal, $\exp(-i\omega t)$, on a grid at x = 0. Wave density maxima are released for $t = 2\pi n/\omega$, where n is an integer running from $-\infty$ to $+\infty$. The wave propagates in the x direction with a phase velocity v_{ph}. The full lines represent the position of the wave density maxima as functions of time, i.e. the slope of these lines is v_{ph}^{-1}. The electric fields associated with the wave are indicated by small arrows. It is clear that without collective interaction, i.e. without the electric fields, the amplitude of the perturbed distribution function as measured at any position $x = x_a$ would be equal to g(v). The effect of collective interaction in the wave case is somewhat more complicated than in the pulse case discussed in Sec. 8.2. A particle in the background plasma, which has a velocity that is slow compared to the phase velocity, will be overtaken by several wave maxima as it moves from x = 0 to $x = x_a$ and will therefore be subjected to several accelerations and decelerations. A particle with velocity close to v_{ph} will more or less follow the same wave between x = 0 and $x = x_a$, while a fast particle will overtake a number of waves and again be subject to several accelerations and decelerations. The net effect of these accelerations and decelerations on the amplitude of the perturbed distribution function at $x = x_a$ is difficult to predict in detail. One would, however, expect the effect to be about the same for particles that have crossed 1, 2, 3 or 4, etc., wavelengths between x = 0 and $x = x_a$. Therefore we expect to see a periodicity in the amplitude of the perturbed distribution function at $x = x_a$ with

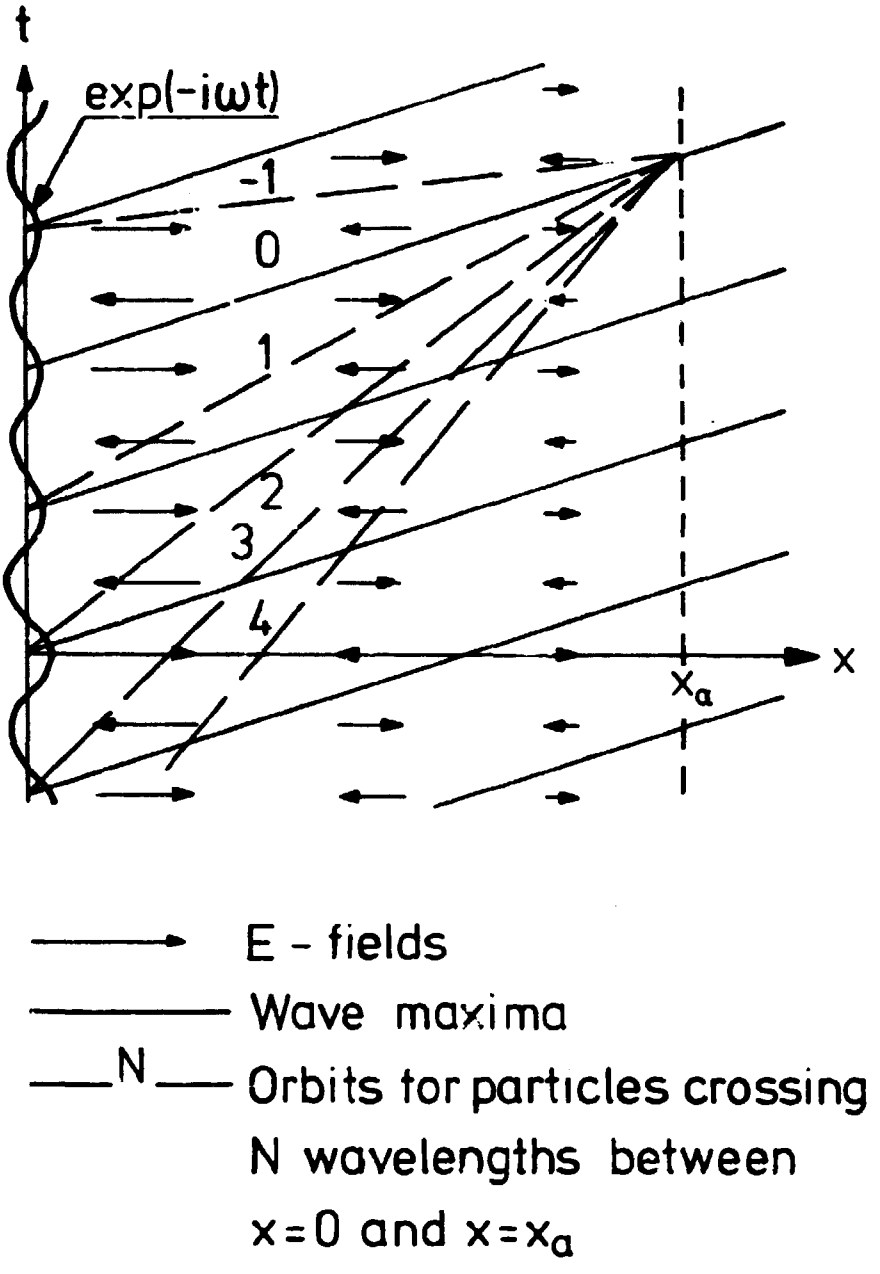

Fig. 4. Schematics of wave propagation.

a period in v-space that is determined by the velocity of those particles which have crossed an entire number, N, of wavelengths between $x = 0$ and $x = x_a$. An ion with velocity v_N has crossed N wavelengths if

$$v_N = v_{ph}(1+2\pi N v_{ph}/\omega x_a)^{-1} \qquad (8.5)$$

where N is subject to the condition

$$- x_a \omega / 2\pi v_{ph} \leq N \leq + \infty \ . \qquad (8.6)$$

In the x_a-v diagram in Fig. 5 curves given by Eq. (8.5) are shown for various N-values. It is easy to see that the curves in Fig. 5 coincide with the oscillations on the curves in Fig. 5 of chapter 6. These very characteristic oscillations should in principle be very easy to detect experimentally. However, as discussed in chapter 6, such a detection would require an electrostatic energy analyzer with a resolution much better than that of the one we have built.

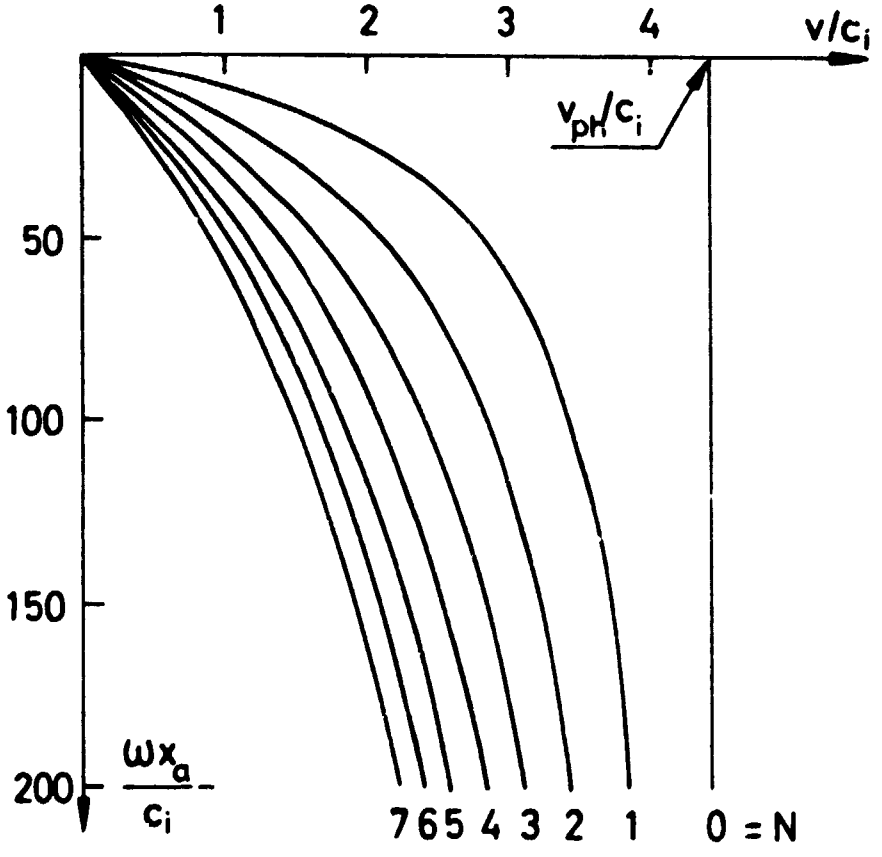

Fig. 5. Curves calculated from Eq. (8.5) for eight N-values. The various parameters used in the calculations were the same as those used in the calculations of Fig. 5 of chapter 5.

The conclusion of this section is that collective interaction in ion acoustic waves has not been demonstrated unambiguously up to now. The best chance for detecting this interaction seems to be to improve the resolution of the electrostatic ion energy analyzer and then to use it to measure the characteristic oscillations in the amplitude of the perturbed ion velocity distribution function in the wave.

8.4. Landau Damping

One of the problems encountered in the study of ion acoustic waves in collisionless plasma (and also in the study of high frequency electron oscillations) that has caused most discussion during the last few decades is the physical mechanism responsible for the damping of the waves. Such damping was first predicted by Landau[5] in his theoretical treatment (briefly summarized in the introduction).

Although the discussion about Landau damping has lasted for more than twenty years, there is still disagreement about the physical mechanism that causes this damping. Some claim that the damping is caused by phase mixing, i.e. that the damping occurs because particles in a wave-crest having a spread in velocity tend to move to the nearby troughs and thereby diminish the wave amplitude. It is clear that this mechanism is responsible for the damping in a case where collective interaction can be neglected. The work of Hirschfield and Jacob[12] mentioned under 2) in the list of unsolved problems in the introduction clearly concerns a case where the damping is caused by phase mixing.

Other authors concentrate on exponential Landau damping. They claim that Landau damping is caused by a resonance effect between the wave and particles in the background plasma that move with a velocity close to the phase velocity of the wave. Two different mechanisms for such a resonance effect have been suggested. To explain one of these mechanisms only particles in the background plasma that move with a velocity so close to the phase velocity that they are trapped in the troughs are considered. If there are more of these particles having a velocity below the phase velocity than there are of trapped particles

having a velocity above the phase velocity, i.e. if $df_o/dv_{v=v_{ph}} < 0$, then the wave must give away energy to the particles and thus it damps. The main argument in favour of this physical explanation of Landau damping is that if Landau[5] technique is used to calculate the propagation properties of a wave, one finds that the exponentially damped mode given by Eq. (1.20) has a damping rate proportional to $df_o(v)/dv_{v=v_{ph}}$. If this explanation is correct, it would certainly imply that exponential Landau damping is a collective effect since no particles can be trapped without collective interaction.

The other resonance mechanism suggested for explaining Landau damping is also based on energy arguments, but not on trapped particles. It can be shown[21] that when a wave with a nearly constant amplitude propagates through a plasma, it will transfer a net energy to the particles and thus damp. The main part of the energy is transferred to plasma particles with velocity close to the phase velocity.

The results of the study presented here help to clarify the discussion about the physical mechanism responsible for Landau damping. We first present arguments against the trapped particle mechanism. As already mentioned in connection with Eq. (8.2), linearization of the Vlasov equation implies that changes in the perturbed ion velocity distribution function are obtained by integration along unperturbed orbits. Therefore there are no trapped particle effects in the linearized equations and solutions to the equations cannot be explained by such particles. It is, of course, correct that trapped particles will absorb energy from the wave if $df_o(v)/dv < 0$ for $v = v_{ph}$, but this can only be seen in a non-linear treatment of the equation.

In order to show more specifically that the damping of a wave does not only depend on $df_o(v)/dv$ for $v = v_{ph}$ and thereby also to have a further argument against Landau damping being caused by energy absorption of trapped particles, we have used our Green's function technique (Eq. (29) of chapter 7) to calculate the propagation properties for small x of an ion acoustic wave generated at $x = 0$ and propagating through a plasma where $f_o'(v_{ph}) = 0$.

We have first performed the calculations for a case where

$$g(v) = n\, c_i^{-1} \pi^{-\frac{1}{2}} \exp[-(v-2.5\, c_i)^2/c_i^2] , \qquad (8.7)$$

$$f_o(v) = n_o c_i^{-1} \pi^{-\frac{1}{2}} \exp[-(v-2.5\, c_i)^2/c_i^2)] \qquad (8.8)$$

and

$$T_i = T_e . \qquad (8.9)$$

The dotted curve marked I in Fig. 6 represents the shape of the $g(v)$ and the $f_o(v)$ functions. The curves marked I in Fig. 7 show the calculated amplitude and phase of the wave as functions of $x\omega/c_i$. We deduce from the phase curve that the phase velocity is very close to $4.05\, c_i$.

To study the effect on the damping of changing the slope of $f_o(v)$ at v_{ph}, the calculations are repeated for a case where $f_o(v)$ is changed into

$$f_o(v) = n_o \left\{ c_i^{-1} \pi^{-\frac{1}{2}} \exp[-(v-2.5\, c_i)^2/c_i^2] \right.$$
$$+ 0.0205(c_i/\sqrt{15})^{-1} \pi^{-\frac{1}{2}} \exp[-(v-4.05\, c_i)^2 15/c_i^2] \qquad (8.10)$$
$$\left. - 0.0205(c_i/\sqrt{15})^{-1} \pi^{-\frac{1}{2}} \exp[-(v-3.55\, c_i)^2 15/c_i^2] \right\} ,$$

while $g(v)$ and T_e/T_i are unchanged.

This $f_o(v)$-function is marked II in Fig. 6. It only differs from (8.8) around $v = v_{ph}$ where the derivative equals zero. The results of the calculations of amplitude and phase for this case are marked II in Fig. 7. We note that the phase velocity has now changed to $3.8\, c_i$, which is the velocity at which $f_o'(v)$, as given in Eq. (8.10), equals zero. The curves showing the amplitude of the wave follow each other closely up to $x\omega/c_i \approx 80$ (about 3 wavelengths). From then on the amplitude for the last case is rather independent of x up to $x\omega/c_i = 150$, where it starts to decrease again.

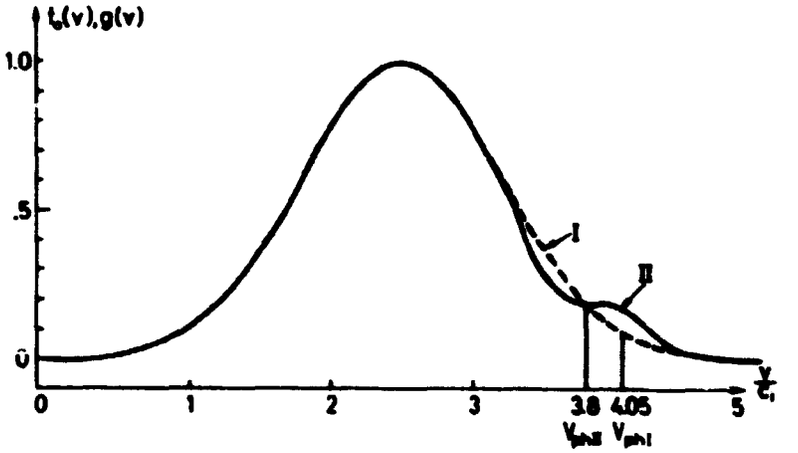

Fig. 6. Shape of the $f_o(v)$ and $g(v)$ functions.

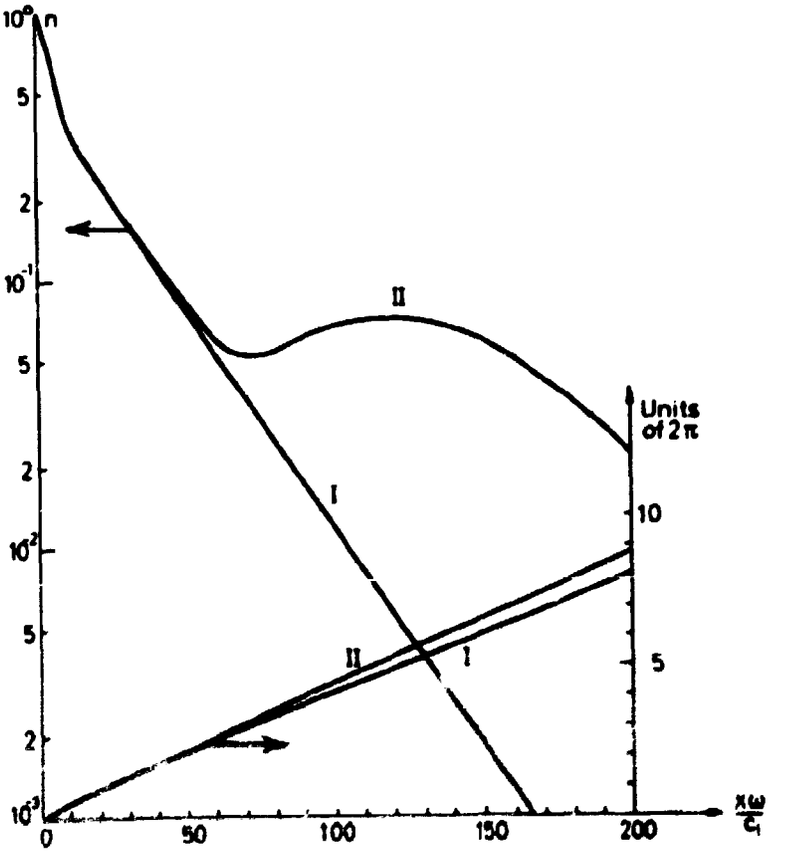

Fig. 7. Amplitude and phase of wave calculated for the two cases.

We conclude from these results that it is not a sufficient condition for an ion acoustic wave in a collisionless plasma to be undamped that $f_o'(v) = 0$ at $v = v_{ph}$. Thus the damping cannot be caused by trapped particles; it depends on the gross structure of the velocity distribution function rather than just on its slope at $v = v_{ph}$. Further evidence for this last statement will be given on the following pages.

We now return to the other two explanations of Landau damping. We first notice that, when used for the case without collective interaction, Fqs. (28) and (29) of chapter 5 are just the mathematical expression for a wave damped by phase mixing in the sense discussed above. When collective interaction is active the equations show that phase mixing is not alone responsible for the damping of the waves. The collective forces change the propagation properties and thereby the damping. Nevertheless, it should again be stressed that any wave pattern obtained from Eqs. (28) and (29) of chapter 5 for a case with collective interaction can also be obtained with free-streaming alone; one must just choose the proper g(v)-functions, as discussed in Sec. 8.3. This indicates that, at least for low T_e/T_i-values where collective interaction is relatively unimportant, the phase mixing arguments describe the damping mechanism quite well.

If we consider the Green's functions of the self-similar type found in chapters 4 and 5

$$n_G(x,t) = \frac{1}{t}\, h(\frac{x}{t}) \ , \tag{8.11}$$

and

$$f_G(x,v,t) = \frac{1}{t}\, k(\frac{x}{t},v) \ , \tag{8.12}$$

we see that first-order quantities such as the total number of ions in a pulse

$$N_T = \int_o^\infty \frac{1}{t}\, h(\frac{x}{t})\, dx \ , \tag{8.13}$$

the total moment of the ions in a pulse

$$M_T \propto \int_0^\infty dx \int_0^\infty \frac{v}{t} k(\tfrac{x}{t},v)\, dv \ , \tag{8.14}$$

and the total ion kinetic energy in a pulse

$$E_{kin} \propto \int_0^\infty dx \int_0^\infty \frac{v^2}{t} k(\tfrac{x}{t},v)\, dv \tag{8.15}$$

are conserved as the pulse moves through the plasma. If we calculate corresponding first-order quantities in a wave by means of expressions like Eq. (29) in chapter 5, we see immediately that they vary with the time as exp(-iωt) and therefore vanish when averaged over one period. If we look at the potential energy, which is a second-order quantity proportional to the square of the density perturbation, it is clear that this energy is not conserved in a pulse as it moves through the plasma; to obtain energy conservation the work done by the expanding pulse on the electron fluid of the background plasma has to be included. It is, however, interesting that in the wave case the small amplitude theorem, as used by Dawson[21] for high frequency oscillations, shows that the wave damping is accompanied by a transfer of potential wave energy to second-order kinetic energy of the ions in the background plasma; the transfer takes place in such a way that the total amount of energy is conserved. Dawson[21] discussed the physical mechanism of the damping of nearly undamped, high frequency, electrostatic waves and found that a wave would transfer energy to the plasma electrons with a velocity very close to the phase velocity, in such a way that it would damp according to the results of a Landau treatment of the problem. Rather than performing a very complicated analysis, we obtain a strong indication that second-order energy is conserved in ion acoustic waves by applying a somewhat simplified version of Dawson's[21] method.

Although as stated in chapter 5 and as will be shown later in more detail, a strictly exponentially damped ion wave is not a solution to the Vlasov equation with given boundary conditions, we shall, for convenience, approximate the electric field by

$$E = E_o e^{i(kx-\omega t)} \ , \tag{8.16}$$

where $k = k_r + ik_i$, $k_i > 0$ and $k_r > 0$.

We calculate the change in velocity, Δv, of an ion entering at $x = 0$ at $t = t_o$ with velocity v by integrating Newton's second law

$$m_i \frac{dv}{dt} = eE_o e^{i(kx-\omega t)} \tag{8.17}$$

along the unperturbed orbit

$$x = v(t-t_o) \tag{8.18}$$

from $x = 0$ to $x \to \infty$ and get

$$\Delta v = \frac{eE_o}{m_i} \int_{t_o}^{\infty} e^{i(kvt-\omega t-kvt_o)} dt = \frac{i\, eE_o}{m_i} \frac{e^{-i\omega t_o}}{(kv-\omega)} . \tag{8.19}$$

From this we get

$$\langle \Delta v^2 \rangle = \frac{1}{2} (\Delta v \cdot \Delta v^*) = \frac{1}{2} \frac{(eE_o)^2}{m_i^2} \frac{1}{(k_r v-\omega)^2+(k_i v)^2} . \tag{8.20}$$

Here $\langle\ \rangle$ stands for a t_o-average over a period of $2\pi/\omega$, and $*$ means complex conjugate.

The change in kinetic energy of the particle as it moves through the wave region is

$$\Delta E_{kin} = \frac{1}{2} m_i \{(v+\Delta v)^2 - v^2\} = \frac{1}{2} m_i \{\Delta v^2+2\Delta v v\} . \tag{8.21}$$

Averaging over one period in t_o gives

$$\langle \Delta E_{kin} \rangle = \frac{1}{2} m_i \langle \Delta v^2 \rangle \tag{8.22}$$

The rate at which energy is delivered from potential energy in the wave to kinetic energy in the background plasma is per unit area of a cross-section of the plasma column

$$W_{kin} = \frac{1}{4} \frac{(eE_o)^2}{m_i} \int_o^\infty \frac{v f_o(v)}{(k_r v-\omega)^2+(k_i v)^2} \, dv \tag{8.23}$$

Averaged over a wavelength, the potential energy density in an ion acoustic wave is

$$E_p = \frac{\kappa T_e}{4} \frac{n^2}{n_o} , \tag{8.24}$$

where n is the wave amplitude. Thus the rate at which potential energy is fed into a unit area of the wave at the grid is given by

$$W_p = \frac{\kappa T_e}{4} \frac{n^2}{n_o} v_{ph} , \tag{8.25}$$

which, by means of the electron fluid equation (1.10), can be re-written in the form

$$W_p = \frac{(eE_o)^2}{4\kappa T} \frac{n_o}{k_r^2} \frac{\omega}{k_r} . \tag{8.26}$$

For the general cases as those treated in chapter 5, where the damping is not exponential, it is difficult to show that W_{kin} equals W_p. It is, however, easy to make plausible that they are equal by evaluating W_{kin} from the approximate expression (8.23).

As an example we take the situation treated in Fig. 3 of chapter 5. For this case the unperturbed distribution function is

$$f_o(v) = \frac{n_o}{\sqrt{\pi} c_i} e^{-\{(v-3c_i)^2/c_i^2\}} \tag{8.27}$$

and

$$T_e = T_i \tag{8.28}$$

By taking the first wavelength as representative of the propagation properties, we deduce from the figure the following approximate values

$$v_{ph} = \frac{\omega}{k_r} = 4\ c_i \quad \text{and} \quad k_i/k_r = 1/5 \tag{8.29}$$

The denominator in the integrant of Eq. (8.23) constitutes the absorption spectrum of energy from the wave. By inserting the values of (8.29) into this spectrum, we find that it has a maximum at $v = 3.85\ c_i$ and half-value points at $v = 3.08\ c_i$ and $v = 4.62\ c_i$. Because a great number of the particles in the undisturbed distribution (8.27) lies between these half-value points, we may conclude that for relatively heavily damped waves, such as ion acoustic waves, wave energy is transferred to the bulk of the particles in the background plasma rather than just to the resonance particles, as is the case for weakly damped waves[21].

By inserting (8.27), (8.28) and (8.29) into (8.23) we get

$$W_{kin} = \frac{1}{32\sqrt{\pi}} \frac{(eE_o)^2}{\kappa T_e} \frac{n_o}{k_r^2} v_{ph} \int_o^\infty \frac{u e^{-(u-3)^2}}{(u-4)^2+(\frac{u}{5})^2}\, du \tag{8.30}$$

By graphical evaluation, the integral in (8.30) is found to be very close to 5, thus we get

$$W_{kin} \approx \frac{1}{11} \frac{(eE_o)^2}{\kappa T_e} \frac{n_o}{k_r^2} \frac{\omega}{k_r} . \tag{8.31}$$

This is about 40% of W_p given in (8.26). The agreement is acceptable taking into account that the damping of the wave is substantially smaller than the assumed exponential damping at large distances from the grid. As a matter of fact, if the damping had been evaluated one wavelength from the grid the agreement would have been within 10%. Complete agreement is not expected because the energy absorbed or delivered by the ions in the perturbed distribution functions g(v) at x = 0 gives a contribution to W_{kin} that was not taken into account. Because the

wave propagation depends on $g(v)$[19], it is clear that this contribution is not negligible, but a rough estimate indicates that it is relatively small for most choices of $g(v)$.

Accepting that W_{kin} and W_p are equal we may draw the following conclusion from this discussion of Landau damping of ion acoustic waves: trapped particles are not responsible for linear Landau damping. The damping can best be described as a phase mixing of almost freely streaming particles; the deviation from pure free streaming is caused by collective interaction acting in such a way that the potential energy lost by the wave per time unit is transferred to the ions in the background plasma. The energy absorption spectrum is centered around the phase velocity of the wave, but in the case of the relatively strongly damped ion acoustic waves, the spectrum has a rather wide shape so that energy is absorbed by the bulk of the ion distribution function. It is a matter of taste whether one explains Landau damping as a phase mixing effect subject to energy conservation between waves and particles, or whether one prefers to explain it by the transfer of wave energy to the particles - there is no conflict between the two interpretations.

From Eq. (29) in chapter 5 we can gain deeper insight into the propagation properties of an ion acoustic wave. especially regarding the behaviour relatively close to the exciter where most experimental results are obtained. To do so we rewrite the equation in the form

$$n(x,t) = \exp(-i\omega t)A(x) \ . \tag{8.32}$$

Here $A(x)$ is a complex quantity. $|A(x)|$ represents the amplitude of the wave, while the argument of $A(x)$ represents the phase of the wave as a function of x. $A(x)$ is given by

$$A(x) = \pi^{-1} \int_0^\infty \exp(i\omega \frac{x}{v}) \, v^{-1} \, \mathrm{Im} \, N_b(v) \, dv \ . \tag{8.33}$$

By inspecting the definition of $N_b(v)$ given in Eq. (12) of chapter 5, we note that

$$v^{-1} \, \mathrm{Im} \, N_b(v) \to 0 \quad \text{for} \quad v \to \infty \ , \tag{8.34}$$

that

$$\text{Im } N_b(\nu) \to 0 \quad \text{for} \quad \nu \to 0_+ \ , \tag{8.35}$$

and that $N_b(\nu)$ is limited in the interval $0 \leq \nu < \infty$.

We substitute $y = \nu^{-1}$ into Eq. (8.33) and get

$$A(x) = \pi^{-1} \int_c^\infty \exp(i\omega xy)\, G(y)\, dy \tag{8.36}$$

where

$$G(y) \equiv y^{-1} \text{ Im } N_b(y^{-1}) \ . \tag{8.37}$$

From Eqs. (8.34) and (8.35), we get $G(0) = 0$ and $G(y) \to 0$ for $y \to \infty$, and we also know that $G(y)$ is limited in the interval $0 \leq y < \infty$. The shape of $G(y)$ depends on the functions $g(v)$ and $f_o(v)$ and on T_e. The properties mentioned above guarantee that $G(y)$ is integrable in the interval $0 \leq y < \infty$, and thereby we can use Riemann's lemma for further discussion of Eq. (8.36). First of all, Riemann's lemma tells us that $|A(x)| \to 0$ as $x \to \infty$, which means that the wave does damp to zero, but there is no reason to believe that the damping is exponential. Riemann's lemma says nothing of the dependence of $|A(x)|$ for small x, and there might be intervals in which $|A(x)|$ increases. As a matter of fact, examples of numerical calculations reported in [19] show cases where $A(x)$ oscillates for small x. It is interesting to note that such amplitude oscillations were seen experimentally by Kawai and Ikegami[23]. These authors claim that the oscillations are caused by non-linear effects. Our results show that such oscillations can be easily explained in a linear theory; they can, as we have seen, even occur in situations where collective interactions are neglected.

Furthermore, there is no reason to believe that the argument of $A(x)$, as given in Eq. (8.36), increases linearly with x. In fact the calculations in [14] show that it generally does not. This means that the wavelength, and thereby the phase velocity of the wave, depends on x. This fact gives evidence against exponential Landau damping being caused by a trapped particle resonance effect between the wave and particles in the background

plasma moving with a velocity close to the phase velocity. Because no constant phase velocity exists, it is difficult to imagine that such a resonance effect is responsible for the damping.

It was found above that infinitely many amplitude patterns, $|A(x)|$, can be obtained from Eq. (8.36) just by varying $G(y)$. As much experimental work on ion acoustic waves in collisionless plasmas has been performed in order to show that the waves are exponentially damped, it is of interest (perhaps only of academic interest) to show that among the infinitely many patterns obtainable from Eq. (8.36) there are none that are strictly exponentially damped. The proof of this statement is as follows[24]. Let us assume that an exponentially damped wave exists; if that is the case then

$$A(x) \propto \exp(-i\alpha x) , \tag{8.38}$$

where $\alpha = \alpha_r + i\alpha_i$ is a complex number with $\alpha_i \neq 0$. We substitute $p = -i\omega x$ into Eq. (8.36) and get

$$A(x=ip/\omega) = \int_0^\infty \exp(-py)\, G(y)\, dy , \tag{8.39}$$

which shows that $A(x=ip/\omega)$ can be obtained as the Laplace transform of $G(y)$ evaluated on the imaginary axis of the p-plane. The properties of $G(y)$ discussed in connection with Eq. (8.37) above guarantee that the Laplace transform (8.39) exists and that it is convergent and analytic in the half-plane Re. $p \geq 0$. Our requirement that $A(x)$ should take the form $\exp(-i\alpha x)$ is equivalent to requiring that the Laplace transform should take the form $\exp(\alpha p/\omega)$. This function, however, is not convergent on the imaginary p-axis if $\alpha_i \neq 0$. Hence we have indirect proof that an ion acoustic wave, strictly exponentially damped in space, cannot exist.

8.5. Fluid Description contra Kinetic Description

Many theoretical treatments of problems ir plasma physics are based on fluid equations rather than on Vlasov equations. Fluid equations can be derived from Vlasov equations by apply-

ing various simplifying assumptions and approximations[14]. Because the variable quantities in the fluid equations are functions only of space and time, and not of velocity, these equations are in general much easier to use than the Vlasov equations. It has been widely discussed for some time to what extent one can rely on results obtained from fluid equations. Our Green's function study provides us with a few new arguments in this discussion. In the most commonly used form the linearized fluid equations for the ion acoustic wave problem discussed in this paper are[14]:

The continuity equation

$$\frac{\partial \rho}{\partial t} + \rho_o \frac{\partial v}{\partial x} = 0 \ , \tag{8.40}$$

the momentum equation

$$\rho_o \frac{\partial v}{\partial t} + \frac{\partial p}{\partial x} = 0 \ , \tag{8.41}$$

and the adiabatic equation

$$\frac{1}{p_o} \frac{\partial p}{\partial x} = \gamma \frac{1}{n_o} \frac{\partial n}{\partial x} \ . \tag{8.42}$$

In these equations n is the particle density, ρ ($= nm_i$) is the mass density, v is the fluid velocity, and p ($= 2n \kappa T$) is the plasma pressure. The symbols p_o, ρ_o, n_o and T_o represent the conditions in the undisturbed plasma while the perturbations are represented by the same symbols without indices. γ is the adiabatic ratio. From Eqs. (8.40), (8.41) and (8.42) it is easy to derive the dispersion relation for ion acoustic waves described by the fluid equations:

$$v_{ph}^2 = \left(\frac{\omega}{k}\right)^2 = \frac{2\gamma \kappa T_o}{m_i} \tag{8.43}$$

where ω and k are real numbers. This equation shows that the phase velocity is independent of frequency, which again means

that a plasma as described by the fluid equations is dispersionless. Therefore, if we calculate the Green's function for the fluid equations we find that this function retains its δ-function shape as it propagates through the plasma.

The fact that the Green's function, as described by the fluid equations, does not take the self-similar form $\frac{1}{t} h(\frac{x}{t})$ shows serious flaws in a fluid treatment. Fluid equations cannot be used for a detailed study of a problem, but only to obtain rough estimates of some gross properties of the plasma.

8.6. Unstable Plasmas and Future Work

The theoretical results obtained for the unstable plasma in chapter 6 have not been verified so far. Verifications of these results would be very interesting as they would constitute a detailed experimental investigation of the rise of an instability growing from a low level. During the last few months the Risø Q-machine group has been involved in an attempt to study experimentally the development of an instability of the kind treated in chapter 6. The preliminary results obtained so far are not very encouraging, as they more or less only constitute a reprtition of the results obtained by Baker[25]. It seems to be difficult to resolve the oscillations in the exponentially growing part of the pulse, whereas acceptable agreement with theory has been obtained for the self-similar part. One of the reasons for the difficulties with the growing part is that the propagation velocity of this signal depends on the density of the background plasma, and therefore varies across the plasma column.

A natural, long-term continuation of the work described in this paper would be a study of non-linear effects in unstable plasmas. Such an investigation would eventually turn into a study of plasma turbulence, which is a field of utmost importance in fusion research. The Q-machine group intends to follow these lines in the future work.

REFERENCES

1) J.H. Malmberg and C.B. Wharton, Phys. Rev. Lett. 13 (1964) 184-186.

2) A.Y. Wong, N. D'Angelo, and R.W. Motley, Phys. Rev. Lett. 9 (1962) 415-416.

3) A.Y. Wong, R.W. Motley, and N. D'Angelo, Phys. Rev. A133 (1964) 436-442.

4) V.O. Jensen, Risø Report No. 54 (1962) 19 pp.

5) L.D. Landau, J. Phys., USSR 10 (1946) 25-34.

6) G. Backus, J. Math. Phys. 1 (1960) 178-191.

7) H. Weitzner, Phys. Fluids 6 (1963 1123-1127); and in: Magnetofluid and Plasma Dynamics. Edited by H. Grad (American Mathematical Socity, Providence, 1967) Proceedings of Symposium in Applied Mathematics, 18) 127.

8) G. Joyce, K. Lonngren, I. Alexeff, and W.D. Jones, Phys. Fluids 12 (1969) 2592-2599.

9) N. Sato, H. Ikezi, N. Takahashi, and Y. Yamashita, Phys. Rev. 183 (1969) 278-287.

10) P. Korn, T.C. Marshall, and S.P. Schlesinger, Phys. Fluids 13 (1970) 517-526.

11) H.J. Doucet and D. Gresillon, Phys. Fluids 13 (1970) 773-781.

12) R.W. Gould, Phys. Rev. A136 (1964) 991-997.

13) J.L. Hirschfield and J.H. Jacob, Phys. Fluids 11 (1968) 411-413.

14) L. Spitzer, Jr., Physics of Fully Ionized Gases, 2nd ed., (Interscience, New York, 1962) Chapter 5.

15) J.M. Buzzi, H.J. Doucet, and D. Gresillon, Phys. Fluids 13 (1970) 3041-3049.

16) S.A. Andersen, G.B. Christoffersen, V.O. Jensen, and P. Michelsen, Plasma Phys. 14 (1972) 202-204.

17) S.A. Andersen, V.O. Jensen, and P. Michelsen, Rev. Sci. Instrum. 43 (1972) 945-947.

18) S.A. Andersen, V.O. Jensen, P. Michelsen, and P. Nielsen, Phys. Lett. A32 (1970) 413-414.

19) V.O. Jensen and P. Michelsen, Risø Report No. 257 (1972) 33 pp.

20) G.B. Christoffersen, V.O. Jensen, and L.P. Prahm, in: Fifth European Conference on Controlled Fusion and Plasma Physics, Grenoble, France, August 21-25, 1972. Vol. 1 (Euratom-CEA, Grenoble, 1972) 175.

21) J. Dawson, Phys. Fluids 4 (1961) 869-874.

22) V.O. Jensen and P.I. Petersen, Phys. Lett. A45 (1973) 293-294.

23) Y. Kawai and H. Ikegami, Plasma Phys. 13 (1971) 463-470.

24) H.C.S. Hsuan and V.O. Jensen, Phys. Fluids 16 (1973) 1776-1778.

25) D.R. Baker, Phys. Rev. Lett. 28 (1972) 1189-1192 and Phys. Fluids 16 (1973) 1730-1739.

Dansk resumé af

NOGLE UNDERSØGELSER AF DET ION-AKUSTISKE BØLGEPROBLEM I KOLLISIONFRI PLASMAER

I den foreliggende afhandling beskrives eksperimentelle og teoretiske undersøgelser af udbredelsesforhold for ion-akustiske bølger i et kollisionsfrit plasma. Undersøgelserne er udført på Risø i tiden 1969 til 1974.

I indledningen gives et kort resumé af det arbejde, der var udført inden for dette felt indtil 1969, og der opregnes en række problemer, som ikke var afklarede.

Kapitel 2 indeholder en kort beskrivelse af Risøs Q-maskine og der gives nogle karakteristiske størrelser for de plasmaer, der kan produceres i den.

Kapitlerne 3 til 6 er genoptryk af artikler, som omhandler forskellige dele af arbejdet, og som er publicerede i The Physics of Fluids. I artiklen i kapitel 3 beskrives de resultater, som er opnået med en elektrostatisk energianalysator, der er udviklet for at bestemme ionhastighedsfordelingsfunktionen i plasmaet i Risøs Q-maskine.

I kapitel 4 beregnes Green's funktionerne til det sæt ligninger, der benyttes til at beskrive udbredelsen af ion-akustiske bølger. Eksperimentelt simuleres Green's funktionen ved at indsætte et elektrisk forspændt gitter i plasmasøjlen og påtrykke det en kortvarig elektrisk puls. Der findes god overensstemmelse mellem beregningerne og de opnåede eksperimentelle resultater. Ved disse målinger er der påvist sikre tegn på kollektiv vekselvirkning i et plasma.

I artiklen i kapitel 5 er Green's funktionerne benyttet til at beregne udbredelsesforhold for ion-akustiske bølger under forskellige forhold. Målingerne er i god overensstemmelse med de teoretiske resultater. Det konkluderes i dette kapitel, at kollektiv vekselvirkning i en ion-akustisk bølge, der udbreder sig i et plasma, hvor elektron- og iontemperaturen er næsten lige store, er så svag, at den ikke kan detekteres.

I kapitel 6 præsenteres en teoretisk behandling af et plasma med en ustabil ionhastighedsfordelingsfunktion af den type, som kan opnås i Q-maskiner. Ved hjælp af Green's funktionerne vises det, at en påtrykt tæthedsperturbation i et sådant plasma nor-

malt vil starte med at formindskes og først begynde at vokse efter en vis tid.

Enkelte kommentarer og korrektioner til kapitlerne 3 til 6 er givet i kapitel 7.

Endelig diskuteres de fire artikler under eet i kapitel 8, og der præsenteres en række konklusioner, som er baserede på det udførte arbejde. Der er i dette kapitel lagt vægt på at vise, i hvilket omfang det er lykkedes at medvirke til en afklaring af den række problemer, der blev opregnet i kapitel 1. Specielt præsenteres der her bidrag til diskussionen om den fysiske fortolkning af den mekanisme, der forårsager Landau dæmpning. Dette kapitel indeholder også en diskussion af betydningen af Vlasov ligningens kollektive vekselvirkningsled. Endelig fremføres der også i dette kapitel nogle argumenter i forbindelse med diskussionen om fluidligningernes egnethed til at beskrive et plasma.

ISBN 87-550-0408-3